

November 2020

Well Testing of Fracture Corridors in Naturally - fractured Reservoirs (NFR)

Yingying Guo

Follow this and additional works at: https://digitalcommons.lsu.edu/gradschool_theses



Part of the [Engineering Commons](#)

Recommended Citation

Guo, Yingying, "Well Testing of Fracture Corridors in Naturally - fractured Reservoirs (NFR)" (2020). *LSU Master's Theses*. 5235.

https://digitalcommons.lsu.edu/gradschool_theses/5235

This Thesis is brought to you for free and open access by the Graduate School at LSU Digital Commons. It has been accepted for inclusion in LSU Master's Theses by an authorized graduate school editor of LSU Digital Commons. For more information, please contact gradetd@lsu.edu.

WELL TESTING OF FRACTURE CORRIDORS IN NATURALLY - FRACTURED RESERVOIRS (NFR)

A Thesis

Submitted to the Graduate Faculty of the
Louisiana State University and
Agricultural and Mechanical College
in partial fulfillment of the
requirements for the degree of
Master of Science

in

The Craft & Hawkins Department of Petroleum Engineering

by
Yingying Guo
B.S., New Mexico Institute of Mining and Technology, 2015
December 2020.

All models are wrong, but some are useful.

George Box

This thesis is dedicated to my father and mother, Bin Guo and Yanchun He, who inspired me to go into petroleum engineering and encouraged me to pursue higher education.

ACKNOWLEDGMENTS

I would like to begin by thanking Dr. Andrew K. Wojtanowicz, Dr. Wesley C. Williams, and Dr. Ipsita Gupta for sitting on my committee. Without their supportive help, this thesis would not have been possible.

Secondly, I would like to especially thank my advisor and committee chair, Dr. Andrew K. Wojtanowicz, for offering me a teaching assistant position and financial support for my master's studies in petroleum engineering and applied statistics. His wide range of knowledge, a plethora of new ideas, and a constant thirst for new techniques have broadened my intellectual horizontals. Additionally, his inordinate amount of patience, decent behavior, rigorous attitude, and kind heart taught me how to be a better person, a good student, and a good teaching assistant. I thank him for always opening the door to me, encouraging me, and giving me the freedom to pursue the intellectual interests that changed my mind for the better. There is a long way to go before I can stand on my own feet, but being his student is the best gift the world has ever given to me. His incredible professionalism in teaching as a professor and in research as an advisor gave me the best example for my future career.

Thirdly, I would like to thank all the professors, staff, and fellow graduate students who I have worked with and who have helped me during my study at Louisiana State University. I could not survive without them.

Lastly, I would also like to thank my friend Neil Currie, an experienced professional geologist, for helping me understand the complicated fracture corridor systems. He has helped me develop my geological knowledge since I was in undergraduate school and often walked me word by word through concepts as I learned geology terminology.

There is nothing so thankful as having so many kind people in my life!

TABLE OF CONTENTS

ACKNOWLEDGMENTS	iv
LIST OF TABLES	vii
LIST OF FIGURES	viii
NOMENCLATURE	xi
ABSTRACT	xiv
CHAPTER 1. INTRODUCTION	1
1.1. Introduction.....	1
1.2. Significance of Research.....	1
1.3. Key Research Questions	3
CHAPTER 2. BACKGROUND	4
2.1. Modelling of Naturally Fractured Reservoirs	4
2.2. What are Fracture Corridors?.....	8
2.3. What is Well Testing?.....	18
2.4. What is Statistics?	20
CHAPTER 3. METHODOLOGY	21
3.1. Overview of Methodology	21
3.2. Reservoir Modelling	21
3.3. Model Verification.....	32
3.4. Well Analysis.....	38
CHAPTER 4. RESULTS	54
4.1. Well Placement Identification – Fracture/Matrix Well	54
4.2. Distinguish Matrix Well in Corridor-Type NFR and Well in Conventional NFR.....	57
4.3. Estimation of Well-Corridor Distance	60
4.4. Fracture Corridor Conductivity Estimation for Matrix Well	61
4.5. Fracture Corridor Length Estimation.....	62
4.6. Accuracy Assessments with Cumulative Logit Models	66
CHAPTER 5. DISCUSSION.....	76
5.1. Limitation of Fracture Corridor Length Estimation from Bilinear Flow Regime	76
5.2. Effect of Well-Corridor Configuration on Accuracy of the Fracture Corridor Length Estimation from SSS Flow Regime.....	77
5.3. Implications for Petroleum Engineering.....	79
5.4. Further Research	80
CHAPTER 6. CONCLUSION	82

APPENDIX A. DERIVATION OF EQUATIONS FOR WELLBORE STORAGE REMOVAL.....	84
APPENDIX B. SPACE – FILLING DESIGN DATA AND RESULTS	88
APPENDIX C. SAS CODE FOR CUMULATIVE LOGIT MODELS	90
APPENDIX D. SAS LOG FOR CUMULATIVE LOGIT MODELS.....	92
APPENDIX E. SAS OUTPUT FOR MULTICOLLINEARITY TEST	97
APPENDIX F. SAS OUTPUT FOR ACCURACY OF MATRIX PERMEABILITY ESTIMATION	98
APPENDIX G. SAS OUTPUT FOR ACCURACY OF WELL-CORRIDOR DISTANCE ESTIMATION	99
BIBLIOGRAPHY	100
VITA	107

LIST OF TABLES

2.1.	Engineering classification of NFR (after Nelson)	4
3.1.	Dual porosity NFR with small contrast of diffuse fracture/matrix properties	24
3.2.	Single porosity model of NFR	24
3.3.	Dual porosity NFR with high contract of diffuse fracture/matrix properties	25
3.4.	Well properties.....	31
3.5.	Reservoir properties used to verify the model	34
3.6.	Flow regime diagnostics	41
4.1.	Properties of corridor type NFR (model 1).....	59
4.2.	Properties of conventional NFR.....	60
4.3.	Properties of the example CMG model 2 for corridor type NFR	64
5.1.	The results of fracture corridor approximation for three positions.....	78
B.1.	Space-filling design data generated by JMP (a suite of computer programs for statistical analysis developed by the JMP business unit of SAS Institute)	88
B.2.	Result Table.....	89
E.1.	Pearson correlation coefficients for independent variables	97
E.2.	Collinearity diagnostics for independent variables.....	97
F.1.	Summary for accuracy of the matrix permeability estimation by forward selection method.....	98
F.2.	Parameter estimation of the accuracy of the matrix permeability estimation by forward selection method.....	98
F.3.	Likelihood-ratio test for the accuracy of the matrix permeability estimation	98
G.1.	Summary for accuracy of the well-corridor distance estimation by forward selection method.....	99
G.2.	Parameter estimation of the accuracy of the well-corridor distance estimation by forward selection method.....	99
G.3.	Likelihood-ratio test for the accuracy of the well-corridor distance estimation	99

LIST OF FIGURES

2.1.	Fluids flow when well in connected to fractures in NFR (dual porosity model).....	5
2.2.	Pressure vs. distance to wellbore during initial production in NFR	6
2.3.	Pressure vs. distance to wellbore when crossflow occur in NFR	7
2.4.	Pressure vs. distance to wellbore after matrix and the fracture each reach an equilibrium condition in NFR.....	7
2.5.	Fluids flow when well in connected to fractures in NFR (dual permeability model).....	8
2.6.	A schematic illustration of fracture corridor.....	10
2.7.	Global fracture corridor localities	11
2.8.	A schematic illustration of fault damage zone fracture corridor (FDZ)	12
2.9.	A schematic illustration of the fault tip process zone fracture corridor (FTP)	13
2.10.	Schematic illustration 1 of fold crest – related fracture corridor (FRC).....	14
2.11.	Schematic illustration 2 of fold crest – related fracture corridor (FRC).....	14
2.12.	Schematic illustration 3 of fold crest – related fracture corridor (FRC).....	15
2.13.	Schematic illustration 4 of fold crest – related fracture corridor (FRC).....	16
3.1.	Conceptual model of parallel fracture corridors	22
3.2.	An example of a diagnostic plot for a conventional reservoir and NFRs with low matrix and fracture permeability contrast in Table 3.1 and 3.2	23
3.3.	An example of a diagnostic plot for NFRs with high matrix and fracture permeability contrast in Table 3.3.....	23
3.4.	Single porosity model for matrix/fracture well.....	26
3.5.	Anisotropic flow system of fracture corridor type reservoir with equivalent permeabilities in the X direction (K_{fm_x}) and Y direction (K_{fm_y})	29
3.6.	Simplified flow system with well in the fracture corridor (fracture well).....	30
3.7.	Simplified flow system with well between two fracture corridors (matrix well)	30
3.8.	Model of fracture well with 11 fracture corridors	32
3.9.	Model of matrix well with 11 fracture corridors	33

3.10.	Model of fracture well for simplified flow system in the fracture corridor reservoirs	33
3.11.	Model of matrix well for simplified flow system in the fracture corridor reservoirs	34
3.12.	Model verification for fracture well.....	37
3.13.	Model verification for matrix well.....	37
3.14.	First radial flow regime for a fracture well in corridor type NFR	42
3.15.	Linear flow regime for a fracture well in corridor type NFR	42
3.16.	Bilinear flow regime for a fracture well in corridor type NFR.....	43
3.17.	Second radial flow regime for a fracture well in corridor type NFR.....	43
3.18.	Flow regimes for a fracture well in corridor type NFR	44
3.19.	First radial flow regime for a matrix well in corridor type NFR	45
3.20.	Corridor flow regime for a matrix well in corridor type NFR.....	45
3.21.	Bilinear flow regime for a matrix well in corridor type NFR.....	46
3.22.	Second radial flow regime for a matrix well in corridor type NFR.....	46
3.23.	Flow regimes for a matrix well in corridor type NFR	47
3.24.	Analysis of pressure data of bilinear flow	50
4.1.	An example of a diagnostic plot for fracture well before the removal of the wellbore storage in corridor type NFR (model 1).....	55
4.2.	An example of a diagnostic plot for fracture well after the removal of the wellbore storage in corridor type NFR (model 1).....	55
4.3.	An example of a diagnostic plot for matrix well before the removal of the wellbore storage in corridor type NFR (model 1).....	56
4.4.	An example of a diagnostic plot for matrix well after the removal of the wellbore storage in corridor type NFR (model 1).....	56
4.5.	Diagnostic plot for matrix well in corridor type NFR (model 1).....	58
4.6.	Diagnostic plot in conventional NFR	59
4.7.	Examples of a diagnostic plot from fracture well and matrix wells near fracture corridor in corridor type NFR (model 1)	61

4.8.	Diagnostic plot for bilinear flow.....	62
4.9.	Diagnostic plot for matrix well in corridor type NFR (model 2) in Table 4.3	65
4.10.	An example of a pressure drawdown plot for fracture well in corridor type NFR (model 2) in Table 4.3.....	65
5.1.	Diagnostic plot for fracture and matrix wells in corridor-type NFR (model 1).....	76
5.2.	Diagnostic plot for matrix well in large and small corridor-type NFR.....	77
5.3.	Examples of 3 fracture corridor position and well position in the reservoir	78
5.4.	$(p_R - p_{wf})$ vs. time for three positions from a fracture well	79
5.5.	Conceptual flow chart of well testing for fracture corridor type naturally fractured reservoirs.....	80
A.1.	Sketch of subinterval $[t_{i-1}, t_{i+1}]$ to segment ΔP_w	84
A.2.	Sketch of subinterval $[t_{i-1}, t_i]$ for integration	85
A.3.	Sketch of derivative algorithm.....	86

NOMENCLATURE

A	Area, (ft ²)
B_o	Oil formation volume factor (rb/stb)
C_A	The shape factor of unfractured vertical wells
C_F	The shape factor of fractured vertical wells
$(C_t)_m$	Matrix total compressibility (1/psi)
C_t	Total compressibility (1/psi)
C_{fD}	Dimensionless fracture corridor conductivity
D	Well-corridor distance (ft)
h	Reservoir thickness (ft)
K	Permeability (md)
K_E	Equivalent permeability (md)
K_f	Fracture corridor permeability (md)
$K_f W_f$	Fracture corridor conductivity (md-ft)
K_{fm}	Equivalent permeability of fracture corridors' system and the matrix beds(md)
K_{fm_x}	Equivalent permeability of fracture corridors' system and the matrix beds in the X-direction (md)
K_{fm_y}	Equivalent permeability of fracture corridors' system and the matrix beds in the Y-direction (md)
K_m	Matrix permeability (md)
K_{NFR}	Fracture permeability in NFR (md)
K_r	Radial permeability (md)
K_x	Permeability in the X direction(md)
K_y	Permeability in the Y direction(md)
L_f	Fracture corridor length (ft)

L_{hf}	Fracture half-length (ft)
L_m	Matrix length between two adjacent fracture corridors along fracture corridors (ft)
L_t	Reservoir length along fracture corridors (ft)
W_f	Width of fracture corridor (ft)
W_m	Fracture corridor spacing (ft)
W_t	Reservoir length perpendicular to fracture corridors (ft)
$K_f L_f$	Fracture corridor conductivity (md-ft)
MFCS	Minimum fracture corridors spacing (ft)
m_{BL}	The slope of the bilinear flow regime
N	Initial oil in place (stb)
p	Pressure (psi)
P	Probability
p_f	Pressure in fractures (psi)
p_i	Initial reservoir pressure (psi)
p_m	Pressure in matrix (psi)
p_R	Volumetric reservoir pressure (psi)
p_{wf}	Well bottomhole pressure (psi)
q	Production Rate (stb/d)
r_i	The radius of investigation (ft)
R_{K_m}	The response of matrix permeability
R_D	Response of estimated well-to-corridor distance
t	Production time (hour)
t_{ebf}	The end time of the bilinear flow regime (hour)
$t \times \Delta p'$	Pressure derivative (psi)

v_A	Actual value measured
v_E	Expected value
Δp_s	Constant-rate-pressure drop (psi)
Δp_{sd}	Derivative of pressure drop (psi/hour)
Δp_w	Wellbore-storage-distorted pressure drop (psi)
Δp_{wd}	Derivative of wellbore-storage-distorted pressure-drop (psi/hour)
Δp_{wi}	Integral of wellbore-storage-distorted pressure drop (psi)
Δp_{wid}	Derivative of wellbore-storage-distorted pressure drop Integra (psi/hour)
μ_o	Oil viscosity (cp)
μ	Fluid viscosity (cp)
\emptyset	Porosity
\emptyset_m	Matrix porosity
δ	Relative error
π	Probability

ABSTRACT

Geological folding/faulting may create fractured reservoirs containing a semi-parallel system of sparsely - spaced fracture corridors. Presently, methods for detecting fracture corridor requires borehole image log within a horizontal well, high-resolution 3-D seismic data or dynamic data, which are limited and expensive. Pressure behavior of wells completed either in highly-conductive corridors (fracture wells) or in the exclusion zone (matrix wells) would be quite differently. Therefore, pressure response patterns can be used to identify well's placement in the corridor system. The objectives of this study are to build new simulation model for corridor type NFRs and apply the well testing technique to identify corridor type NFRs from conventional NFRs, detect well's location, and estimate reservoir properties.

In this study, pattern recognition technique is used to analyze diagnostic plots of pressure drawdown generated by simulated flow tests with a commercial software (CMG). A unique simulation model has been built by combining a local model of fracture well or matrix well with adjacent fracture corridor and a "homogenized" global model of the remaining corridor network. The global model generalizes the corridor network using single-porosity and radial permeability approach, which is verified as being sufficiently accurate. This study also employs the cumulative logit models to assess accuracy of estimating permeability of the exclusion zone and well to corridor distance.

The results showed that diagnostic plots of bottom hole pressure response to constant production rate for the matrix and fracture wells clearly indicate the well's location. Moreover, permeability of the exclusion zone and well-to-corridor distance can be determined from the initial radial flow regime after removing the wellbore storage effect by β -deconvolution from a matrix well. It is also shown that diagnostic plot of the bilinear flow regime provides data for estimating

the fracture corridor conductivity and fracture corridor length. The corridor length can be estimated more precision from the pseudosteady-state flow regime. The more distant the well is from the fracture corridor, and the lower the exclusion zone permeability, the more accurate estimation of exclusion zone permeability. Accuracy of the well-to-corridor distance estimation improves for longer corridors and low-permeability exclusion zone.

CHAPTER 1. INTRODUCTION

1.1. Introduction

In the study of naturally fractured reservoirs, more focus has been placed on fracture corridors in the past decade. Fracture corridors, which act as preferential fluid pathways, are typically closely spaced, parallel or sub-parallel fracture clusters that can transect the entire reservoir vertically and extend long distances laterally. Fracture corridors have been observed in the outcrop. However, a cheap and effective way to detect fracture corridors in subsurface reservoirs has not been found. The detection of subsurface fracture corridors is the topic of interest in this study.

1.2. Significance of Research

In 1983, Segall et al. first defined fracture corridors as a narrow zone that contains closely spaced, parallel and subparallel fractures. Subsequently, Ogata et al. (2014) defined fracture corridor types and each type's formation mechanism in detail. After that, Souque et al. (2018) studied the development of fault-related fracture corridors, using the chalk in Isle of Thanet, Kent, England as an example.

The evidence for fracture corridors is primarily derived from outcrop studies. Fracture corridors are commonly observed in carbonate reservoirs. For example, Souque et al. (2018) studied the outcrop of fracture corridors in chalk. Ogata et al. (2014) extended their research to fracture corridors in limestone. Sharp et al. (2014) conducted an outcrop case study of fracture corridors in dolomite. Fracture corridors have also been observed in tight sandstone (Questiaux et al., 2009). Sanderson et al. (2019) characterized fracture corridors as utilizing scanlines. These outcrop studies helped to further understanding fracture corridors in the subsurface.

In 2006, Ozkaya et al. studied horizontal wells in a tight reservoir in south Kuwait to evaluate the low permeability formation's fracture flow potential. Rapid production decline and extremely low bottom hole pressures are commonly observed in tight reservoirs, while fracture corridors can have high flow potential, helping production. This enhanced production emphasizes the importance of locating fracture corridors in tight reservoirs. Detecting fracture corridors in a subsurface reservoir is much more difficult. The width of fracture corridors is, in most cases, much smaller than the seismic data bin. Standard seismic data cannot be used to map fracture corridors (Questiaux et al., 2009). In 2008, Singh et al. developed a workflow to map fracture corridors with 3D seismic data, which was successfully applied to the NW Raudhatain, Sabriyah, Umm Niqqa, and Bahra carbonate fields in Kuwait. However, seismic resolution limits this workflow when fracture corridors are more than 10 to 30 meters or more in width or length. In 2008, El-Gezeery et al. studied the identification fracture corridors by Real-Time Logging While Drilling Resistivity Imaging. Ozkaya studied fracture corridors detection utilizing open-hole logs in horizontal wells (2007), dynamic data by factor analysis (2008), dynamic data by probabilistic decision tree (2007, and 2008), exclusion zones (2010). Ozkaya also studied validating predicted fracture corridors by statistical comparison with well data in 2019.

To date, the best method of simulating fracture corridor type reservoirs remains controversial, although many researchers have attempted to build models of fracture corridor type reservoirs. In 2007, Uba et al. applied a Hybrid Dual Porosity Dual Permeability model to simulate a giant carbonate reservoir with fracture corridors. To avoid dual porosity simulation, Elfeel et al. (2010) combined Discrete Fracture and Matrix (DFM) models with single porosity models to upscale multiphase fluid flow properties of fracture corridors. In 2015, Saputra et al. compared a dual porosity model and a single porosity model and concluded that adapting fracture corridors and

diffuse fractures in a single porosity model was a better way to simulate the Ujing Pangkah fractured carbonate reservoir. Additionally, they found that dual porosity models cannot explain the behavior of some wells. In August 2019, a patent for streamline flow simulation of a model representing fracture corridors was filed by Schlumberger Technology Corporation.

1.3. Key Research Questions

Ozkaya made the most significant contribution to the study of naturally fractured reservoirs containing fracture corridors in recent 15 years. Following his work of mapping fracture corridors using the exclusion zone (2010) and validating predicted fracture corridors by statistical comparison with well data (2019), this research seeks to answer three critical questions.

1. How to build a simulation model for corridor type naturally fractured reservoirs that can simulate well testing?
2. How to develop methods to analyze diagnostic plots including identifying corridor-type naturally fractured reservoirs from the conventional naturally fractured reservoirs, detecting well location with respect to corridors, finding the distance from well to the nearest corridor and minimum corridor spacing, estimating matrix permeability and corridor conductivity and length?
3. How to assess accuracy of these methods mentioned above?

CHAPTER 2. BACKGROUND

2.1. Modelling of Naturally Fractured Reservoirs

Sixty percent of global oil reserves are stored in naturally fractured carbonate reservoirs (Schlumberger). Based on the porosity and permeability characteristics that matrix and fractures create, naturally fractured reservoirs can be classified into four types for engineering purposes (Table 2.1). In Type I naturally fractured reservoirs, the matrix has low porosity and permeability, and fractures provide the bulk of porosity and permeability, which means fractures provide both storage capacity and fluid-flow pathways. In Type II naturally fractured reservoirs, the matrix has low permeability, some porosity, and fractures provide most permeability, which means the matrix provides most storage capacity, and fractures provide most of the fluid-flow pathways. In Type III naturally fractured reservoirs, the matrix has high porosity and producible permeability, which means the matrix provides most storage capacity and fluid-flow pathways while fractures enhance the permeability of the reservoirs. In Type IV naturally fractured reservoirs, the matrix provides most porosity and permeability, and fractures act as seals/barriers.

Table 2.1. – Engineering classification of NFR (after Nelson)

Type I Naturally Fractured Reservoirs	Fractures provide essential reservoir porosity and permeability
Type II Naturally Fractured Reservoirs	Fractures provide the essential reservoir permeability
Type III Naturally Fractured Reservoirs	Fractures assist permeability in an already producible reservoir
Type IV Naturally Fractured Reservoirs	Fractures provide no additional porosity or permeability but create significant reservoir anisotropy (barriers)

2.1.1. Single Porosity Models

Single porosity models are widely used for conventional reservoirs. They can also be used to simulate naturally fractured reservoirs. However, naturally fractured reservoirs may contain hundreds or thousands of matrix and fracture blocks, which are difficult and time consuming to simulate with numerical methods.

2.1.2. Dual Porosity Models

Barenblatt, Zheltov, Kachina (1960) came up with the concept of a “dual continuum” to describe naturally fractured reservoirs, which laid a solid theoretical foundation of naturally fractured reservoirs. Barenblatt considered a naturally fractured reservoir as two overlapping continua. One continuum is a matrix, and the other is a fracture. Subsequently, Warren and Root introduced the pseudosteady-state flow behavior of naturally fractured reservoirs. In practice, a heterogeneous naturally fractured reservoir can be approximated by an equivalent homogeneous dual-porosity model. In the dual porosity model, only fractures can be connected to the well (Figure 2.1).

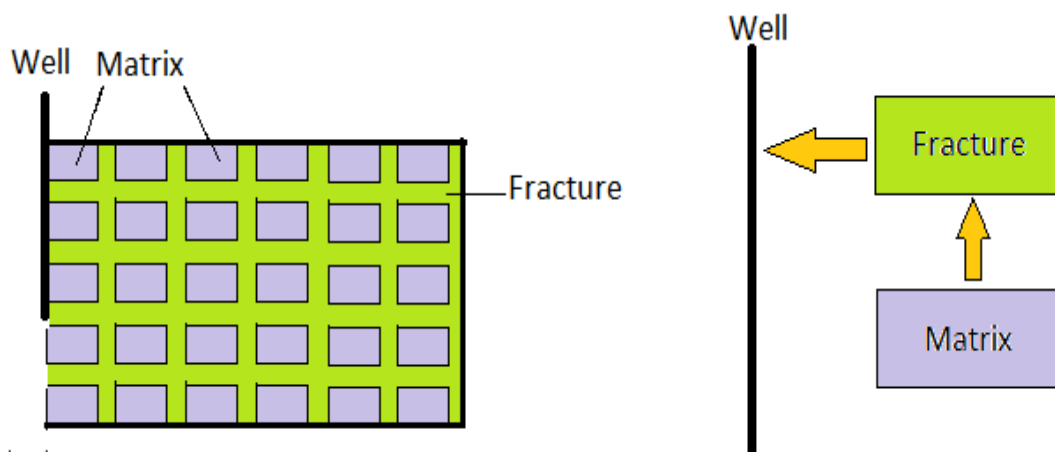


Figure 2.1. Fluids flow when well is connected to fractures in NFR (dual porosity model)

There are two continuous seepage fields in dual continuum reservoirs. Every block in the dual porosity model represents both fracture and matrix. Every point in the naturally fractured reservoirs has two pressures and two velocities because every point there also has two permeabilities. Fracture permeability is usually much more significant than matrix permeability, especially when approximating Type II naturally fractured reservoirs. In the early time of production, fluids flow to the well through fractures (Figure 2.2). During this period, pressure in the fractures decreases, while matrix pressure is relatively constant. Crossflow (Figure 2.3) from the matrix into fractures can occur once a pressure gradient between the matrix and fractures formed. Matrix pressure will then decrease until the pressure in the fracture and matrix equilibrate (Figure 2.4). The fluid transfer during crossflow is estimated using a shape factor. Many researchers, including Warren and Root (1963), Kazemi et al. (1976), Coats (1989), and Lim and Aziz (1995) derived shape factors in their research. The dual porosity model is the preferred method for simulating flow in naturally fracture reservoirs as it saves nodes and time compared to a single porosity model.

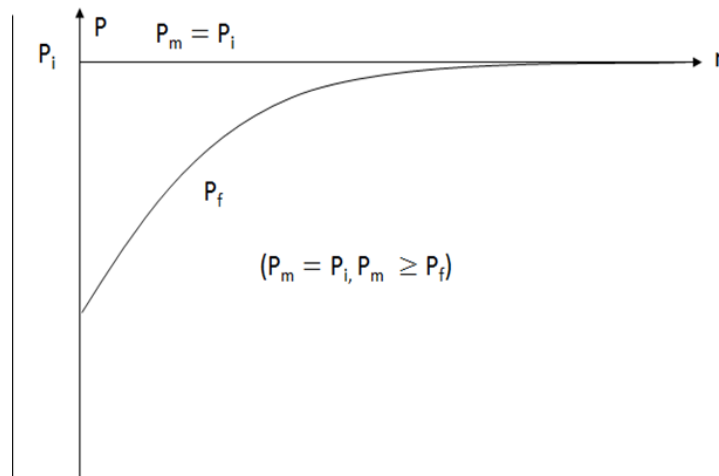


Figure 2.2. Pressure vs. distance to wellbore during initial production in NFR

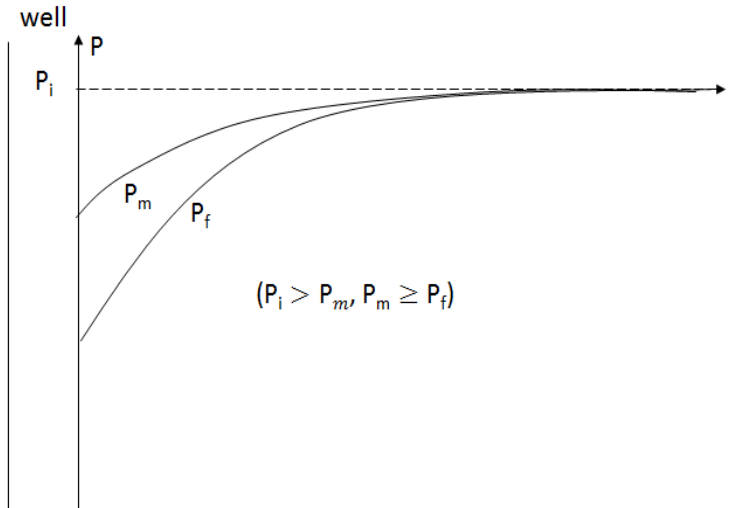


Figure 2.3. Pressure vs. distance to wellbore when crossflow occur in NFR

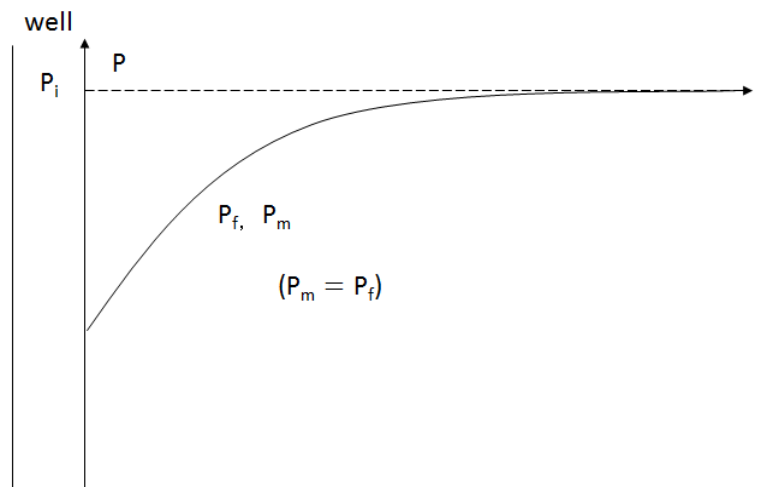


Figure 2.4. Pressure vs. distance to wellbore after matrix and the fracture each reach an equilibrium condition in NFR

2.1.3. Dual Permeability Models

Dual permeability models were suggested to simulate Type III naturally fractured reservoirs. Dual permeability models are similar to dual porosity models. However, they are reported to be more accurate than dual porosity models. In the dual permeability model (Figure 2.5), a well can be connected to fractures and matrix in naturally fractured reservoirs.

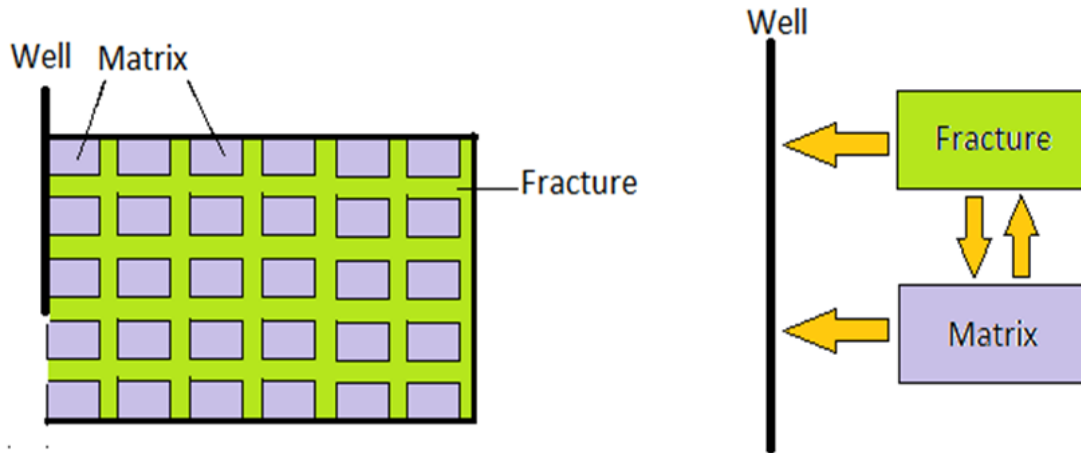


Figure 2.5. Fluids flow when well is connected to fractures in NFR (dual permeability model)

2.1.4. Discrete Fracture Models

In discrete fracture network models (DFN), all fractures are represented as discrete, well defined, and stochastic elements, instead of continuums. DFN can approximate the behavior of random fracture networks with hierarchy (Meyer 1999). Compared to traditional continuum models, the DFN models allow for better parameterization of uncertainty and variability (Dershowitz et al. 2000). They can calibrate grid and fracture spacing factors for continuum models and approximate productivity indices for wells used in continuum models (Dershowitz et al. 2000). However, DFN models are unable to describe the stochastic system under consideration accurately. They are also limited to relatively small-scale modeling due to computational demands (Dershowitz et al. 2000).

2.2. What are Fracture Corridors?

Fracture corridors are narrow and long tabular zones, consisting of sub-parallel and sub-vertical fractures of variable dimensions with high fracture intensity. They are generally fault-related (Ogata et al., 2014; Tiab et al., 2015). Two requirements to form fracture corridors are the brittle rock and stress field. When enough stress is applied to break the brittle rock, fracture

corridors can occur in the hanging wall and footwall zone of a normal fault, around the fault tip process zone, or along the axial of fault-related folds (Ogata et al., 2014). The permeability of fracture corridors can sometimes exceed ten darcies (Singh et al., 2008; Tiab et al., 2015), while the matrix permeabilities in the reservoir are orders of magnitude lower. The permeability differences between a matrix and fracture corridors make the fracture corridors the primary fluid flow pathway. Thus, fracture corridors play a crucial role in oil production. Understanding the location and orientations of fracture corridors in subsurface reservoirs is critical to improving field production and optimizing drilling locations.

2.2.1. Fracture Corridors Geometries

Fracture corridor type reservoirs are Type II naturally fractured reservoirs. They include narrow and long tabular fracture zones. From outcrop studies, geologists have visually observed fracture corridors many tens of meters to hundreds of meters long (Cacas et al., 2001; Questiaux et al., 2009; Tiab et al., 2015). A few of them may be kilometers long (Questiaux et al., 2009). The fractures in the tabular zones can be shorter than the length of fracture corridors with different dimensions (Cacas et al., 2001; Tiab et al., 2015). There can be thousands of parallel or subparallel fractures in fracture corridors closely packed together (Tiab et al., 2015). The fracture corridor's width can range from centimeter to meter scale (Segall et al., 1983; Odling 1997). The thickness of the bed generally limits the height of the fracture corridor. Fracture corridor spacing is defined as the distance between two adjacent parallel fracture corridors. Ozkaya, S. I. & Minton, K. R. (2007) found that conductive fracture corridor spacing varies from 10.9 m to 394.25 m with an average of 90 m. A schematic illustration of the fracture corridor is shown in Figure 2.6.

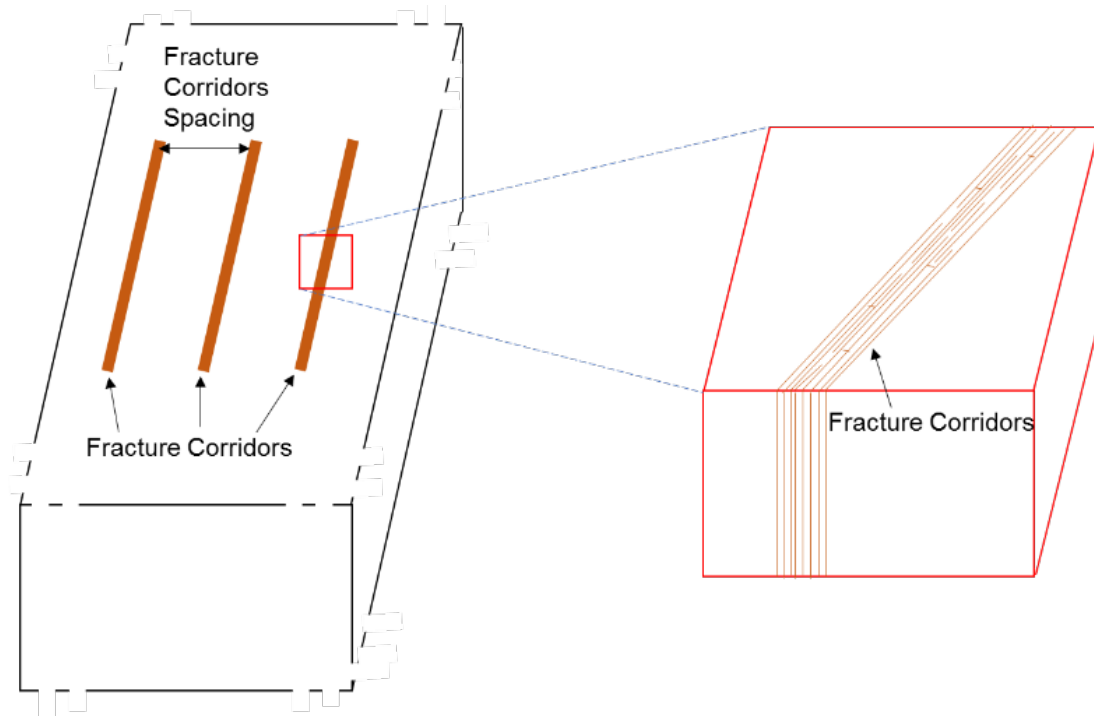


Figure 2.6. A schematic illustration of fracture corridor

2.2.2. Fracture Corridor Locations

Globally, fracture corridors have been found on most continents, with many of these have very high permeability and can help oil production significantly (Figure 2.7). The locations include localities in the Eriboll Formation lies on top of the Torridon Group in Scotland (Watkins et al., 2017), Latemar Platform in northern Italy (Boro et al., 2014), Suez Rift in Egypt (Hollis et al., 2017), Calvisson in France (Chatelée et al., 2017), Utah in the USA (Ogata et al., 2014), Sabriyah Field in North Kuwait (Singh et al., 2008), South Oman Salt basin (Ozkaya et al., 2007), Sichuan in China (Liang et al. 2015).



Figure 2.7. Global fracture corridor localities

2.2.3. Geologic Setting

Fracture corridors are found in carbonate rock, such as chalks (Laubach et al., 1994; Becker et al., 1996; Odling, 1997; Cacas et al., 2001; Barr et al., 2004; Al-Kindi, 2006; Belayneh, 2007; and Souque et al., 2018), limestone (Ogata et al., 2014), and dolomite (Sharp et al., 2014). They also form in sandstones broadly, but they are more relevant in tight sandstones (Questiaux et al., 2009) since permeability is low.

2.2.4. Mechanisms of Corridor Formation

Typically, there are three types of corridors (Ogata et al., 2014), called fault damage zone fracture corridors (FDZ), fault tip process zone fracture corridors (FTP), and lastly, fold crest – related fracture corridor (FRC).

FDZs (Figure 2.8) is the fracture corridors developed on the footwall and hanging wall. They are parallel to the fault. The mechanisms that explain the formation of FDZs are listed below,

- 1) A normal fault is formed when an extension force breaks a lithologic sequence, and gravity force drops the hanging wall downward.
- 2) Joints form on the footwall and hanging wall simultaneously, parallel to the normal fault due to exposure to the same stress field.
- 3) The fractures near the normal fault are sealed by dust and clay generated by movement (cataclastic material), while the fractures further away from the normal fault experience less absolute motion and remain open, forming fracture corridors.

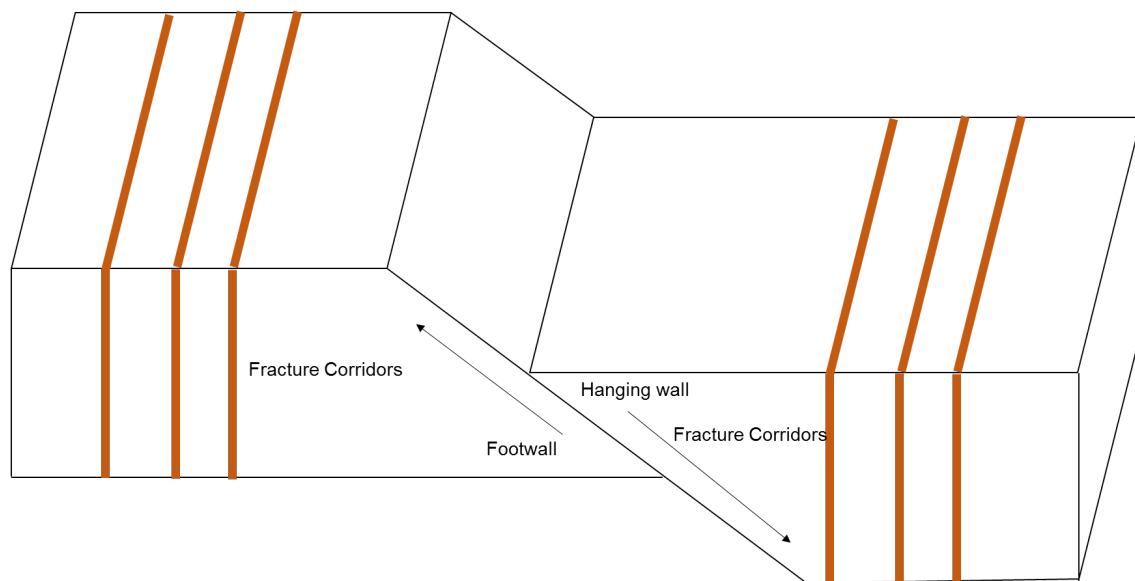


Figure 2.8. A schematic illustration of fault damage zone fracture corridor (FDZ)

FTPs (Figure 2.9) are fracture corridors formed around fault tips. The mechanisms that explain the formation of FTPs are listed below,

- 1) Fault tips form when the fault stops extending due to the lack of energy to overcome the surface energy.
- 2) As the force driving fault growth lessens, remaining fractures express as tip points forming fracture corridors with a “horse-tail” pattern.

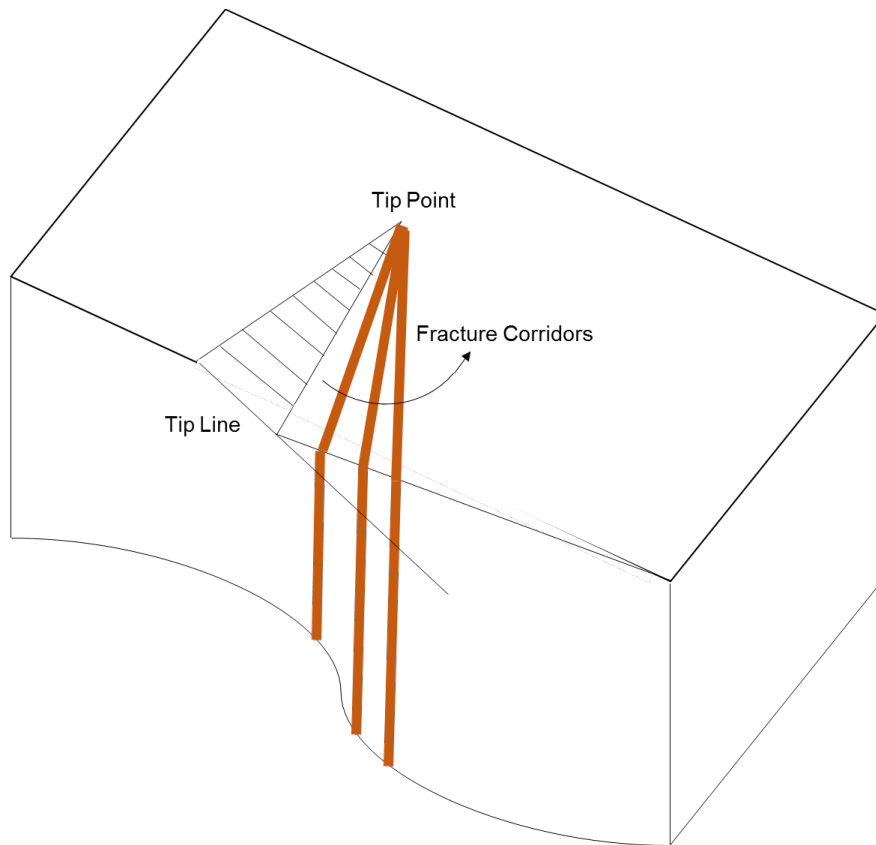


Figure 2.9. A schematic illustration of the fault tip process zone fracture corridor (FTP)

FRCs (Figure 2.10, Figure 2.11, Figure 2.12, and Figure 2.13) are fracture corridors formed on fault-related folds. The development of FRC is very complicated. They can be parallel to the associated fault or perpendicular to the main fault. They also can be orthogonal. The following are the four possible scenarios.

The mechanisms of scenario one are listed below (Figure 2.10),

- 1) Extension force creates a normal fault and fracture corridors, which are parallel to the normal fault.
- 2) The stress parallel to the normal fault creates a fold. Nevertheless, the curvature is not sufficient to form the fracture corridor perpendicular to the normal fault.

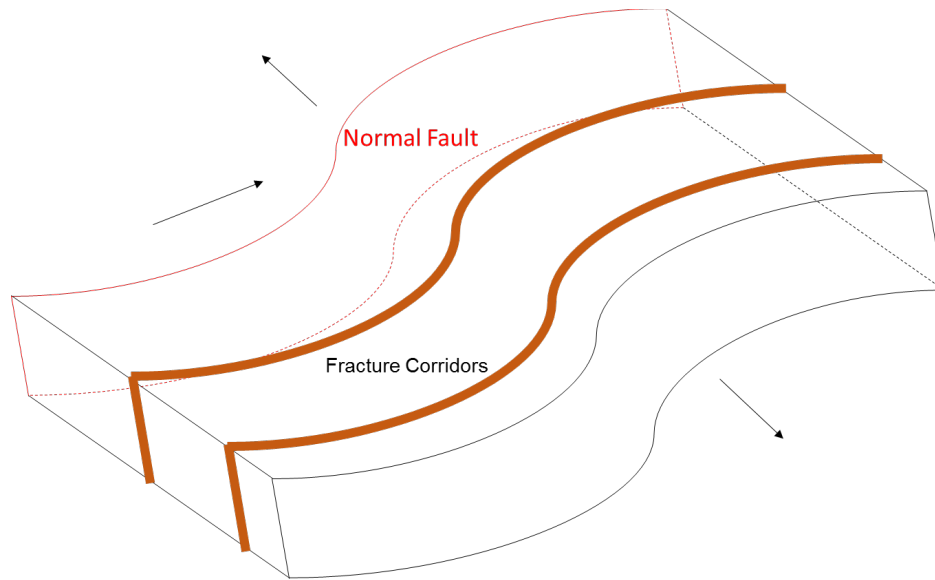


Figure 2.10. Schematic illustration 1 of fold crest – related fracture corridor (FRC)

The mechanisms of scenario two are listed below (Figure 2.11),

- 1) The stress creates the fault-bend fold or fault-propagation fold.
- 2) The rock breaks at the bed's highest curvature positions, forming the fracture corridors parallel to the fault.

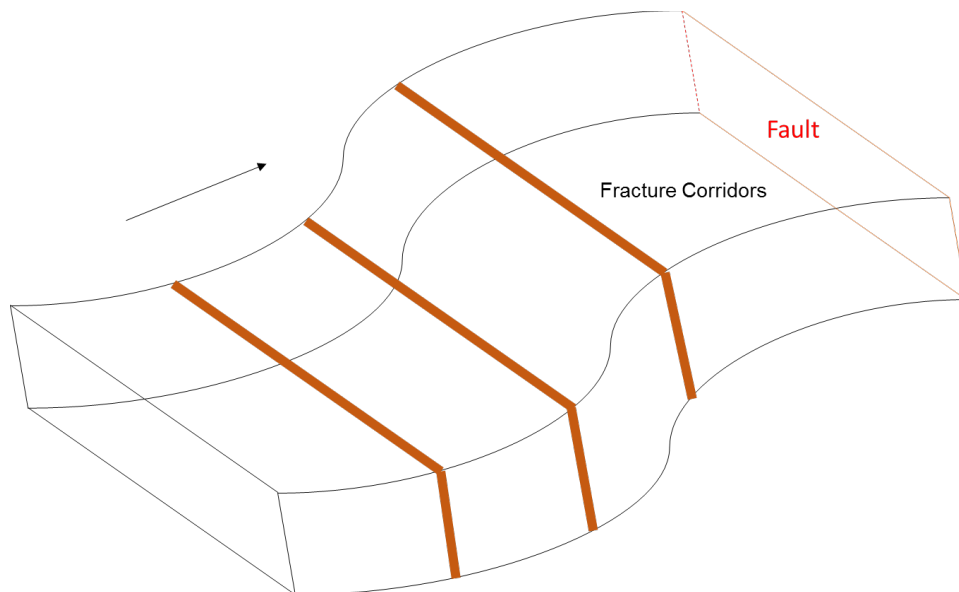


Figure 2.11. Schematic illustration 2 of fold crest – related fracture corridor (FRC)

The mechanisms of scenario three are listed below (Figure 2.12),

- 1) The extension force creates a normal fault and fracture corridors, which are parallel to the normal fault.
- 2) The stress parallel to the normal fault creates the fold.
- 3) The rock breaks at the bed's highest curvature positions, forming the fracture corridors parallel to the fault.

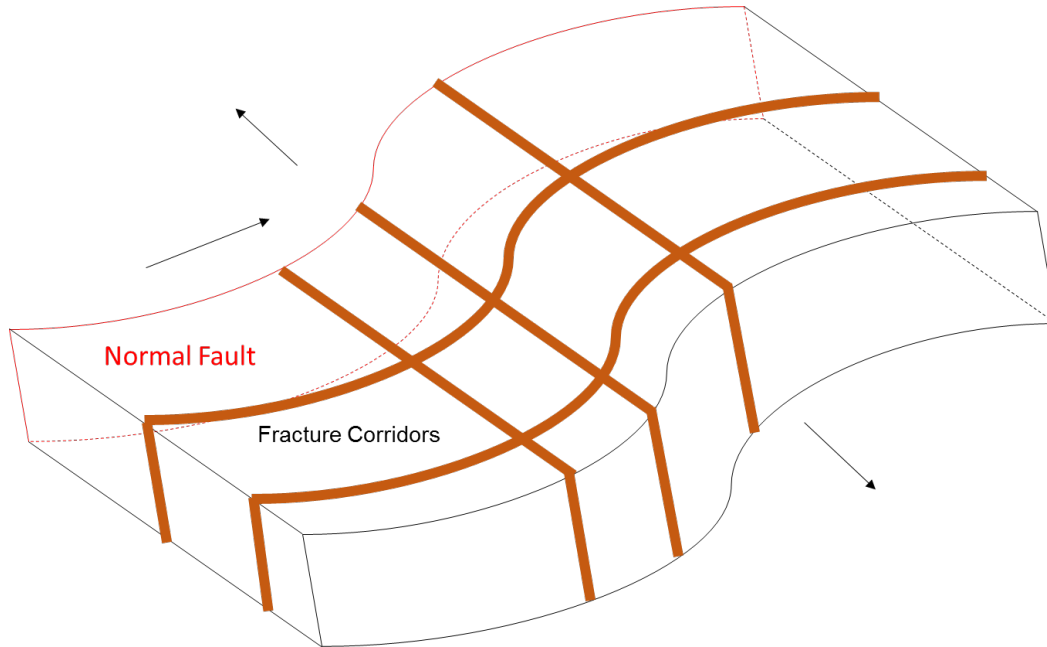


Figure 2.12. Schematic illustration 3 of fold crest – related fracture corridor (FRC)

The mechanisms of scenario four are listed below (Figure 2.13),

- 1) The stress creates the strike-slip fault and a fold, whose axis is perpendicular to the strike-slip fault.
- 2) The rock breaks at the bed's high curvature, forming the fracture corridors perpendicular to the strike-slip fault.

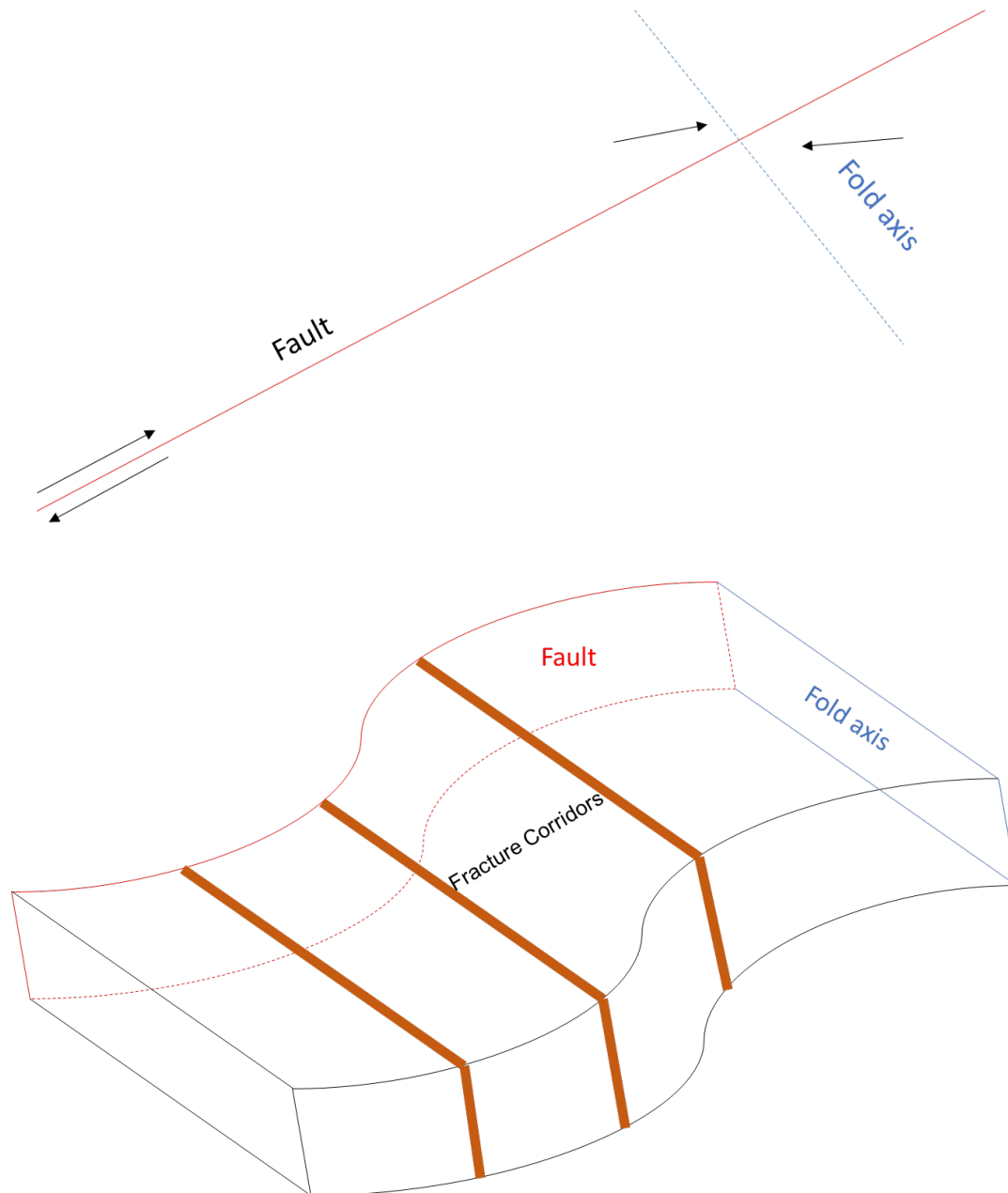


Figure 2.13. Schematic illustration 4 of fold crest – related fracture corridor (FRC)

2.2.5. Reservoir Parameters

Fracture corridor porosity is supposed to be less than matrix porosity. Fracture corridor permeability is much higher than matrix permeability (Ozkaya, 2009). A permeability contrast of

at least 1000 was documented in a Middle East carbonate reservoir by Singh et al. (2008). Fracture compressibility is 10 to 100 higher than matrix compressibility (Tiab et al., 2015).

The type of fracture corridors expressed in the reservoir varies in different fields due to different geologic conditions. The type of fracture corridors can be predicted based on regional tectonic history and field mapping/geophysical data in many cases, even if fracture corridors cannot be observed. The matrix in a tight reservoir with fracture corridors usually has low porosity and low permeability, such as Kuwait's large carbonate reservoir (Singh et al., 2008). For example, matrix porosity is 1% to 2% in tight sandstone, Moine Thrust Belt, NM Scotland (Watkins et al., 2017). The fractured basement reservoir's total matrix porosity in Yemen is 1.15% (Legrand et al., 2010). However, some of the reservoirs, even for the tight reservoirs, can have high porosity. For example, porosity is high 12-28% in Kuwait's tight reservoir (Ozkaya et al., 2005). The matrix porosity in the Clastic Field, Southern Basin-Oman, is as high as 25% to 35 (Ozkaya et al., 2005).

The significant permeability contrast exists in fracture corridor type reservoirs. For example, the matrix permeability is less than 0.001 md, while the fracture permeability is up to 1 md in the fractured basement reservoir in Yemen (Legrand et al., 2010). The matrix permeability is 0 -10 md, while fracture corridor permeability is above one darcy in Kuwait's tight reservoir (Ozkaya et al., 2005). Diffuse fractures can further enhance matrix permeability, and in some cases, diffuse fractures have been documented to increase matrix permeability by 20 md in a tight carbonate reservoir in the Middle East (Ray et al., 2012).

2.2.6. Impacts of Fracture Corridors on Production

In reservoirs containing fracture corridors systems, incredibly tight reservoirs such as chalk reservoirs, and tight sandstone reservoirs, conductive fracture corridors can play an essential role in improving productivity (Nelson, 2001; Agar and Geiger, 2014; Tiab et al., 2015). Identifying

these locations and the geometry of these corridors is critical to optimizing reservoir development and field production.

2.2.7. Importance of Fracture Corridors in Reservoir Modelling

Hybrid Dual Porosity Dual Permeability model (Uba et al., 2007), combined Discrete Fracture and Matrix (DFM) models with single porosity models (Elfeel et al., 2010), and adapting fracture corridors and diffuse fractures in single porosity model (Saputra et al., 2015) have all been historically applied to simulate reservoirs with fracture corridors. There is no official correct way to simulate fracture corridor type reservoirs. In order to get the correct well behavior, it is imperative to select the reservoir model.

2.3. What is Well Testing?

Well testing is a method to test specific reservoir parameters such as flow conductance and skin factor from a diagnostic plot by well behavior when some changes occur during production time. This method is widely used for both conventional reservoirs and naturally fractured reservoirs. Ozkaya, S. I. & Minton, K. R. (2007) found that conductive corridor spacing varies from 10.9 m to 394.25 m with an average of 90 m (which is from 36 ft to 1293.5 ft with an average of 295 ft). Conductive fracture corridor spacing is substantially longer than other types of natural fractures, which ensures enough well testing data would have a high probability of locating the well in the matrix concerning the nearest fracture corridor. Ozkaya, S. I., (2010) proposed well testing as a method to examine the conductivity of fracture corridors, identify wells completed in a matrix, and place exclusive zones. An exclusive zone is a region with no conductive fracture corridors. He briefly described the idea of locating an exclusive circular zone based on well-test data from a matrix well. The radius of the exclusive circular zone equals the radius of the investigation.

2.3.1. Alternate Methods of Detection

Core samples cannot detect fracture corridors because the scale of core samples (several inches) is much less than the fracture corridors (Tiab et al., 2015). The scale of core samples is too small to determine whether fractures are corridors or natural fractures.

The resolution of standard seismic data is too low to identify and map fracture corridors (Questiaux et al., 2009). High-resolution 3-D seismic data can be used to map fracture corridors, but only if fracture corridors are more than 10 to 30 meters or more in width or length (Singh et al., 2008). Frequently 3-D seismic data is uneconomic.

Dynamic data, such as water production, can detect fracture corridors due to the much higher conductivity within fracture corridors. However, this method has two disadvantages. The first is that this method can only be used when many wells have been drilled in the reservoir, which means the reservoir has been well developed. Secondly, the result can yield false identification when impacted by production methods such as injection wells.

A borehole image log within a horizontal well is the best way to detect fracture corridors to date (Tiab et al., 2015). However, the number of borehole image log from the horizontal well is minimal. Additionally, low resolution and contrast within the image can make it challenging to distinguish conductive fractures and non-conductive fractures. Also, consideration is a high cost for borehole image logs within horizontal wells.

2.3.2. Why Apply Well Testing?

The alternate methods, such as 3-D seismic data, dynamic data, borehole image log, can detect fracture corridors in some cases, but all of these methods have limitations. In cases where the reservoir is not well characterized, there is no bottom water under the reservoir, or when fracture

corridors are less than 10 to 30 meters in width or length, these methods will fail, leading to how to detect and characterize fracture corridors. In these cases, well testing provides a viable alternative to characterize the corridors. Also, 3-D seismic data and borehole image log are costly. However, well testing data, especially drawdown well testing data is relatively inexpensive, and always available for all the wells. What is more, well testing has the potential to estimate variety of naturally fractured reservoirs' properties.

2.4. What is Statistics?

Statistics, which is well known as the science of data, is a scientific way to collect, organize, summarize, and analyze information for the purpose of drawing conclusions. Statistics can be divided into three areas: description statistics, exploration statistics, and designed research studies. The three areas of statistics are widely used in any research. Description statistics are used to condense and describe the information within a data set. Exploration statistics are used to conclude a population from samples collected from the population because it is tough to get population information in most cases. Designed research studies can be further broken down into two areas. The two areas are experimental design and sample survey. The difference between experimental design and sample survey is whether the study's individuals are controlled or not. Researchers control the individuals in the experimental design. In contrast, individuals are not controlled in the sample survey. The main aim of designing research studies is to test the difference or estimate values with confidence intervals reliable using statistical techniques at minimum cost.

CHAPTER 3. METHODOLOGY

3.1. Overview of Methodology

The methodology used in this research can be divided into three categories: reservoir modeling, well testing, and statistical techniques. Single porosity with combined local and global models were selected to simulate fracture corridor type reservoirs. Well testing, including removing wellbore storage and drawdown well testing, were applied to detect fracture corridors and estimate matrix permeability, fracture corridor conductivity, well-corridor distance, and fracture corridor length. Statistics technologies, including space-filling designs and multicategory logit models, were used to design the experiment and analyze data.

3.2. Reservoir Modelling

The fracture corridors can be parallel to each other, orthogonal to each other, or form a horse-tail shape depending on the fracture corridor types. In this study, we just consider the parallel fracture corridors.

The conceptual model of parallel fracture corridors is shown in Figure 3.1. The dual porosity model or dual permeability model, which is the standard way to simulate naturally fractured reservoirs, is supposed to model the matrix and diffuse fractures. The diffuse fractures can be regarded as part of the matrix in corridor type naturally fractured reservoirs (Figure 3.4), as the permeability of the diffuse fractures is a little bit higher than the permeability of the matrix. The cross flow (Figure 2.3) from the matrix to diffuse fractures (Figure 3.2) is negligible in corridor type naturally fractured reservoirs compared with that in common naturally fractured reservoirs (Figure 3.3). Tables 3.1, 3.2, and 3.3 give properties of the example CMG models for NFR used for the results in Figure 3.2 and Figure 3.3. As shown in Figure 3.2, for low matrix and fracture

permeability contrast, the plots are the same for single and dual porosity models. So, a single porosity model of diffuse fractures is selected for this study. Grids with high permeability are assigned to the fracture corridors, while grids with low permeability are assigned to the matrix. A fracture well is defined as the well drilled in a fracture corridor. A matrix well is defined as the well drilled in the matrix in this study (Figure 3.4).

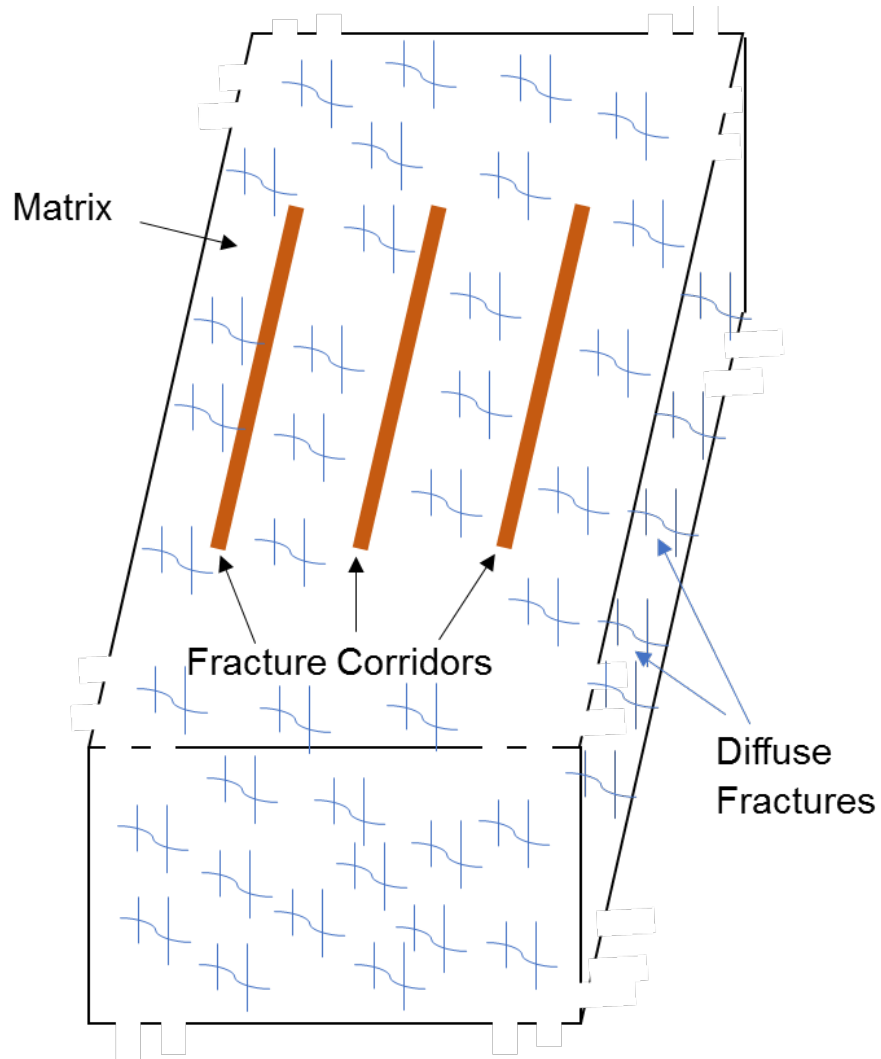


Figure 3.1. Conceptual model of parallel fracture corridors

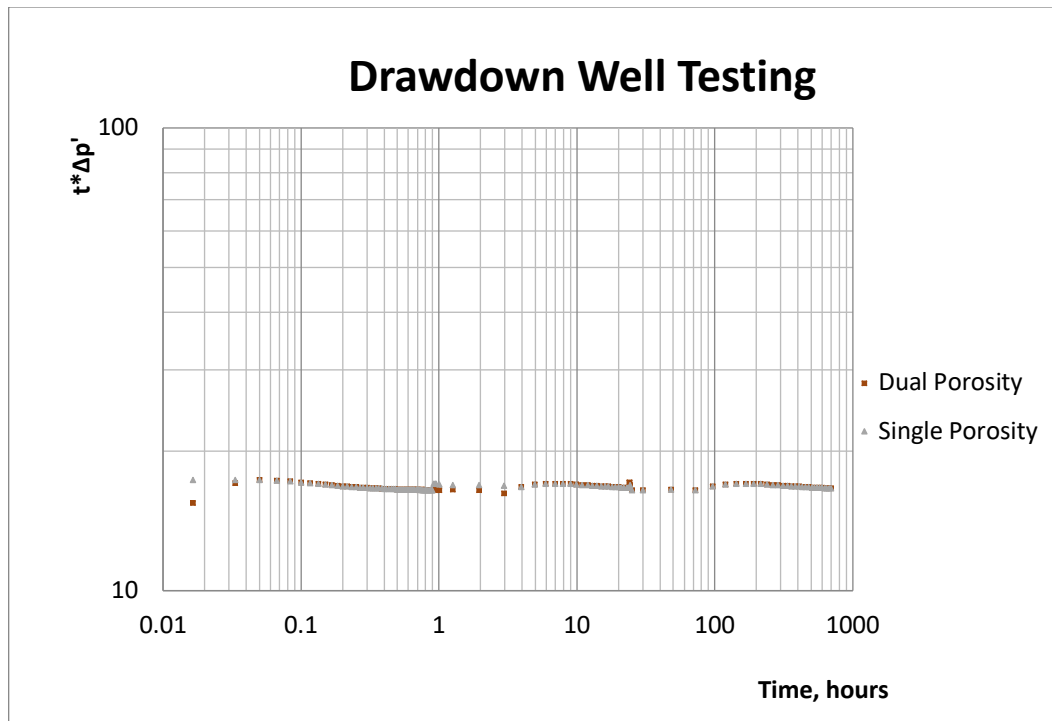


Figure 3.2. An example of a diagnostic plot for a conventional reservoir and NFRs with low matrix and fracture permeability contrast in Table 3.1 and 3.2

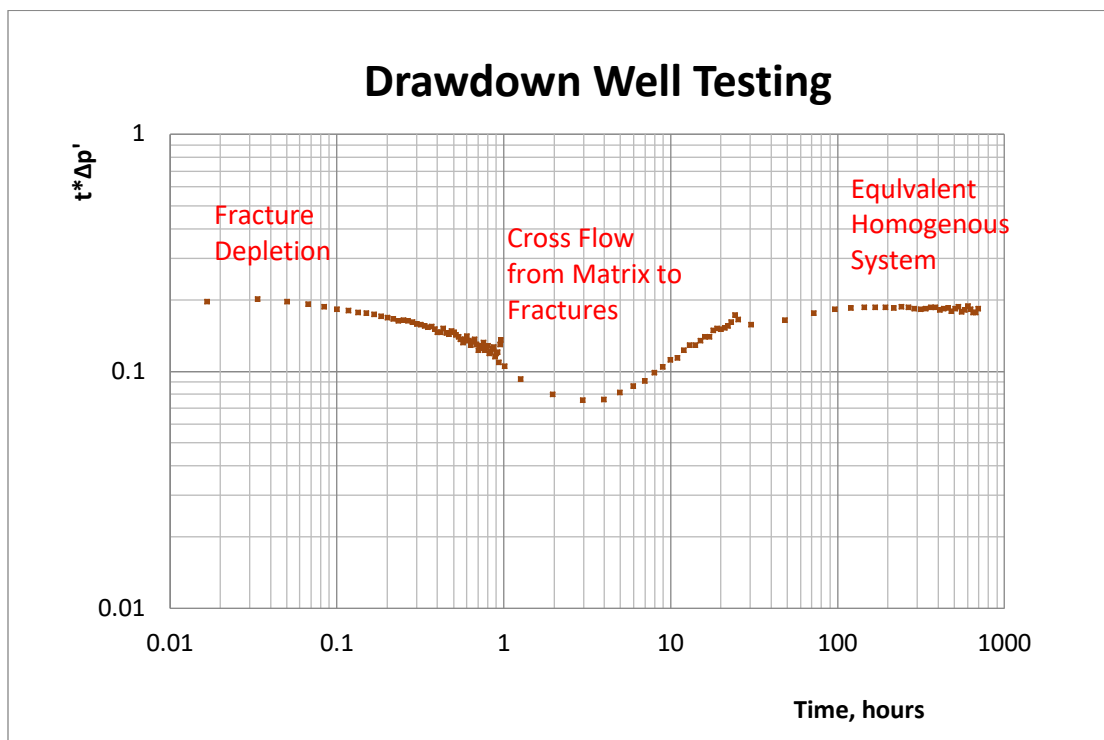


Figure 3.3. An example of a diagnostic plot for NFRs with high matrix and fracture permeability contrast in Table 3.3

Table 3.1. Dual porosity NFR with small contrast of diffuse fracture/matrix properties

Reservoir Temperature	200	F
Reservoir Top	10035	ft
Reservoir thickness	30	ft
Average Reservoir Pressure	4362.66	psi
Matrix Compressibility	4.00E-06	1/psi
Fracture Compressibility	4.00E-05	1/psi
Matrix Porosity	0.1	Fraction
Fracture Porosity	0.001	Fraction
Matrix Permeability	1	md
Fracture Permeability	10	md
Reservoir Wettability	Oil Wet	
Oil Formation Volume factor	1.1	rb/stb
Oil Viscosity	7	cp
Oil Density	56	lb/ft ³
Oil Compressibility	1.50E-06	1/psi
Fracture Spacing	1	ft
Production Rate	10	stb/d

Table 3.2. Single porosity model of NFR

Reservoir Temperature	200	F
Reservoir Top	10035	ft
Reservoir thickness	30	ft
Average Reservoir Pressure	4362.66	psi
Matrix Compressibility	4.00E-06	1/psi
Matrix Porosity	0.1	Fraction
Matrix Permeability	10	md
Reservoir Wettability	Oil Wet	
Oil Formation Volume factor	1.1	rb/stb
Oil Viscosity	7	cp
Oil Density	56	lb/ft ³
Oil Compressibility	1.50E-06	1/psi
Production Rate	10	stb/d

Table 3.3. Dual porosity NFR with high contract of diffuse fracture/matrix properties

Reservoir Temperature	200	F
Reservoir Top	10035	ft
Reservoir thickness	30	ft
Average Reservoir Pressure	4362.66	psi
Matrix Compressibility	4.00E-06	1/psi
Fracture Compressibility	4.00E-05	1/psi
Matrix Porosity	0.1	Fraction
Fracture Porosity	0.001	Fraction
Matrix Permeability	1	md
Fracture Permeability	1000	md
Reservoir Wettability	Oil Wet	
Oil Formation Volume factor	1.1	rb/stb
Oil Viscosity	7	cp
Oil Density	56	lb/ft3
Oil Compressibility	1.50E-06	1/psi
Fracture Spacing	1	ft
Production Rate	10	stb/d

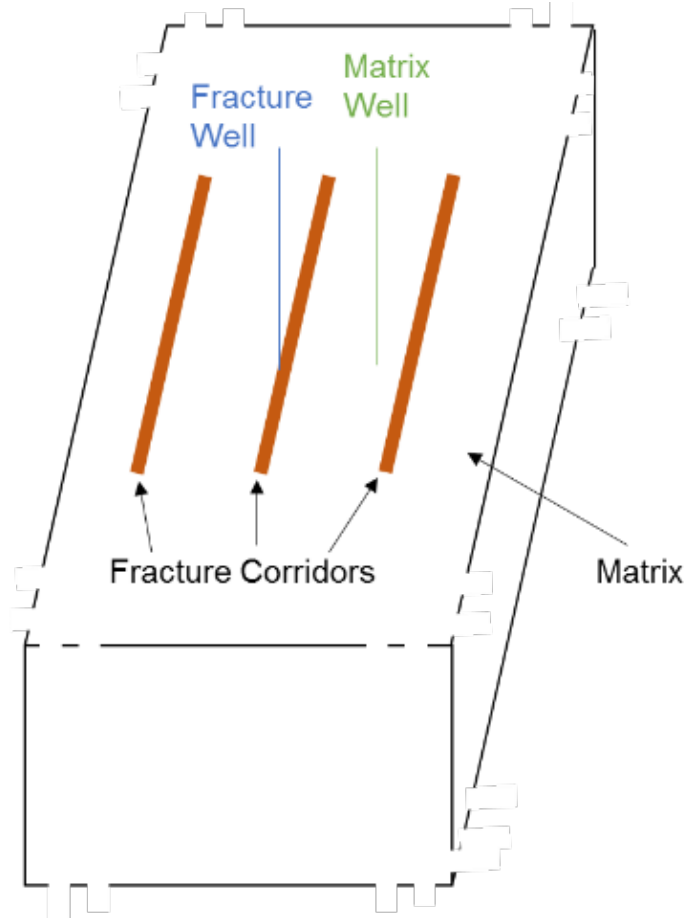


Figure 3.4. Single porosity model for matrix/fracture well

In this study, we model the fracture corridor type reservoirs considering horizontal flow and radial anisotropic permeability. General diffusivity equation for slightly - compressible fluid having constant viscosity and flowing through anisotropic (K_x , K_y) porous medium with no gravity effects (horizontal flow) is the following, for 2D case (radial flow):

$$\frac{\partial}{\partial x} \left(k_x \frac{\partial p}{\partial x} \right) + \frac{\partial}{\partial y} \left(k_y \frac{\partial p}{\partial y} \right) = c\phi\mu \frac{\partial p}{\partial t} \quad (3.1)$$

To convert this anisotropic two-dimensional flow system into an isotropic radial flow, a mathematical transformation of coordinates is made as follows:

The coefficients in the right part of the equation have to be the same to change the Cartesian coordinate to a radial coordinate. To cancel K_x and K_y , let

$$x' = \frac{x}{\sqrt{K_x}} \quad y' = \frac{y}{\sqrt{K_y}} \quad (3.2)$$

Substituting (3.2) to (3.1) gives,

$$\frac{\partial}{\partial x} \left(K_x \frac{\partial p}{\partial x} \right) = \frac{\partial}{\partial x'} \left(K_x \frac{\partial p}{\partial x'} \frac{\partial x'}{\partial x} \right) \frac{\partial x'}{\partial x} = \frac{\partial}{\partial x'} \left(K_x \frac{\partial p}{\partial x'} \frac{1}{\sqrt{K_x}} \right) \frac{1}{\sqrt{K_x}} = \frac{\partial^2 p}{\partial x'^2}$$

and,

$$\frac{\partial}{\partial y} \left(K_y \frac{\partial p}{\partial y} \right) = \frac{\partial^2 p}{\partial y'^2}$$

which gives Eq (3.1) as,

$$\frac{\partial^2 p}{\partial x'^2} + \frac{\partial^2 p}{\partial y'^2} = C_t \mu \phi \frac{\partial p}{\partial t} \quad (3.3)$$

Writing Eq. (3.3) for radial flow defines radial distance as,

Now we can switch to

$$r = \sqrt[4]{K_x K_y} \sqrt{x'^2 + y'^2} \quad (3.4)$$

$$x' = r \cos \theta$$

$$y' = r \sin \theta$$

$$\frac{\partial^2 p}{\partial r^2} + \frac{1}{r} \frac{\partial p}{\partial r} + \frac{1}{r^2} \frac{\partial^2 p}{\partial \theta^2} = \frac{C_t \mu \phi}{\sqrt{K_x K_y}} \frac{\partial p}{\partial t}$$

P did not change with θ , thus, $\frac{1}{r^2} \frac{\partial^2 p}{\partial \theta^2} = 0$

$$\frac{\partial^2 p}{\partial r'^2} + \frac{1}{r'} \frac{\partial p}{\partial r'} = \frac{c \mu \phi}{\sqrt{K_x K_y}} \frac{\partial p}{\partial t} \quad (3.5)$$

The diffusivity equation for slightly compressible fluids of radial coordinates is,

$$\frac{\partial^2 p}{\partial r^2} + \frac{1}{r} \frac{\partial p}{\partial r} = \frac{c_t \mu \phi}{K} \frac{\partial p}{\partial t}$$

Comparing the equation with equation (3.5) defines radial permeability as,

$$K_r = \sqrt{K_x K_y} \quad (3.6)$$

There has been a controversy about the definition of radial permeability.

Notably, Sheng (2010) claims that Earlougher (1977) made a typo in defining $K_r = \sqrt{K_x K_y}$.

In this study, we use the definition in equation (3.6).

In our model, there are j number of fracture corridors having the same length L_f , the same permeability K_f , and fracture corridor width W_{fi} shown in Figure 3.5.

According to the theory, for serial flow in beds, equivalent permeability (K_{fm}) of the system of fracture corridors (K_f) and the matrix beds (K_m) in the x-direction, K_{fm_x} , can be calculated as

$$K_{fm_x} = \frac{W_t}{\frac{\sum_{i=1}^{j+1} W_{mi}}{K_m} + \frac{\sum_{i=1}^j W_{fi}}{K_f}} \quad (3.7)$$

According to the theory, for parallel flow in beds, equivalent permeability (K_{fm}) of the system of fracture corridors (K_f) and the matrix beds (K_m) in the y-direction, K_{fm_y} , can be calculated as

$$K_{fm_y} = \frac{1}{W_t} (\sum_{i=1}^{j+1} W_{mi} K_m + \sum_{i=1}^j W_{fi} K_f) \quad (3.8)$$

Then, for parallel flow in beds, the equivalent permeability in X-direction is,

$$K_x = \frac{1}{L_t} [K_{fm_x} L_f + K_m (L_t - L_f)] \quad (3.9)$$

For serial flow in beds, the equivalent permeability in Y-direction is,

$$K_y = \frac{L_t}{\frac{L_f}{K_{fm_y}} + \frac{L_t - L_f}{K_m}} \quad (3.10)$$

Consequently, radial permeability of the corridor type naturally fractured reservoirs can be calculated by the equation,

$$K_r = \sqrt{K_x K_y} = \sqrt{\frac{1}{L_t} [K_{fm_x} L_f + K_m (L_t - L_f)] \times \frac{L_t}{\frac{L_f}{K_{fm_y}} + \frac{L_t - L_f}{K_m}}} = \sqrt{\frac{K_{fm_x} L_f + K_m (L_t - L_f)}{\frac{L_f}{K_{fm_y}} + \frac{L_t - L_f}{K_m}}} \quad (3.11)$$

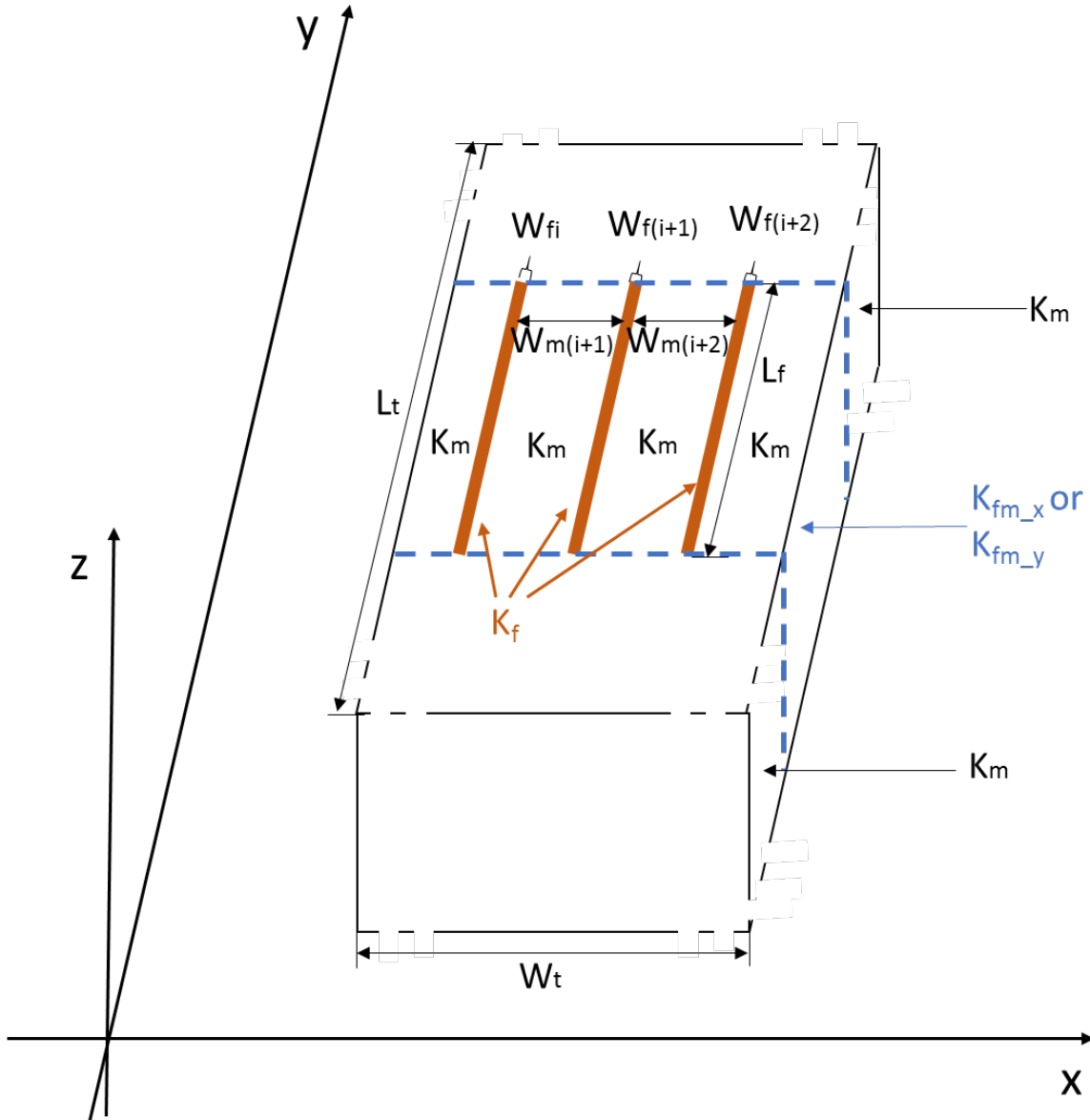


Figure 3.5. Anisotropic flow system of fracture corridor type reservoir with equivalent permeabilities in the X direction (K_{fm_x}) and Y direction (K_{fm_y})

Using the radial permeability concept, flow into a fracture well is further simplified, as shown in Figure 3.6. For a matrix well, the flow system is shown in Figure 3.7.

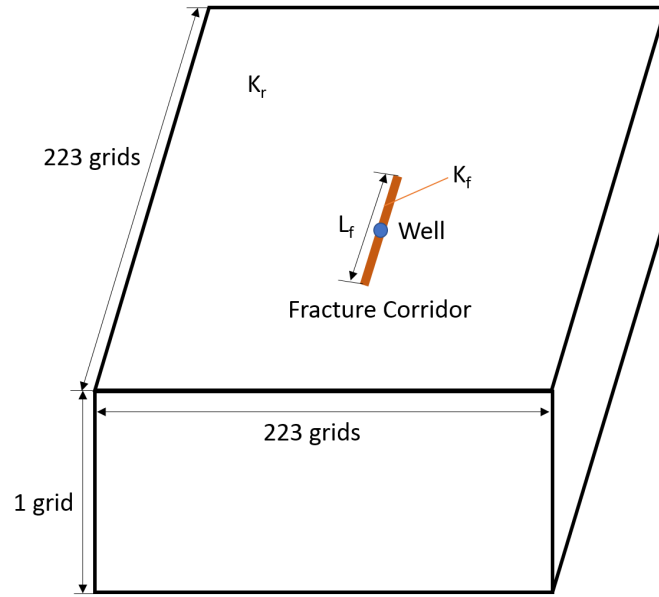


Figure 3.6. Simplified flow system with well in the fracture corridor (fracture well)

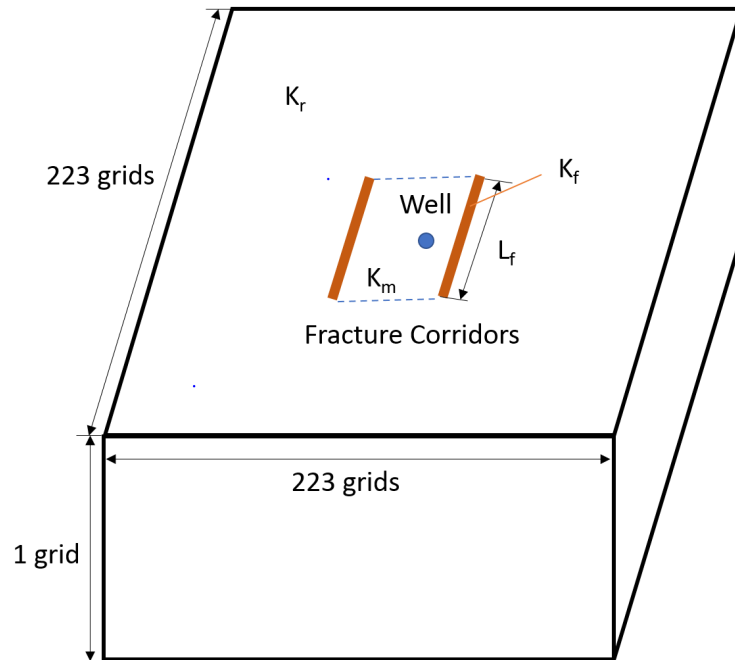


Figure 3.7. Simplified flow system with well between two fracture corridors (matrix well)

The single porosity model software, IMEX, is used in this study to simulate fracture corridor type naturally fractured reservoirs (NFR). The model comprises 49,729 cells with $223 \times 223 \times 1$ grids. The grids are built in the Cartesian coordinates with no corner point geometry. The cartesian grid system is convenient for modeling the NFR with parallel fracture corridors because production well can be easily placed anywhere in the reservoir. Permeability K_f is assigned to all grids representing fracture corridors. While radial permeability K_r is assigned to all matrix grids, as shown in Figures 3.6 and 3.7. For a fracture well, the system in Figure 3.6 radial permeability is included, matrix permeability assumed to be homogeneous and isotropic. This assumption is based upon empirical data from one well test in Oman's carbonate field, which showed a homogeneous matrix (Ozkaya, S. I. 2007). For a matrix well, matrix permeability K_m is assigned to all grids between the two corridors, while the radial permeability, K_r , is assigned to all other grids outside the corridors. Grid sizes in the horizontal directions are equal to each other to ensure radial flow. The volume of the grid comprising vertical well is increased to model wellbore storage. We assume matrix well is completion intercepting only diffusion zone and fracture well fully completed within one fracture corridor. Properties of the well used in this study are shown in Table 3.4. There is no free gas initially or water in the reservoir. In the simulations, dimensions of the grid cells vary from case to case in both X and Y direction depending on the study's purpose because the number of grids is limited to 50,000 due to the CMG license.

Table 3.4. Well properties

Well Radius	0.25	ft
Skin	0	
Block Volume Modifier	500	

3.3. Model Verification

To verify that the fracture and matrix well in the simplified flow systems perform the same as the fracture and matrix well in the naturally fractured reservoirs with fracture corridors for all the flow regimes, models of fracture and matrix well in the reservoirs with 11 fracture corridors are created, as shown in Figures 3.8 and 3.9. Models of fracture and matrix well in the simplified flow systems are created, as shown in Figures 3.10 and 3.11. Table 3.5 gives the properties of the CMG models shown in Figures 3.8, 3.9, 3.10, and 3.11. The radial permeability (K_r) of the corridor type naturally fractured reservoirs shown in Figures 3.10 and 3.11 is calculated. As shown in figure 3.12 and 3.13, the diagnostic plots for fracture and matrix well in the simplified flow systems and the reservoirs with 11 fracture corridors match well.

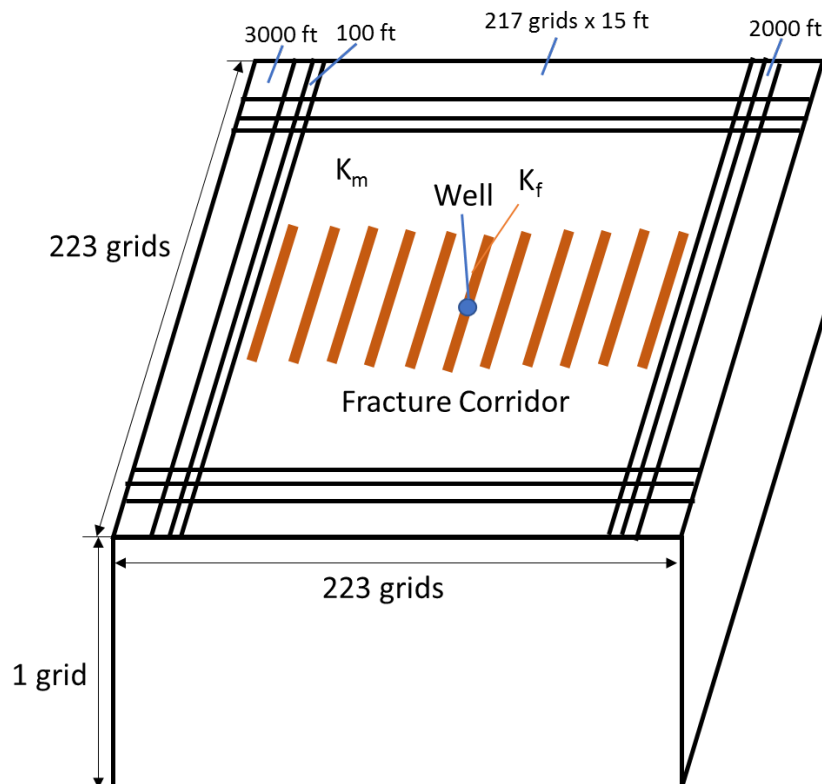


Figure 3.8. Model of fracture well with 11 fracture corridors

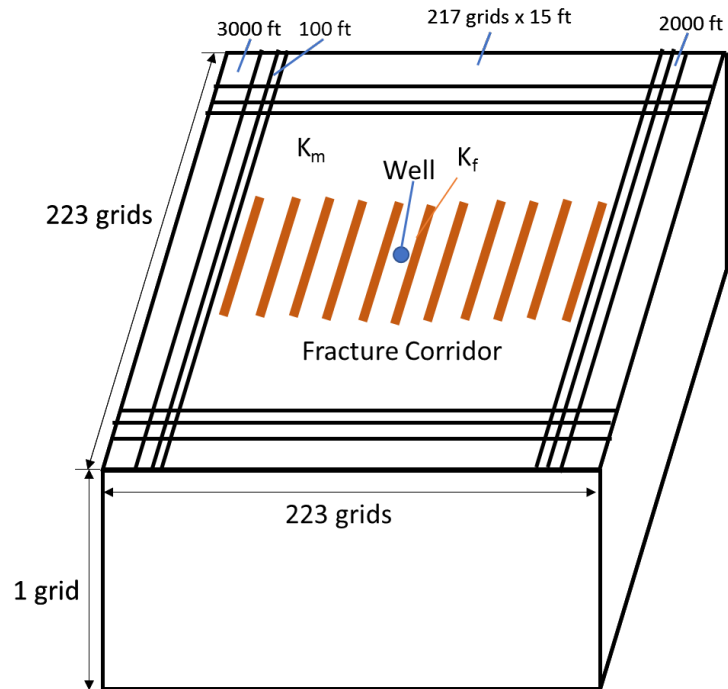


Figure 3.9. Model of matrix well with 11 fracture corridors

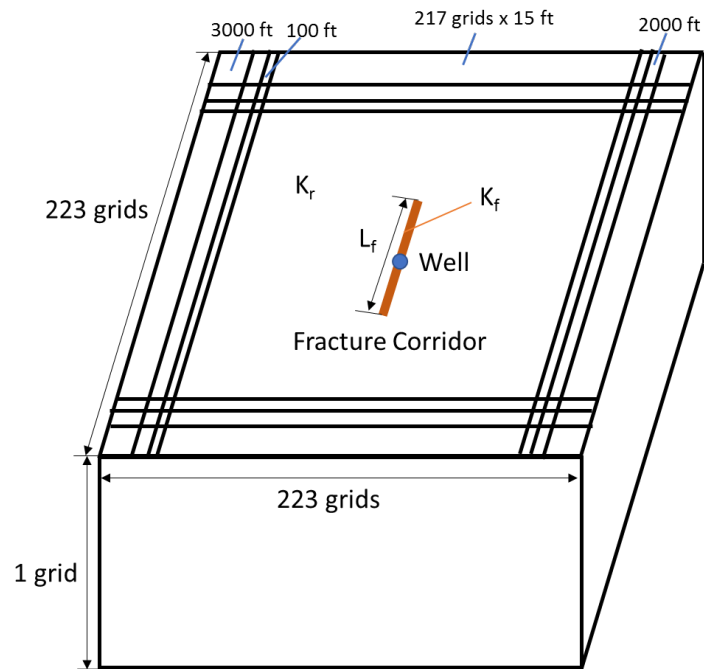


Figure 3.10. Model of fracture well for simplified flow system in the fracture corridor reservoirs

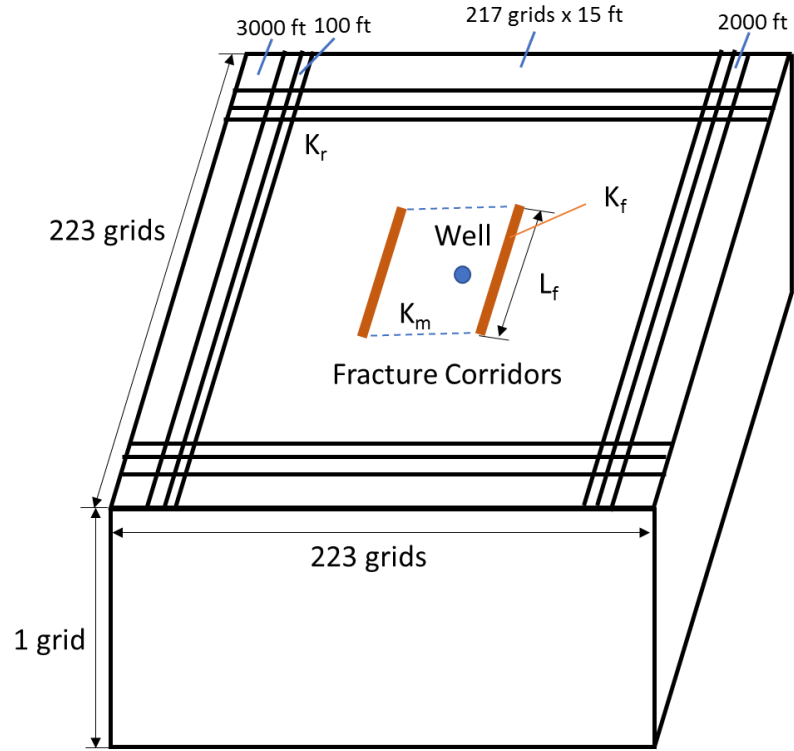


Figure 3.11. Model of matrix well for simplified flow system in the fracture corridor reservoirs

Table 3.5. Reservoir properties used to verify the model

Reservoir Temperature	200	F
Reservoir Top	10035	ft
Grid Size in Vertical Direction	30	ft
Grid Size in Horizontal Direction	15, (100, 2000, 3000)	ft
Initial Average Reservoir Pressure	4362.66	psi
Rock Compressibility	4.00E-06	1/psi
Water Compressibility	0.0000032	1/psi
Oil Compressibility	1.50E-06	1/psi
Matrix Porosity	0.01	Fraction
Fracture Corridor Porosity	0.001	Fraction
Matrix Permeability	10	md
Fracture Corridor Permeability	10000	md
Oil Formation Volume factor	1.1	rb/stb
Oil Viscosity	7	cp
Production Rate	10	stb/d

Well is assigned in the middle of the fracture corridor and the reservoir for fracture well. The fracture corridor spacing is 300 ft for all the fracture corridors shown in Figures 3.8, 3.9, and 3.11. Well is assigned 45 feet away from the nearest fracture corridor.

The three most outside grids are 3000 ft, 2000 ft, and 100 ft, respectively. All the other grids are 15 ft long. So the reservoir width (W_t) and the reservoir length are

$$W_t = L_t = 15 \times 217 + 2 \times 100 + 2 \times 2000 + 2 \times 3000 = 13455 \text{ ft}$$

One hundred grids are used to create the fracture corridors. Thus, the fracture corridor length is

$$L_f = 1500 \text{ ft}$$

The total pure matrix length is

$$L_t - L_f = 11955 \text{ ft}$$

The total pure matrix width is

$$\sum_{1}^{j+1} W_{mi} = 2 \times 100 + 2 \times 2000 + 2 \times 3000 + 206 \times 15 = 13290 \text{ ft}$$

The total fracture corridor width is

$$\sum_{i=1}^{11} W_{fi} = 11 \times 15 = 165 \text{ ft}$$

The equivalent permeability of the system of fracture corridors and the matrix beds in the X-direction is

$$K_{fm_x} = \frac{W_t}{\frac{\sum_{i=1}^{j+1} W_{mi}}{K_m} + \frac{\sum_{i=1}^j W_{fi}}{K_f}} = \frac{13455}{\frac{13290}{10} + \frac{165}{10000}} = 10.124 \text{ md}$$

The equivalent permeability of the system of fracture corridors and the matrix beds in the Y-direction is

$$K_{fm_y} = \frac{1}{W_t} \left(\sum_{i=1}^{j+1} W_{mi} K_m + \sum_{i=1}^j W_{fi} K_f \right) = \frac{1}{13455} [13290 \times 10 + 165 \times 10000] \\ = 132.508 \text{ md}$$

The equivalent permeability in X-direction is,

$$K_x = \frac{1}{L_t} [K_{fm_x} L_f + K_m (L_t - L_f)] = \frac{1}{13455} [10.124 \times 1500 + 10 \times 11955] = 10.0138 \text{ md}$$

The equivalent permeability in X-direction is,

$$K_y = \frac{L_t}{\frac{L_f}{K_{fm_y}} + \frac{L_t - L_f}{K_m}} = \frac{13455}{\frac{1500}{132.508} + \frac{11955}{10}} = 11.149 \text{ md}$$

The radial permeability of the corridor type naturally fractured reservoirs is

$$K_r = \sqrt{K_x K_y} = \sqrt{10.0138 \times 11.149} = 10.566 \text{ md}$$

The radial permeability of the corridor type naturally fractured reservoirs is very close to matrix permeability because the total area of the fracture corridors is much smaller than the reservoir area, and the fracture corridors are far away from each other.

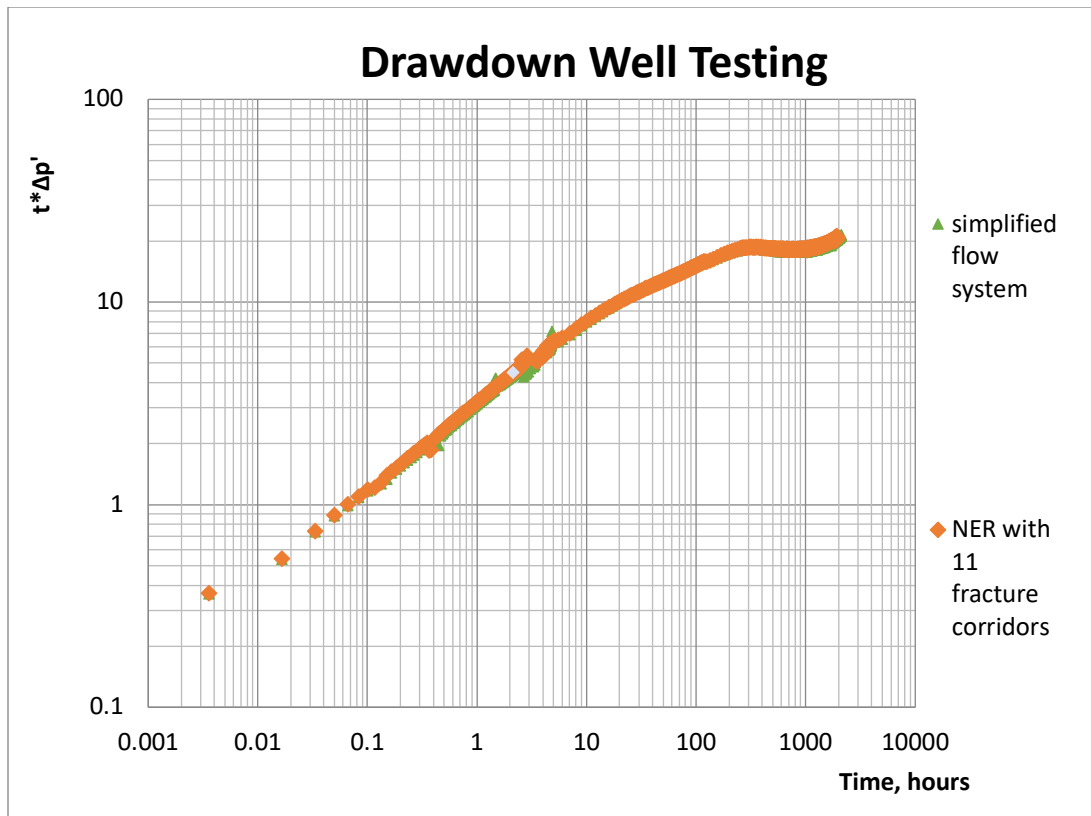


Figure 3.12. Model verification for fracture well

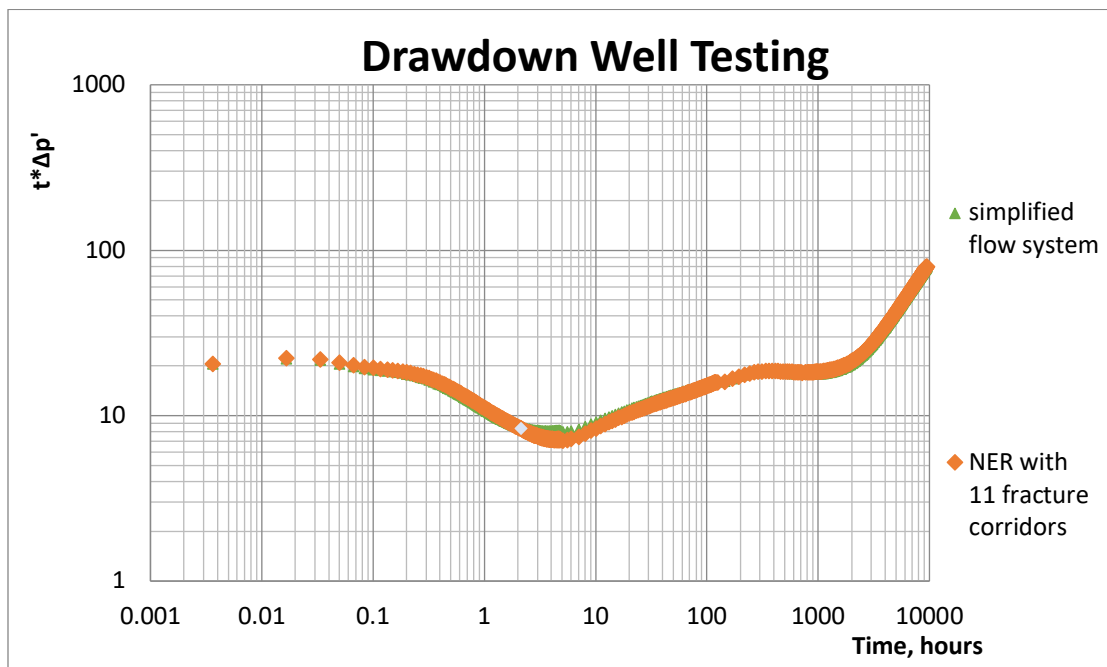


Figure 3.13. Model verification for matrix well

3.4. Well Analysis

Firstly, the β -deconvolution with integral-derivative approach is used to remove the wellbore storage effect from the simulated well testing data. Secondly, the analysis identifies if the well is completed in the fracture corridor or in the matrix (fracture well vs. matrix well) using a Log-log diagnostic plot of the corrected well data. Thirdly, radius of investigation is determined and used to estimate the well-to-corridor distance and minimum spacing of fracture corridors for a matrix well. Fourthly, fracture corridor conductivity and length can be approximated from the recorded bilinear flow stage for a fracture well or a matrix well nearby the fracture corridor.

3.4.1. Wellbore Storage

During well testing, the initially produced fluids come from the wellbore rather than the reservoir. The actual rock-face flow rate is lower than the surface production rate during the initial production due to the wellbore storage effect. Thus, the wellbore storage effect distorts initial well-test data.

To analyze fracture corridors with well testing, wellbore storage should be removed first. Different methods have been developed to remove this initial distortion. Gladfelter et al. (1995), Fetkovich, and Vienot (1984) used rate normalization to remove wellbore storage. Johnston (1992) employed material balance deconvolution to remove wellbore storage. Joseph and Koederitz (1982) and Kuchuck (1987) applied β -deconvolution to remove the wellbore storage effect. Denney, D. (2007) compared rate normalization, material balance deconvolution, and the β -deconvolution methods and concluded that rate normalization is unstable at earlier times. Material balance deconvolution gives the most accurate results, but the β -deconvolution is also reasonably stable.

In the commercial simulator used in this study, wellbore storage is modeled by increasing the volume of the well block (CMG Manual). Then, the slope of the wellbore storage slope plot is needed for using the β -deconvolution method to remove the wellbore storage effect. The equations used in this study was derived by Bahabanian in 2006 as follows:

$$\Delta p_w = p_i - p_{wf} \quad (3.12)$$

$$\Delta p_{wd} = t \frac{d\Delta p_w}{dt} \quad (3.13)$$

$$\Delta p_{wi} = \frac{1}{t} \int_0^t \Delta p_w d\tau \quad (3.14)$$

$$\Delta p_{wid} = t \frac{d\Delta p_{wi}}{dt} \quad (3.15)$$

$$\Delta p_s = \Delta p_w + \frac{1}{\frac{1(\Delta p_w - \Delta p_{wd})}{t} \Delta p_{wid}} \frac{d\Delta p_w}{dt} \quad (3.16)$$

However, the functions $\Delta p_w = f(t)$ and $\Delta p_{wi} = f(t)$ are unknown. Only p_{wf} at different times can be determined by utilizing well testing. Equation (3.13), (3.14), (3.15), and (3.16) cannot be solved simultaneously. The quadratic spline interpolation method was used to estimate equation (3.12). Then, Simpson's rule for numerical integration was applied to estimate equation (3.14) as

$$\begin{aligned} \Delta p_{wi} &= \frac{1}{t} \int_0^t \Delta p_w d\tau = \\ &= \frac{1}{t} \sum_{i=1}^{n-1} \left[\frac{(t_{i-1}^2 + t_{i-1}t_i + t_i^2) \times (t_{i-1}\Delta p_{wi} - t_{i-1}\Delta p_{w(i+1)} - t_i\Delta p_{w(i-1)} + t_i\Delta p_{w(i+1)} + t_{i+1}\Delta p_{w(i-1)} - t_{i+1}\Delta p_{wi})}{3(t_i - t_{i+1})(t_{i-1} - t_{i+1})} - \right. \\ &\quad \left. \frac{(t_{i-1} + t_i) \times (t_{i-1}^2\Delta p_{wi} - t_{i-1}^2\Delta p_{w(i+1)} - t_i^2\Delta p_{w(i-1)} + t_i^2\Delta p_{w(i+1)} + t_{i+1}^2\Delta p_{w(i-1)} - t_{i+1}^2\Delta p_{wi})}{2(t_i - t_{i+1})(t_{i-1} - t_{i+1})} - \right. \\ &\quad \left. \frac{(t_{i-1}^2t_i\Delta p_{w(i+1)} - t_{i-1}^2t_{i+1}\Delta p_{wi} - t_{i-1}t_i^2\Delta p_{w(i+1)} + t_{i-1}t_{i+1}^2\Delta p_{wi} + t_i^2t_{i+1}\Delta p_{w(i-1)} - t_it_{i+1}^2\Delta p_{w(i-1)})}{(t_i - t_{i+1})(t_{i-1} - t_{i+1})} \right] \end{aligned} \quad (3.17)$$

Equation (3.13) $\Delta p_{wd} = t \frac{d\Delta p_w}{dt}$ at each time j can be estimated as

$$\Delta p_{wdj} = \left[t \frac{d\Delta p_w}{dt} \right]_j = \left[\frac{d\Delta p_w}{d\ln t} \right]_j = \frac{\frac{(\Delta p_{wj} - \Delta p_{w(j-1)})}{(\ln t_j - \ln t_{j-1})}(\ln t_{j+1} - \ln t_j) + \frac{(\Delta p_{w(j+1)} - \Delta p_{wj})}{(\ln t_{j+1} - \ln t_j)}(\ln t_j - \ln t_{j-1})}{(\ln t_{j+1} - \ln t_{j-1})} \quad (3.18)$$

Plot Δp_{wd} vs. t to get the log-log diagnose plot before removing wellbore storage.

Equation (3.15) $\Delta p_{wid} = t \frac{d\Delta p_{wi}}{dt}$ at each time j can be estimated by finite difference quotient

as

$$\Delta p_{widj} = \left[t \frac{d\Delta p_{wi}}{dt} \right]_j = \left[\frac{d\Delta p_{wi}}{d\ln t} \right]_j = \frac{\frac{(\Delta p_{wij} - \Delta p_{wi(j-1)})}{(\ln t_j - \ln t_{j-1})}(\ln t_{j+1} - \ln t_j) + \frac{(\Delta p_{wi(j+1)} - \Delta p_{wij})}{(\ln t_{j+1} - \ln t_j)}(\ln t_j - \ln t_{j-1})}{(\ln t_{j+1} - \ln t_{j-1})} \quad (3.19)$$

Equation (3.16) $\Delta p_s = \Delta p_w + \frac{1}{\frac{1(\Delta p_w - \Delta p_{wd})}{t \Delta p_{wid}}} \frac{d\Delta p_w}{dt}$ at each time j can be estimated by finite

difference quotient as

$$\Delta p_{sj} = \left[\Delta p_w + \frac{1}{\frac{1(\Delta p_w - \Delta p_{wd})}{t \Delta p_{wid}}} \frac{d\Delta p_w}{dt} \right]_j = \left[\Delta p_w + \frac{1}{\frac{(\Delta p_w - \Delta p_{wd})}{\Delta p_{wid}}} \left(t \frac{d\Delta p_w}{dt} \right) \right]_j = p_i - p_{wfj} + \frac{1}{\frac{1(p_i - p_{wfj} - \Delta p_{wdj})}{t_j \Delta p_{widj}}} \frac{\frac{(\Delta p_{wj} - \Delta p_{w(j-1)})}{(\ln t_j - \ln t_{j-1})}(\ln t_{j+1} - \ln t_j) + \frac{(\Delta p_{w(j+1)} - \Delta p_{wj})}{(\ln t_{j+1} - \ln t_j)}(\ln t_j - \ln t_{j-1})}{(\ln t_{j+1} - \ln t_{j-1})} \quad (3.20)$$

Then, the derivative of pressure drop, Δp_{sd} , is $\Delta p_{sd} = t \frac{d\Delta p_s}{dt}$ is

$$\Delta p_{sd} = \left[t \frac{d\Delta p_s}{dt} \right]_j = \left[\frac{d\Delta p_s}{d\ln t} \right]_j = \frac{\frac{(\Delta p_{sj} - \Delta p_{s(j-1)})}{(\ln t_j - \ln t_{j-1})}(\ln t_{j+1} - \ln t_j) + \frac{(\Delta p_{s(j+1)} - \Delta p_{sj})}{(\ln t_{j+1} - \ln t_j)}(\ln t_j - \ln t_{j-1})}{(\ln t_{j+1} - \ln t_{j-1})} \quad (3.21)$$

Plotting Δp_{sd} vs. t gives the log-log diagnostic plot after removing wellbore storage. The derivation of the above equation is in Appendix A.

3.4.2. Diagnostic Plot

Following the conventional well test interpretation procedure, a log-log diagnostic plot of the pressure drop derivative vs. time used for flow regime diagnostics shown in Table 3.6, indicating the reservoir type and well location with respect to fracture corridors. Additionally, the diagnostic plot can be used to approximate matrix permeability, fracture corridor conductivity, well-corridor distance, and fracture corridor length.

Table 3.6. Flow regime diagnostics

Flow Regime	Derivative Slope
Wellbore storage	1
Bilinear flow	1/4
Linear flow (fracture)	1/2
Radial flow	0
Boundary-dominated flow	1

3.4.3. Diagnostic Plot Analysis in Fracture Corridor NFR

A. Telling fracture well from matrix well

For a fracture well, after removing the wellbore storage effect, a very short radial flow regime may occur in the beginning until the pressure transient passes the width of the fracture corridor (Figure 3.14). A short linear flow regime may be exhibited by a high conductive fracture corridor (Figure 3.15). After that, a bilinear flow regime may be shown as two linear flows co-occur (Figure 3.16). One flow is the linear flow within the high conductive fracture corridor. The other flow is the linear flow within the low conductive matrix. Next, the system may reach a second radial flow regime (Figure 3.17) before the pressure transient finally travels to the reservoir boundary. Figure 3.18 shows all the possible flow regimes in the log-log diagnostic plot. The slope of the log-log diagnostic plot may change from 0 (radial flow regime) to 1/2 (linear flow regime), then to 1/4

(bilinear flow regime), next to 0 (radial flow regime), until 1 (Boundary-dominated flow regime). Not all the flow regimes can be presented in one single well test. For example, if the fracture corridor's width is too short, the first regime may disappear. The bilinear flow regime may not be established if the fracture corridor is very short.

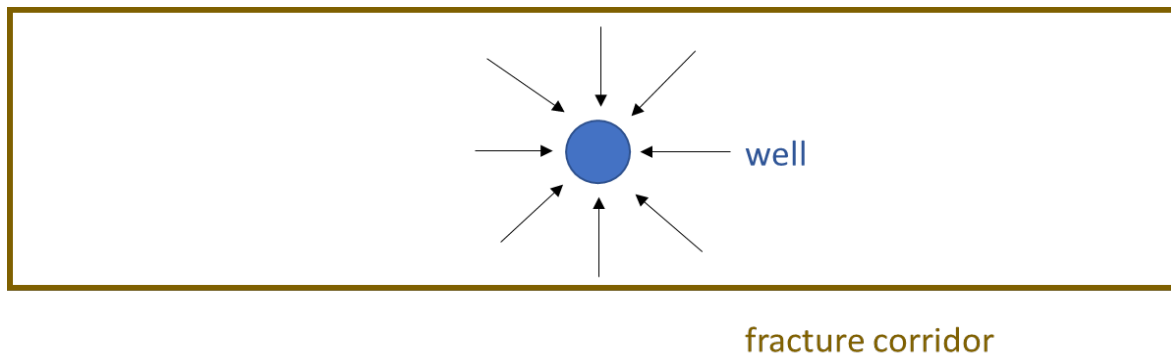


Figure 3.14. First radial flow regime for a fracture well in corridor type NFR



Figure 3.15. Linear flow regime for a fracture well in corridor type NFR

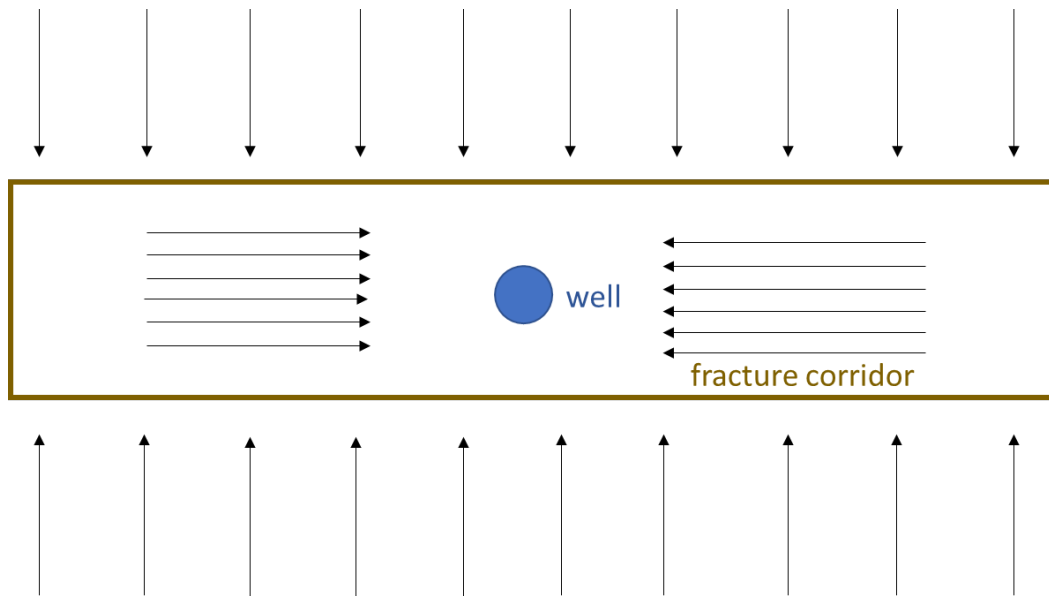


Figure 3.16. Bilinear flow regime for a fracture well in corridor type NFR

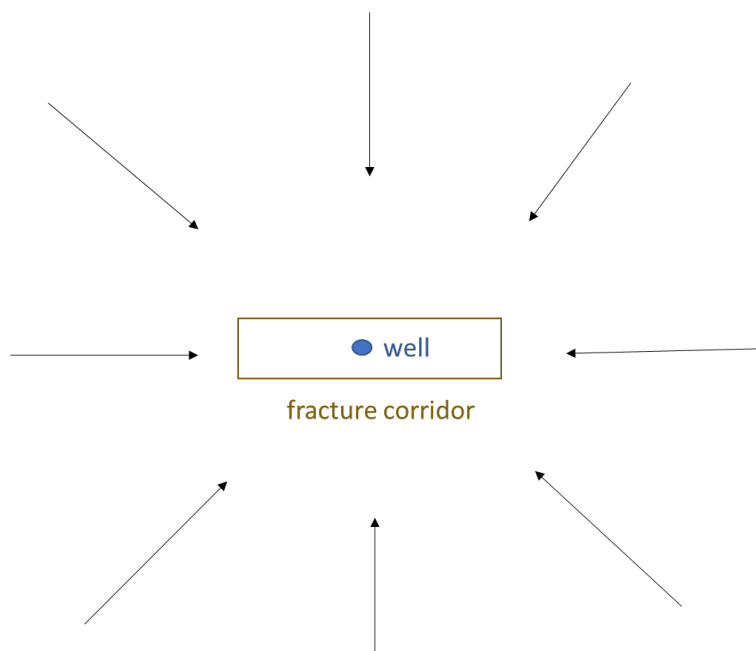


Figure 3.17. Second radial flow regime for a fracture well in corridor type NFR

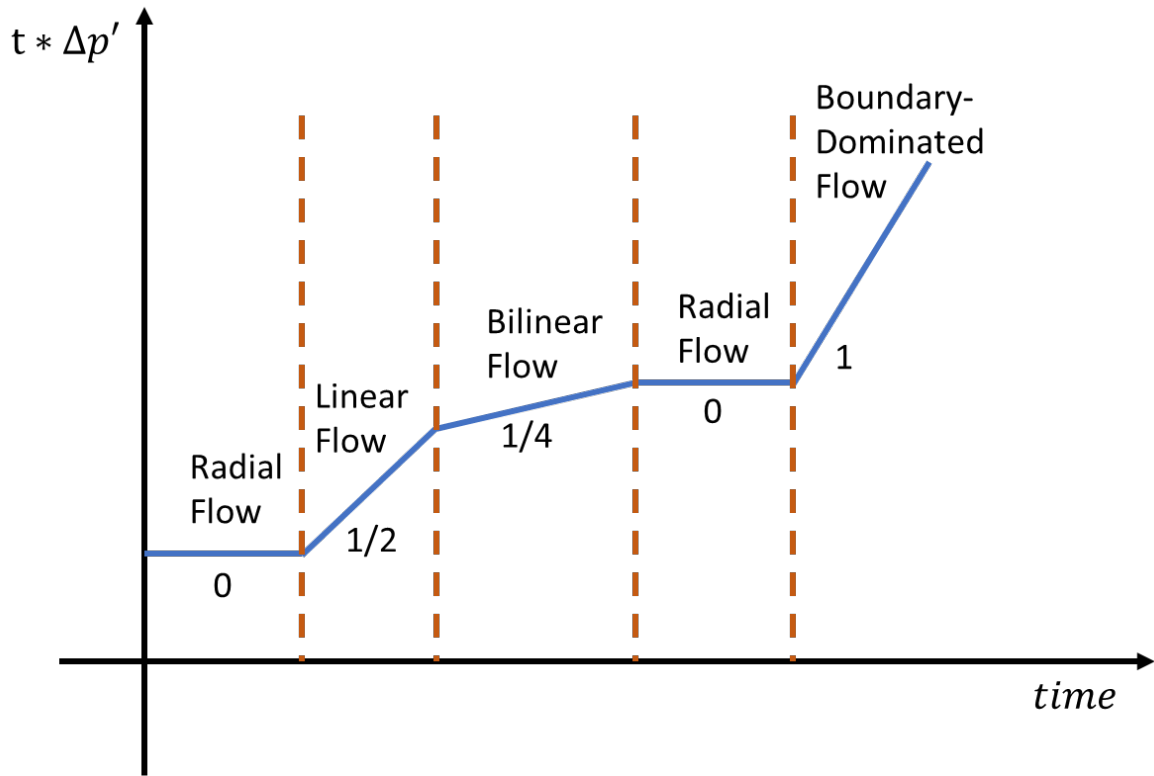


Figure 3.18. Flow regimes for a fracture well in corridor type NFR

For a matrix well, after removing the wellbore storage effect, a radial flow regime may occur at the beginning (Figure 3.19) until the pressure transient travels to the fracture corridor. The pressure drop rate will then decrease as the pressure transient travels in the high conductive fracture corridor. Next, as pressure transient enters the matrix, pressure drops faster, so a trough will show on the log-log diagnostic plot (Figure 3.20). After that, a bilinear flow regime may be shown as two linear flows co-occur (Figure 3.21). One flow is the linear flow within the high conductive fracture corridor. The other flow is the linear flow within the low conductive matrix. Next, the system may reach a second radial flow regime (Figure 3.22) before the pressure transient finally travels to the reservoir boundary. Figure 3.23 shows all the possible flow regimes in the log-log diagnostic plot. The slope of the log-log diagnostic plot may change from 0 (radial flow regime) to 1/4 (bilinear flow regime), then to 0 (radial flow regime), until 1 (Boundary-dominated flow

regime). Not all the flow regimes can be presented in one single well test. For example, if the matrix well is too close to the fracture corridor, the first regime may disappear. The bilinear flow regime may not be established if the fracture corridor is very short or the matrix well is far from its nearest fracture corridor.

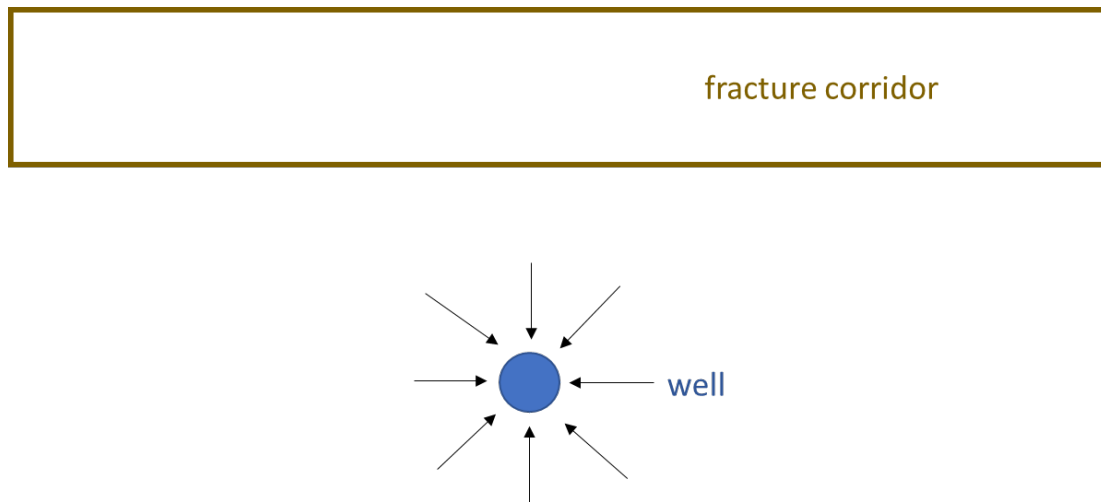


Figure 3.19. First radial flow regime for a matrix well in corridor type NFR

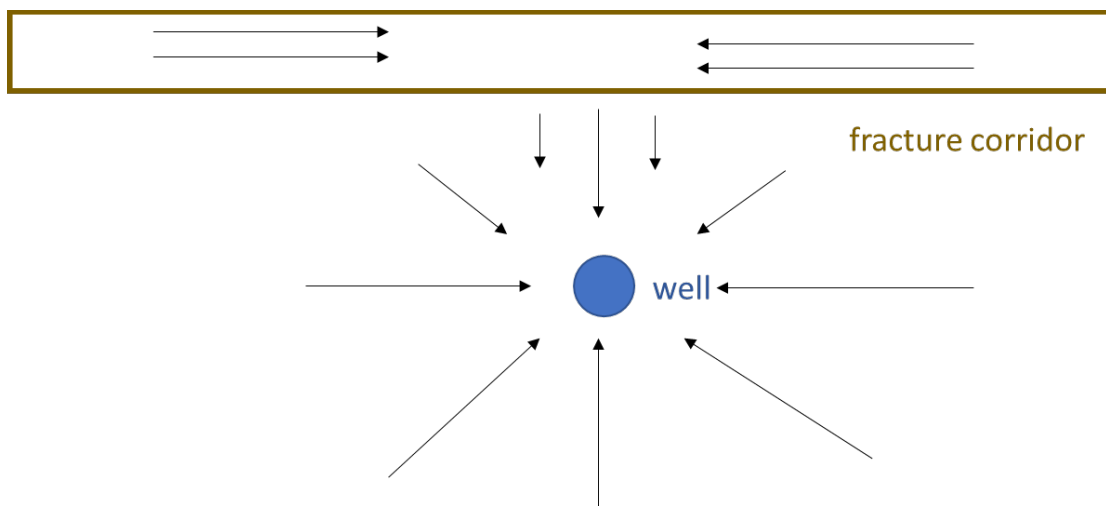


Figure 3.20. Corridor flow regime for a matrix well in corridor type NFR

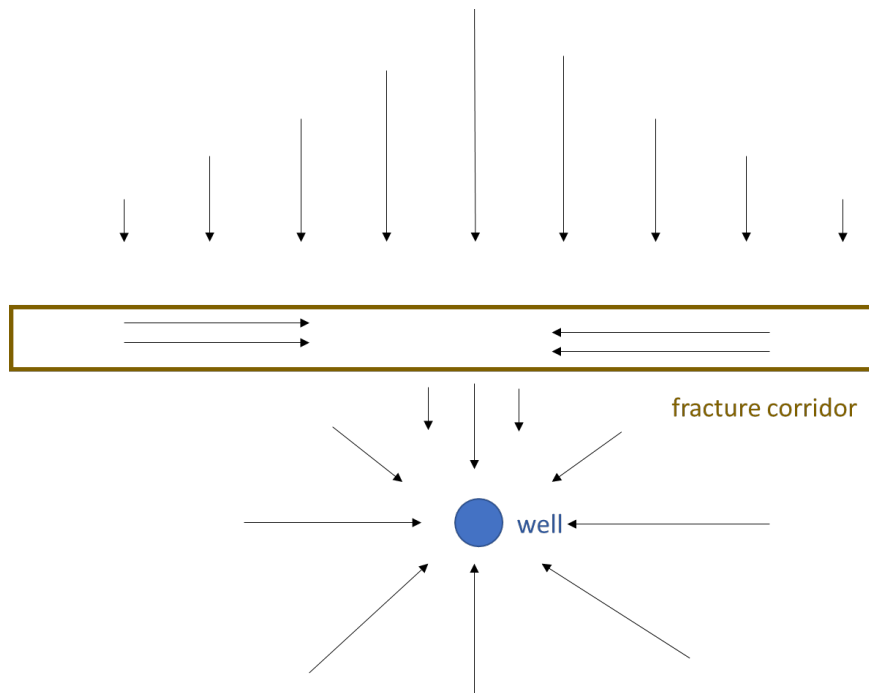


Figure 3.21. Bilinear flow regime for a matrix well in corridor type NFR

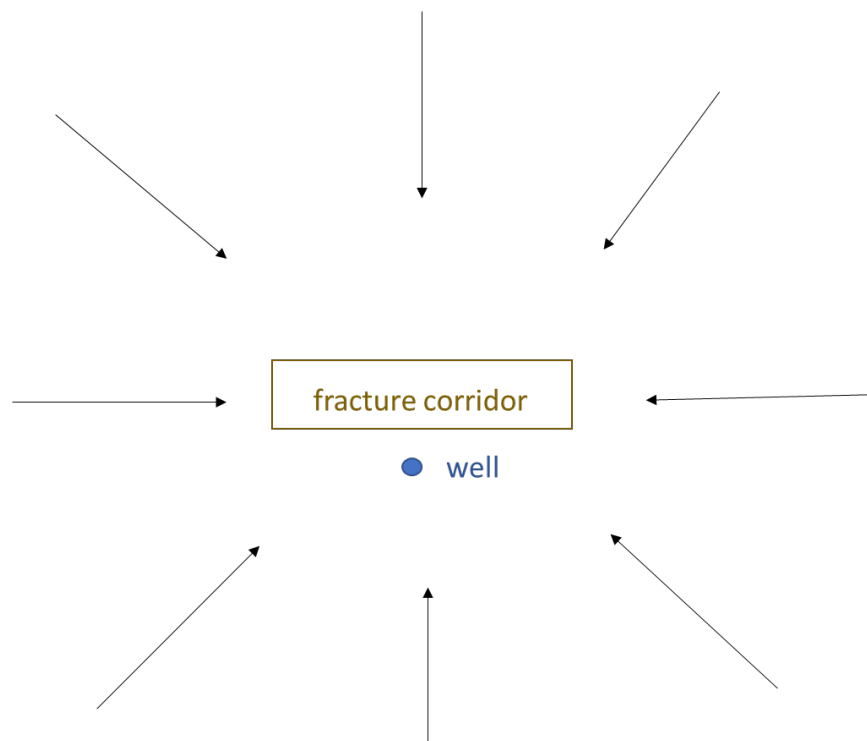


Figure 3.22. Second radial flow regime for a matrix well in corridor type NFR

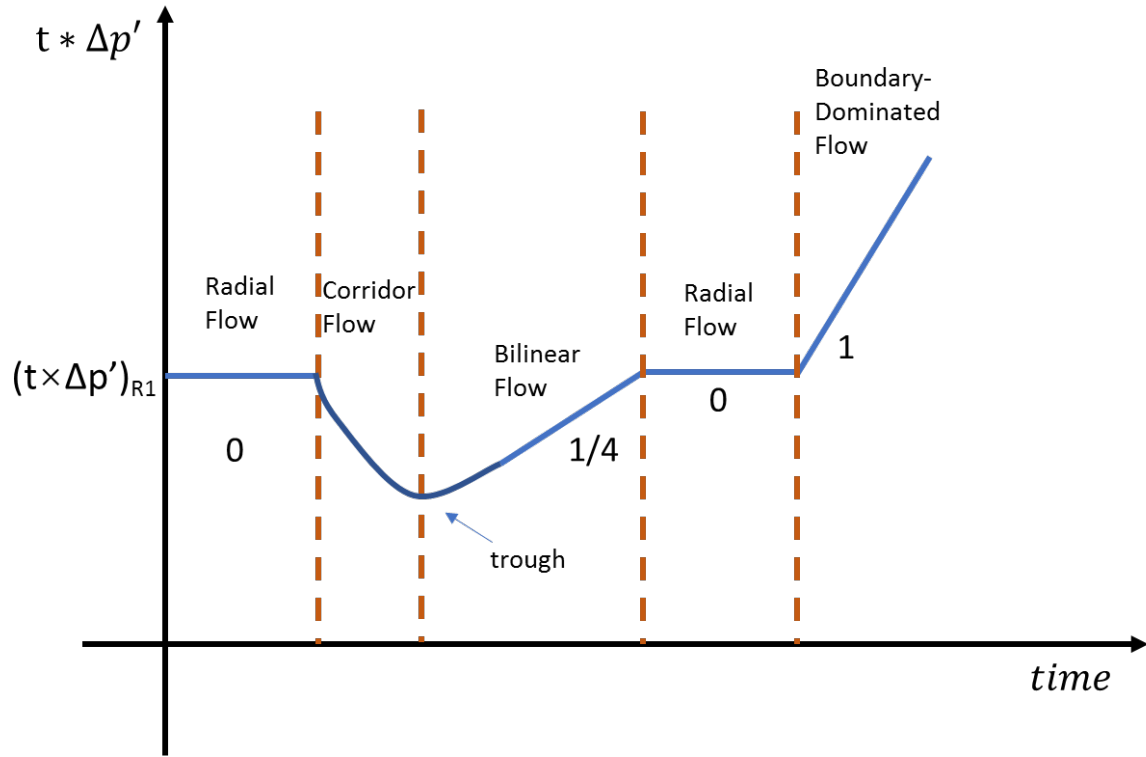


Figure 3.23. Flow regimes for a matrix well in corridor type NFR

Figures 3.18 and 3.23 can be used to tell fracture well from matrix well. Also, a high-pressure depletion is a sign of matrix well due to low matrix permeability.

B. Deciding if the well is in the area with fracture corridors

Compared well test from a common naturally fractured reservoirs (Figure 3.3) and a matrix well in corridor type NFR (Figure 3.23), the shape of the two plots look similar. It is necessary to calculate the radial permeability from the first radial flow regime to distinguish a matrix well in corridor type NFR and a well in NFR. The radial permeability of a homogeneous system can be estimated by the equation:

$$K_r = \frac{70.6q\mu_o B_o}{h(t \times \Delta p')_{R1}} \quad (3.22)$$

Low estimated radial permeability from the first radial flow regime indicates a matrix well in the corridor-type NFR.

C. Finding minimum spacing of fracture corridors

Note that radius of investigation is defined as the distance a pressure transient has moved into a formation following a rate change in a well. The radius of investigation values depends only on the matrix's properties and oil viscosity. Other properties of the NFR will not affect the estimation of the radius of investigation. One benefit of this method is that the production rate does not affect the radius of investigation. For well located between two fracture corridors, radius of investigation is the distance to the nearest fracture corridor and can be estimated as,

$$D = r_i = \sqrt{\frac{K_m t}{948 \phi_m \mu_o (C_t)_m}} \quad (3.23)$$

The minimum possible fracture corridor spacing is twice the radius of investigation and can be estimated as

$$MFCS = 2r_i = \sqrt{\frac{K_m t}{237 \phi_m \mu_o (C_t)_m}} \quad (3.24)$$

D. Estimation of corridor length and conductivity

If a well is completed in the fracture corridor or well is completed close to the fracture corridor, and the bilinear flow regime appears ultimately (Figure 3.24), fracture corridor conductivity and fracture corridor length can be estimated. The fracture corridor conductivity can be estimated with the equation

$$K_f W_f = \left[\frac{44.1 q \mu_o B_o}{m_{BL} h (\phi_m \mu_o (C_t)_m K_m)^{1/4}} \right]^2 \quad (3.25)$$

Then, if $C_{fD} < 1.6$, the fracture corridor length can be estimated by equation

$$L_f = 2L_{hf} = 2 \left(\frac{2.5}{4.55 \sqrt{\frac{K_m}{K_f W_f}} + \sqrt{\frac{\phi_m \mu_o (C_f) m}{0.0002637 K_m t_{ebf}}} \right)^2 \quad (3.26)$$

If a well is drilled in the fracture corridor and boundary-dominated flow can be observed, fracture corridor length can be estimated by the equation

$$L_f = 2L_{hf} = \sqrt{\frac{34.2A}{C_A e^{\frac{(\overline{p}_R - p_{wf})K_m h}{70.6qB_o \mu_o}}}} \quad (3.27)$$

During the boundary-dominated flow regime of a fractured vertical well, pressures and flow rate are related by

$$\frac{(\overline{p}_R - p_{wf})K_m h}{70.6qB_o \mu_o} = \ln \left(\frac{A}{1.871 C_F L_{hf}^2} \right) \quad (3.28)$$

Where,

$$p_R = p_i - \frac{qt}{NC_t} \quad (3.29)$$

$$C_F = C_A/16 \quad (3.30)$$

The above equations are well known in any reservoir and well testing textbooks.

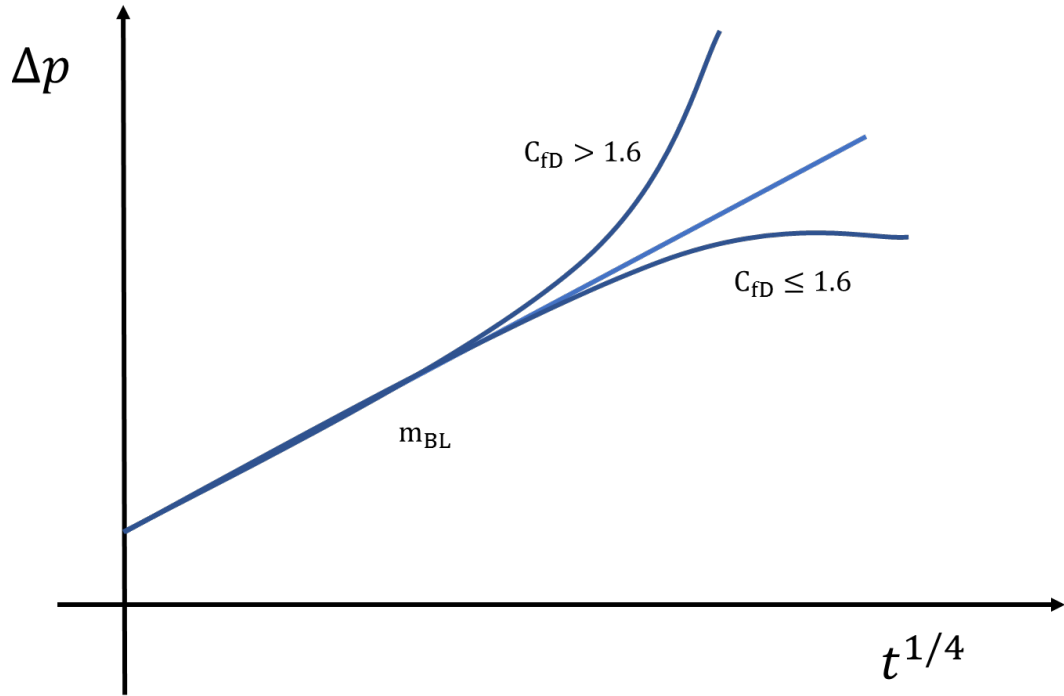


Figure 3.24. Analysis of pressure data of bilinear flow

3.4.4. Assessment of Well Test Analysis

Ozkaya applied statistical methods to study fracture corridor NFR, such as the probabilistic decision tree (2007 and 2008) and reliability (2019). There are three branches of statistics (Geaghan, 2014), including descriptive statistics (graphs and charts), exploration statistics, and designed research studies (experimental design and sample survey). Statistics has become more and more important in recent years. Moreover, increased applications of statistics technology to the petroleum industry will be the trend in the future.

3.4.4.1. Space – Filling Design

Experimental Design is a statistical procedure to evaluate the influence of input design effects and their interaction on the outcome that researchers are interested in to determine the critical information more cheaply and quickly (Schaschke, 2014; Blouin, 2019). The basic idea of experimental design came from a great British statistician, Fisher, for agriculture application.

Fisher and Mackenzie published the first example of experimental design on their crop variation studies in 1923. Fisher's principles are comparison, randomization, statistical replication, blocking, orthogonality, and factorial experiments. The most widely used experimental designs are Completely Randomized Design (CRD), Randomized Block Design (RBD), and Latin Squared Design (LSD).

The uncertainty of a physical experiment comes from random errors and bias. A fundamental reason to do experimental design is to control and estimate random errors by replicating and blocking physical experiments. However, the results obtained using numerical simulations in computer experiments are considered the best estimate. In the numerical simulation, responses are identical for the same sets of inputs in computer experiments, meaning random error can be ignored in these experiments. Controlling bias becomes a critical component of quantifying uncertainty. Typically, the space-filling design is recommended for computer experiments to bound bias (Santner et al., 2018). The software package, JMP, was used to create the tables of experiment design for this study.

A set of computer experiments were conducted by CMG to analyze the effects of matrix permeability, fracture corridor permeability, well-corridor distance, fracture corridor length, and their interactions on the estimation accuracy of matrix permeability and well-corridor distance. The range of matrix permeability is from 1 md to 10 md. The range of fracture corridor permeability is from 1000md to 10000md. The range of well-corridor distance is from 0 ft to 650 ft. The range of the fracture corridor is from 30ft to 3300ft. JMP used sphere packing design to choose design points for matrix permeability, fracture corridor permeability, well-corridor distance, fracture corridor length to maximize the minimum distance between pairs of design points (Table B.1 in Appendix B).

3.4.4.2. Analysis of Polytomous Data – Cumulative Logit Model

The estimation of the NFR parameters may be different from their actual values. Accuracy of the estimation is calculated in this study by relative error ($v_E \neq 0$) as,

$$\delta = \begin{cases} \left| \frac{v_A - v_E}{v_E} \right| \times 100\%, & v_E \text{ can be measured} \\ \text{null}, & v_E \text{ cannot be measured} \end{cases}.$$

Each well test's relative errors are calculated and divided into c categories based on the range.

Cumulative logit models, $\text{logit}[P(Y \leq j)] = \log \left[\frac{P(Y \leq j)}{1 - P(Y \leq j)} \right] = \log \left(\frac{\pi_1 + \dots + \pi_j}{\pi_{j+1} + \dots + \pi_c} \right) = \alpha_j + \beta \mathbf{x}$, ($j = 1, 2, \dots, c - 1$) was used to interpret the effect of an explanatory variable X on the logit of category j to the baseline-category (the last category c). The likelihood ratio test is used to evaluate if the model is a good fit or not. SAS was used to analyze the data. The written code is shown in APPENDIX C.

3.4.4.3. Multicollinearity Test

Multicollinearity exists when the independent variables in the model are perfectly correlated or highly correlated. The consequences of the multicollinearity problem are listed below (Guo, 2020).

1. The estimates of parameter coefficients can have a large variance.
2. A small change in the data can cause a significant change in parameter estimates.
3. The model can give a wrong sign or implausible magnitude of the parameter estimates.
4. The parameter estimates can be unbiased.

Therefore, the multicollinearity problem can result in a wrong interpretation of the parameter coefficients and mislead the results. Usually, pairwise correlations, the Variance Inflation Factor

(VIF), and the condition index are commonly used to detect multicollinearity problems. There is a multicollinearity problem if one or more absolute values of the correlations are more significant than 0.9, one or more VIF values are greater than 10, or the last number of the condition index is greater than 40. To remedy the multicollinearity problem, one can increase the sample size, drop one or more highly correlated independent variables, redefine the independent variables, or fit a ridge regression. The tricky part of the multicollinearity test is that SAS cannot directly give the Variance Inflation Factor (VIF) and the condition index for cumulative logit models. One can fit a multiple linear regression model with the response variable and all independent variables since the multicollinearity is just about the independent variables instead of the model.

3.4.4.4. Variable Selection

Many independent variables will be added to fit a model to estimate the corresponding response variable. However, not every independent variable and their interactions have a significant effect on the corresponding response variable. Thus, variable selection is essential to build a model. There are three most commonly used to select variables. The three standard methods are backward selection, forward selection, and stepwise selection. Backward selection starts with the model with all variables that are interested in it. The most non-significant variable is then removed based on the t-test of the regression coefficient one by one until no non-significant variable exists in the model. The forward selection starts with the most significant variable in the model. Each time, it adds the next most significant variable based on the t-test of the regression coefficient one by one until no remaining variable is significant to the model. The stepwise selection is like the forward selection. The only difference is that the stepwise selection will remove the model's non-significant variable after adding a new variable. Usually, the three variable selection methods work well to select the best model.

CHAPTER 4. RESULTS

This section presents an example application of the technique described in the fracture corridor NFR described in Tables 4.1 and 4.3. The technique is demonstrated and evaluated in the following steps: (a) Identification of well placement; (b) Detection of fracture corridors; (c) Estimation of matrix permeability; (d) Estimation of well-corridor distance; (e) Estimation of fracture corridor conductivity; (f) Estimation of fracture corridor length. Statistical analysis includes determining relative errors for space-filling design, calculated and displayed in Table B.2 in Appendix B. The relative errors were divided into three categories. Category 1 is $\delta \leq 10\%$. Category 2 is $10\% < \delta \leq 20\%$. Category 3 is ‘cannot measure’. The section also presents a statistical assessment of the technique’s accuracy by cumulative logit models.

4.1. Well Placement Identification – Fracture/Matrix Well

The β -deconvolution method was used to remove wellbore storage. Figure 4.1 and Figure 4.2 presented an example of a diagnostic plot for a fracture well before and after removing the wellbore storage in corridor type NFR, respectively. Figure 4.3 and Figure 4.4 presented an example of a diagnostic plot for a matrix well before and after removing the wellbore storage in corridor type NFR, respectively. Results showed that wellbore storage almost did not affect fracture well due to the fracture corridor's high conductivity. In contrast, wellbore storage distorted initial well-test data from the matrix well a lot. Also, wellbore storage can be removed pretty well for the well test data from the matrix well by β -deconvolution.

Figures 4.2 and 4.4 can be used to identify fracture well and matrix well. A trough is observed in the diagnostic plot for a matrix well in the corridor type NFR because pressure transient travels in the matrix before it goes to the fracture corridor. Also, pressure depletion is much lower in a fracture well than that in a matrix well.

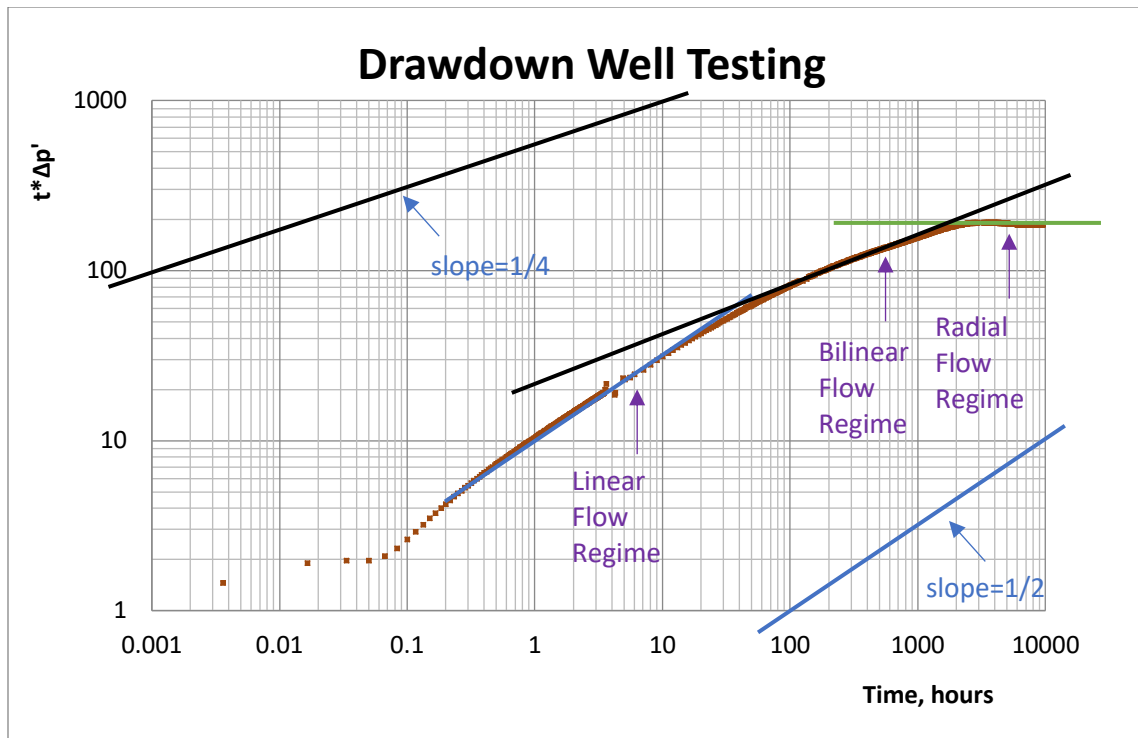


Figure 4.1. An example of a diagnostic plot for fracture well before the removal of the wellbore storage in corridor type NFR (model 1)

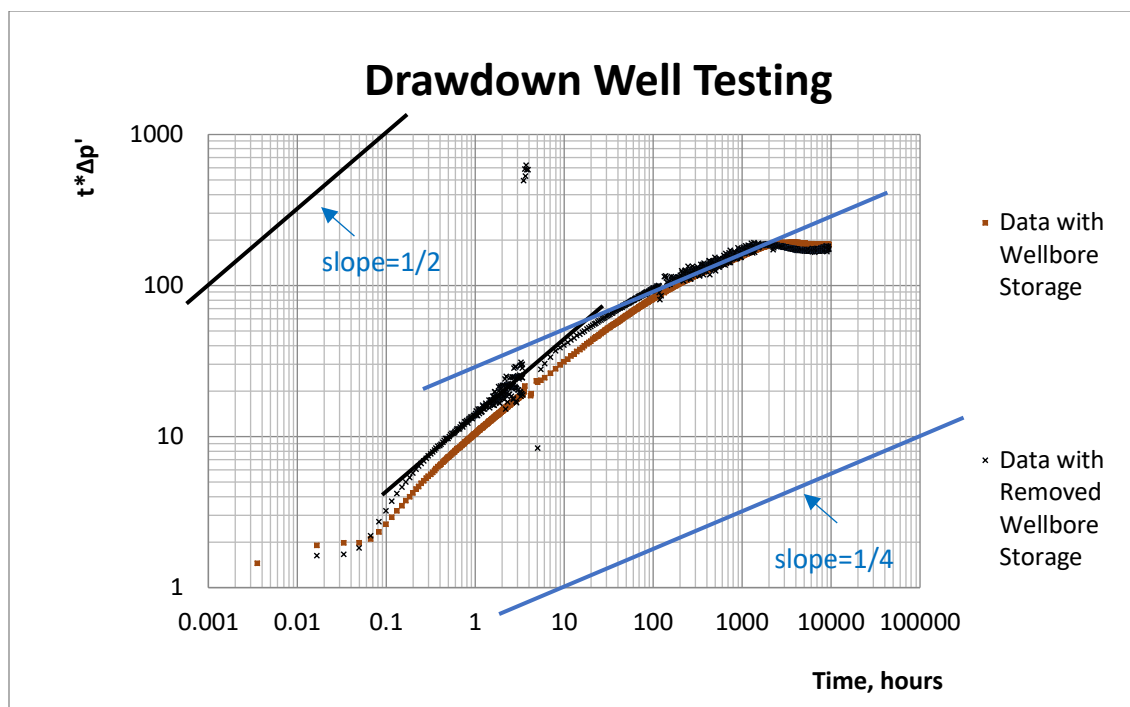


Figure 4.2. An example of a diagnostic plot for fracture well after the removal of the wellbore storage in corridor type NFR (model 1)

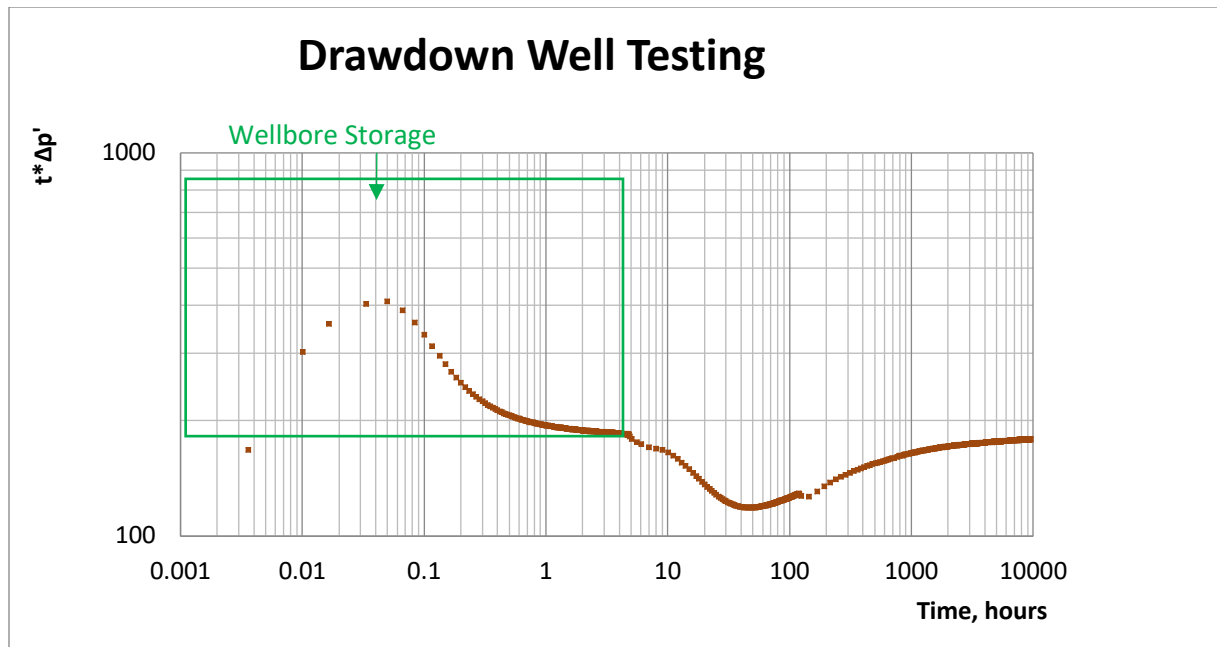


Figure 4.3. An example of a diagnostic plot for matrix well before the removal of the wellbore storage in corridor type NFR (model 1)

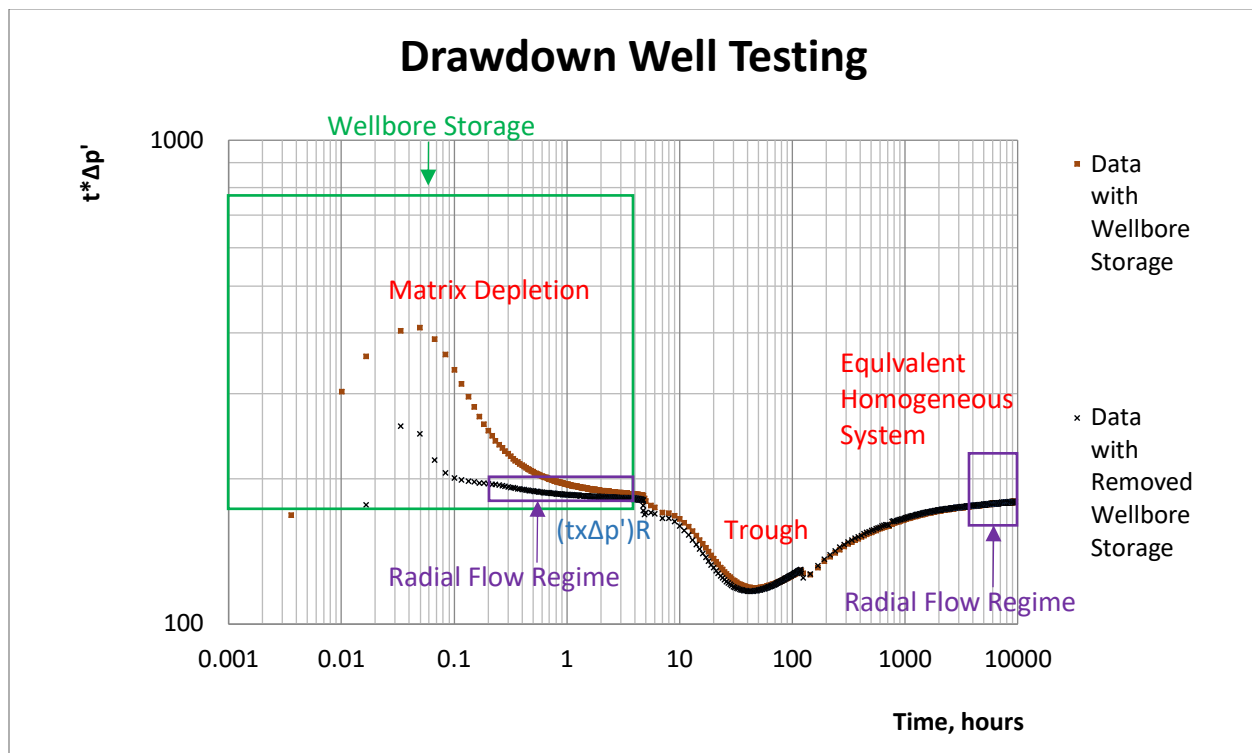


Figure 4.4. An example of a diagnostic plot for matrix well after the removal of the wellbore storage in corridor type NFR (model 1)

4.2. Distinguish Matrix Well in Corridor-Type NFR and Well in Conventional NFR

The shape of the diagnostic plot for matrix well in a corridor type NFR looks similar to that for well in conventional NFR. To distinguish those two diagnostic plots, permeability should be estimated. Figure 4.5 shows an example of a diagnostic plot for matrix well (after removing the wellbore storage) in corridor-type NFR. Figure 4.6 is an example of a diagnostic plot for matrix well in conventional NFR. Properties of the corridor-type NFR and conventional NFR are shown in Tables 4.1 and 4.2, respectively. In order to show all the possible flow regimes in the corridor-type NFR, the sizes of the three outmost grids are increased to 100 ft, 2000 ft, 3000 ft, respectively. Permeability estimated from the radial flow regime and their corresponding relative errors are calculated below.

$$K_{\text{Figure 4.5}} = \frac{70.6q\mu_o B_o}{h(t \times \Delta p')_{R1}} = \frac{70.6 \times 10 \times 7 \times 1.1}{30 \times 185} = 1\text{md} = K_m$$

$$K_{\text{Figure 4.6}} = \frac{70.6q\mu_o B_o}{h(t \times \Delta p')_{R1}} = \frac{70.6 \times 10 \times 7 \times 1.1}{30 \times 0.18} = 1007\text{md} \cong K_{\text{NFR}} = 1000\text{ md}$$

$$\delta_{\text{Figure 4.5}} = \left| \frac{v_A - v_E}{v_E} \right| \times 100\% = 0$$

$$\delta_{\text{Figure 4.6}} = \left| \frac{v_A - v_E}{v_E} \right| \times 100\% = \left| \frac{1000 - 1007}{1007} \right| \times 100\% = 0.7\%$$

The matrix permeability estimation from Figure 4.5 is 1 md - the same as its value in Table 4.1 for corridor type NFR. The permeability approximated in Figure 4.6 is 1000 md, which is slightly higher than the fracture permeability in Table 4.2. The permeability difference calculated from the very early radial flow regime can distinguish matrix well in corridor type NFR and well in NFR. In conventional NFR (no fracture corridors), the permeability value is high due to the occurrence

of finely distributed fractures. In corridor-type NFR, the value is small as it represents only the low permeability matrix.

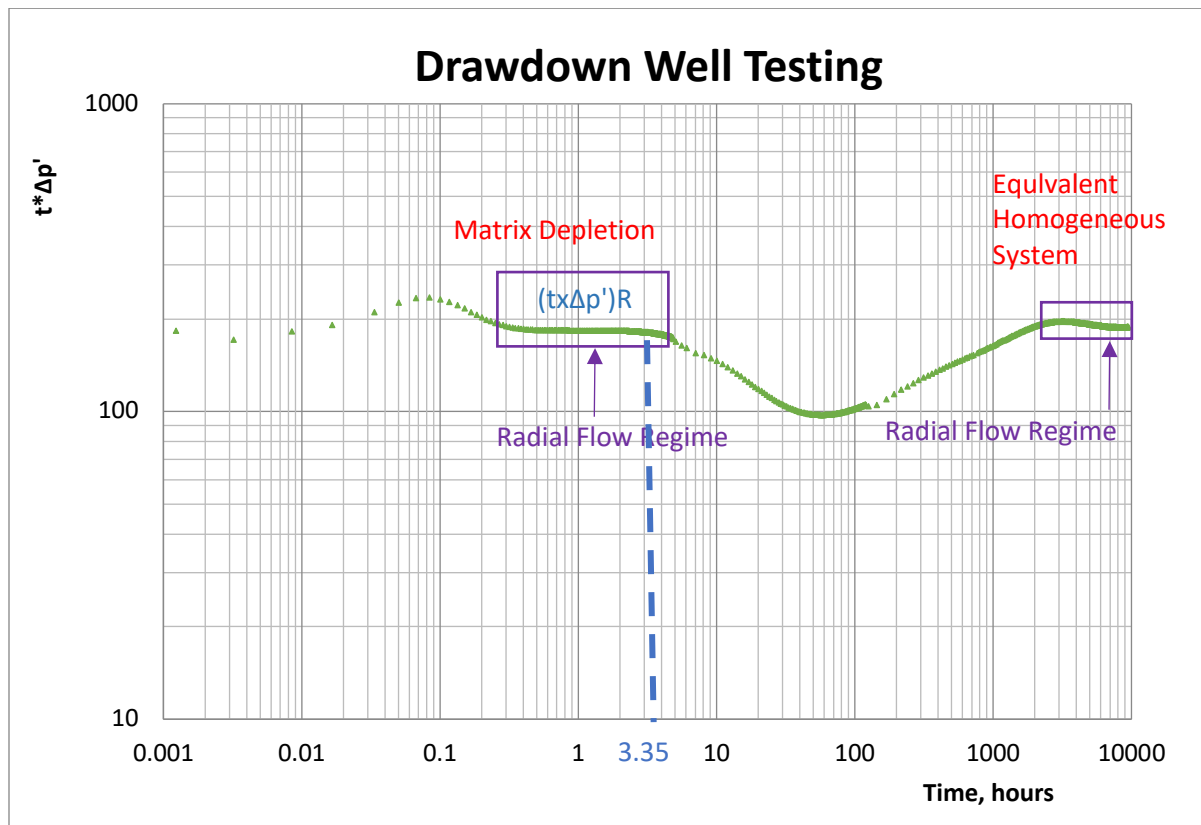


Figure 4.5. Diagnostic plot for matrix well in corridor type NFR (model 1)

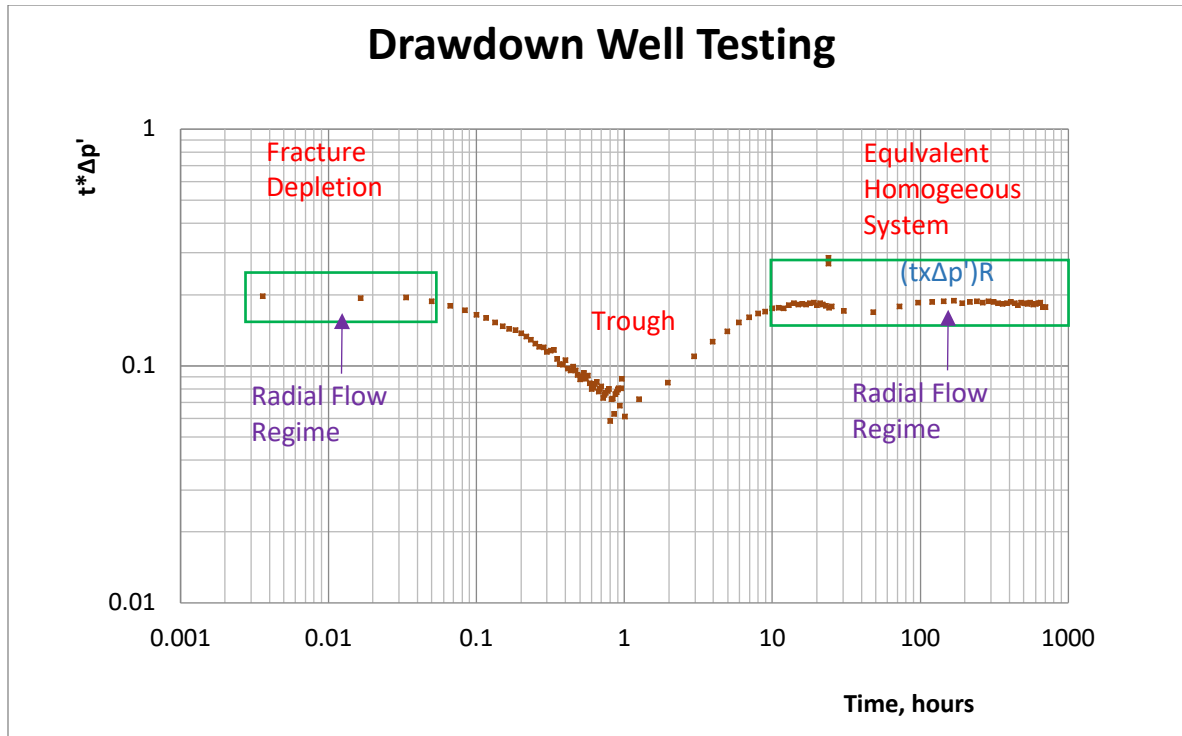


Figure 4.6. Diagnostic plot in conventional NFR

Table 4.1. Properties of corridor type NFR (model 1)

Reservoir Temperature	200	F
Reservoir Top	10035	ft
Grid Size in Vertical Direction	30	ft
Grid Size in Horizontal Direction	15, (100, 2000, 3000)	ft
Initial Average Reservoir Pressure	4362.66	psi
Rock Compressibility	4.00E-06	1/psi
Water Compressibility	3.2E-06	1/psi
Oil Compressibility	1.50E-06	1/psi
Matrix Porosity	0.01	Fraction
Fracture Corridor Porosity	0.001	Fraction
Matrix Permeability	1	md
Radial Permeability	1.06	md
Fracture Corridor Permeability	10000	md
Oil Formation Volume factor	1.1	rb/stb
Oil Viscosity	7	cp
Production Rate	10	stb/d

Table 4.2. Properties of conventional NFR

Reservoir Temperature	200	F
Reservoir Top	10035	ft
Reservoir thickness	30	ft
Reservoir Radius	50000	ft
Average Reservoir Pressure	4362.66	psi
Matrix Compressibility	4.00E-06	1/psi
Fracture Compressibility	4.00E-05	1/psi
Matrix Porosity	0.1	Fraction
Fracture Porosity	0.001	Fraction
Matrix Permeability	1	md
Fracture Permeability	1000	md
Reservoir Wettability	Oil Wet	
Oil Formation Volume factor	1.1	rb/stb
Oil Viscosity	7	cp
Oil Density	56	lb/ft ³
Oil Compressibility	1.50E-06	1/psi
Fracture Spacing	30	ft
Production Rate	10	stb/d

4.3. Estimation of Well-Corridor Distance

For fracture well (Figure 4.1), Well-corridor distance is 0 ft ($D = 0$ ft). For matrix well, the well-corridor distance (Figure 4.5) is estimated by the radius of investigation at $t=3.35$ hours as,

$$D = r_i = \sqrt{\frac{K_m t}{948 \phi_m \mu_o (C_t)_m}} = \sqrt{\frac{1 \times 3.35}{948 \times 0.01 \times 7 \times 5.5 \times 10^{-6}}} = 96 \text{ ft}$$

The relative error is

$$\delta_{\text{Figure 4.5}} = \left| \frac{v_A - v_E}{v_E} \right| \times 100\% = \left| \frac{100 - 96}{96} \right| \times 100\% = 4.16\%$$

And minimum possible fracture corridor spacing is $\text{MFCS} = 2r_i = 192$ ft

4.4. Fracture Corridor Conductivity Estimation for Matrix Well

A complete bilinear flow regime can be observed for fracture well (D=0) and matrix wells (D=15 ft or 45 ft) in corridor type NFR (Figure 4.7). In the diagnostic plot for bilinear flow, the slope of the straight line is 113 (Figure 4.8). From the bilinear flow regime, fracture corridor conductivity can be estimated as,

$$K_f W_f = \left[\frac{44.1 q \mu_o B_o}{m_{BL} h (\phi_m \mu_o (C_t)_m K_m)^{1/4}} \right]^2 = \left[\frac{44.1 \times 10 \times 7 \times 1.1}{113 \times 30 \times (0.01 \times 7 \times 5.5 \times 10^{-6} \times 1)^{1/4}} \right]^2$$

$$= 1617 \text{ md} - \text{ft}$$

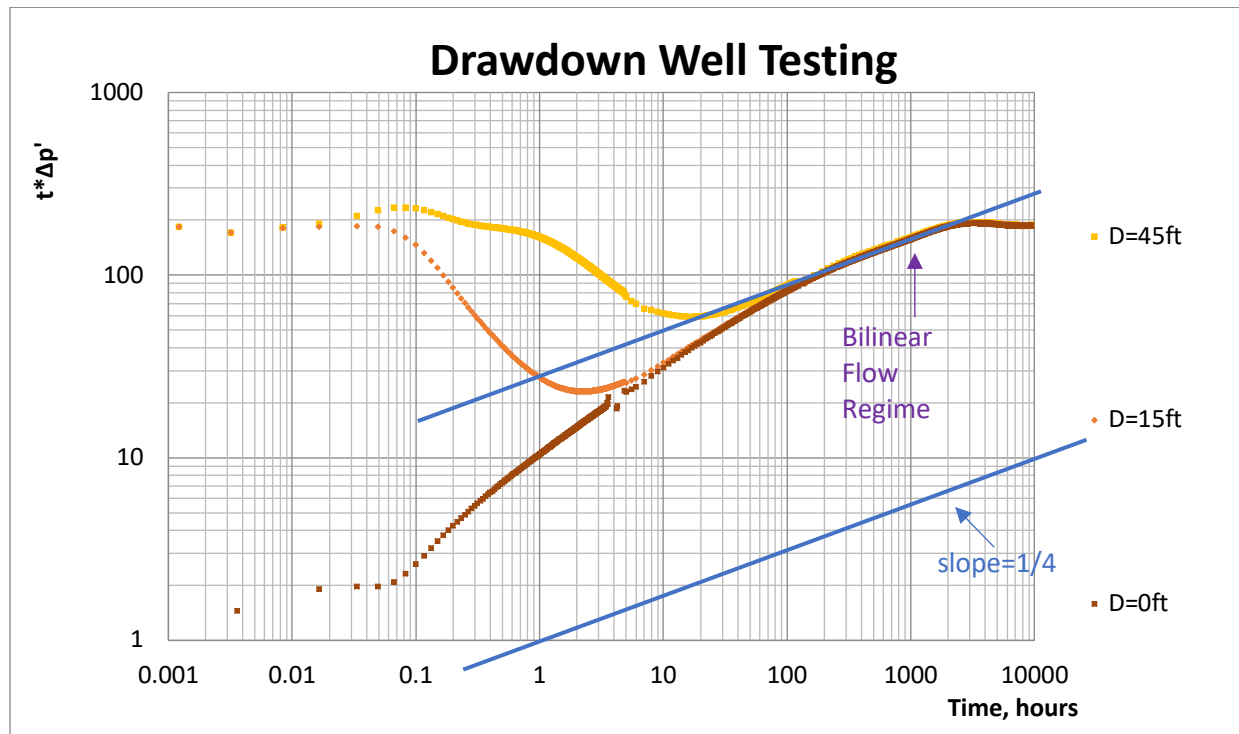


Figure 4.7. Examples of a diagnostic plot from fracture well and matrix wells near fracture corridor in corridor type NFR (model 1)

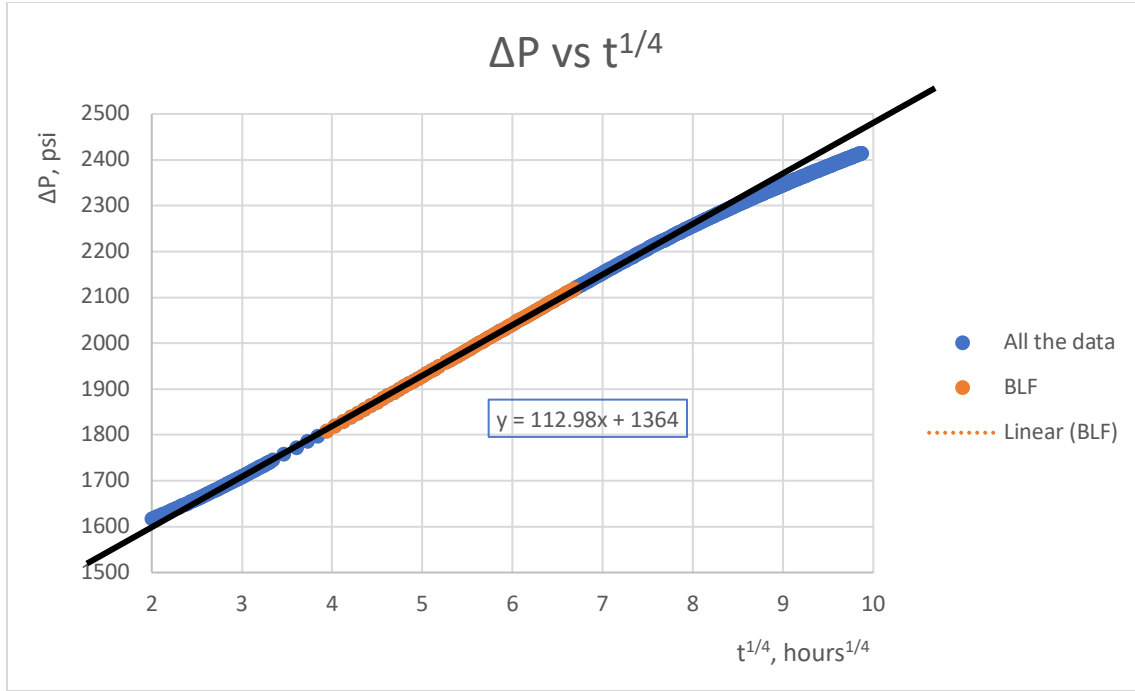


Figure 4.8. Diagnostic plot for bilinear flow

4.5. Fracture Corridor Length Estimation

Fracture corridor length can be estimated from the bilinear flow regime plot for fracture wells and matrix wells nearby a fracture corridor or from the boundary-dominated flow regime for fracture wells.

4.5.1. Estimation of Fracture Corridor Length from Bilinear Flow Regime for Matrix Well

From Figure 4.8, $C_{fD} \leq 1.6$. The fracture corridor length can be estimated using equation (3.26)

$$L_f = 2L_{hf} = 2 \left(\frac{2.5}{4.55 \sqrt{\frac{k_m}{K_f W_f}} \pm \sqrt{\frac{\phi_m \mu_o (C_t)_m}{0.0002637 K_m t_{ebf}}}} \right)^2 = 2 \left(\frac{2.5}{4.55 \sqrt{\frac{1}{1617}} \pm \sqrt{\frac{0.01 \times 7 \times 5.5 \times 10^{-6}}{0.0002637 \times 1 \times 2000}}} \right)^2$$

$$L_{f1} = 1775 \text{ft and } L_{f2} = 1207.6 \text{ft}$$

There are two solutions, 1775ft and 1207.6 ft. C_{fD} need to be calculated to find the correct solution. To calculate C_{fD} , half fracture corridor length should be calculated first, as shown below.

$$L_{hf} = \left(\frac{2.5}{4.55 \sqrt{\frac{K_m}{K_f W_f}} \pm \sqrt[4]{\frac{\phi_m \mu_o (C_t)_m}{0.0002637 K_m t_{ebf}}}} \right)^2 = \left(\frac{2.5}{4.55 \sqrt{\frac{1}{1617}} \pm \sqrt[4]{\frac{0.01 \times 7 \times 5.5 \times 10^{-6}}{0.0002637 \times 1 \times 2000}}} \right)^2$$

$$L_{hf1} = 887.5\text{ft and } L_{hf2} = 603.8\text{ft}$$

Then, C_{fD} for the two solutions can be calculated below.

$$C_{fD1} = \frac{K_f W_f}{K_m L_{hf1}} = \frac{1617}{1 \times 887.5} = 1.8$$

$$C_{fD2} = \frac{K_f W_f}{K_m L_{hf2}} = \frac{1617}{1 \times 603.8} = 2.7$$

As $C_{fD1} \approx 1.6$, while C_{fD2} is greater than 1.6. The estimated fracture corridor length was 1775ft. The actual fracture corridor length created by CMG is 1500 ft. The relative error is $\delta = \left| \frac{v_A - v_E}{v_E} \right| \times 100\% = \left| \frac{1500 - 1775}{1775} \right| \times 100\% = 15.5\%$. Thus, the estimated fracture corridor length from the bilinear flow regime is quite inaccurate and is not a good measure of fracture corridor length.

4.5.2. Estimation Fracture Corridor Length from Boundary-Dominated Flow Regime for a Fracture Well

This method is applicable for prolonged flow testing of wells when the pseudosteady state (SSS) flow stage is reached. In order to model such a scenario, we increase matrix permeability and reduce oil viscosity, as shown in Table 4.3. A diagnostic plot from the matrix well and a

pressure drawdown plot from the fracture well were required to approximate fracture corridor length by pseudosteady state flow regime.

Table 4.3. Properties of the example CMG model 2 for corridor type NFR

Reservoir Temperature	200	F
Reservoir Top	10035	ft
Grid Size in Vertical Direction	30	ft
Grid Size in Horizontal Direction	20	ft
Initial Average Reservoir Pressure	4362.66	psi
Rock Compressibility	4.00E-06	1/psi
Water Compressibility	0.0000032	1/psi
Oil Compressibility	1.50E-06	1/psi
Matrix Porosity	0.01	Fraction
Fracture Corridor Porosity	0.001	Fraction
Matrix Permeability	10	md
Fracture Corridor Permeability	10000	md
Oil Formation Volume factor	1.1	rb/stb
Oil Viscosity	5	cp
Production Rate	10	stb/d

From Figure 4.9, matrix permeability is estimated as

$$K_m = \frac{70.6q\mu_o B_o}{h(t \times \Delta p')_{R1}} = \frac{70.6 \times 10 \times 5 \times 1.1}{30 \times 13} = 10 \text{ md}$$

From Figure 4.10, fracture corridor length was calculated as

$$L_f = 2L_{hf} = \sqrt{\frac{34.2A}{C_A e^{\frac{(p_R - p_{wf})K_m h}{70.6qB_o\mu_o}}}} = \sqrt{\frac{34.2 \times 223 \times 223 \times 20 \times 20}{30.8828 \times e^{\frac{46.1 \times 10 \times 30}{70.6 \times 10 \times 1.1 \times 5}}}} = \sqrt{\frac{22028207.29}{e^{0.07726 \times 46.1}}} = 791 \text{ ft}$$

The actual fracture corridor length created by CMG is 800 ft. The relative error is $\delta = \left| \frac{v_A - v_E}{v_E} \right| \times 100\% = \left| \frac{800 - 791}{791} \right| \times 100\% = 1.14\%$. Estimating fracture corridor length from the boundary-dominated flow appears to be sufficiently accurate.

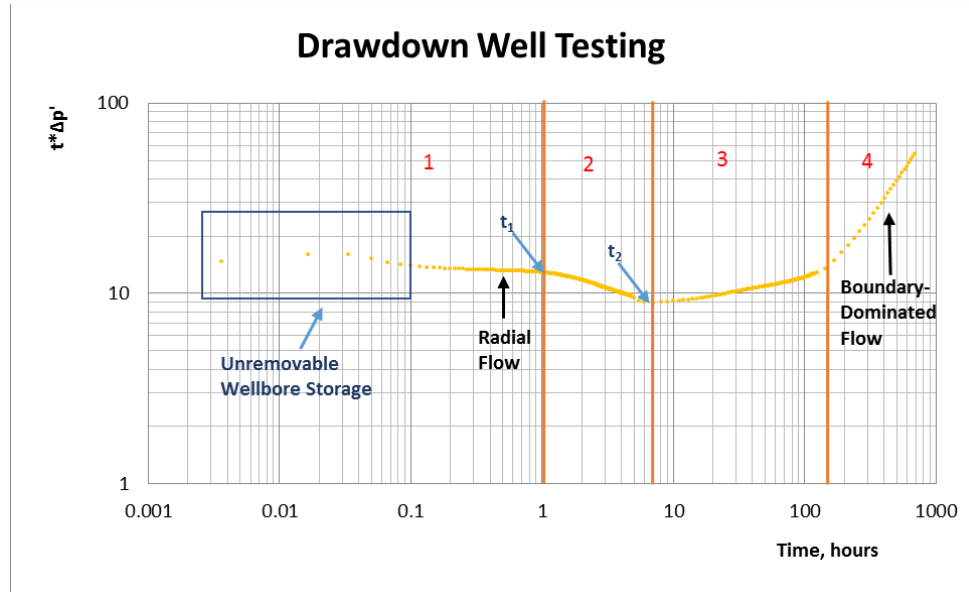


Figure 4.9. Diagnostic plot for matrix well in corridor type NFR (model 2) in Table 4.3

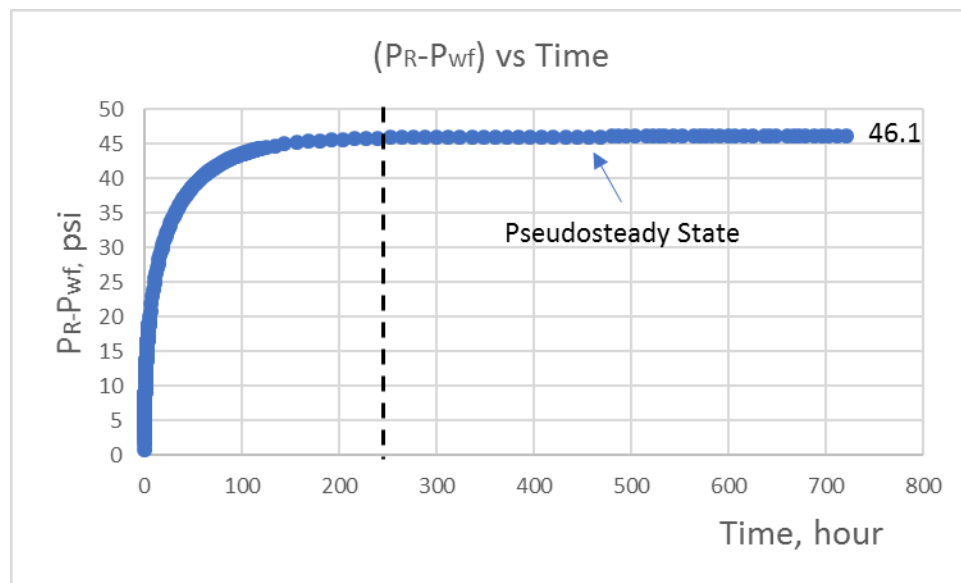


Figure 4.10. An example of a pressure drawdown plot for fracture well in corridor type NFR (model 2) in Table 4.3

4.6. Accuracy Assessments with Cumulative Logit Models

The accuracy of estimation is determined by relative error. The relative errors are in three categories: Category 1 - $\delta \leq 10\%$; Category 2 - $10\% < \delta \leq 20\%$; and Category 3 - ‘can not measure’. The accuracy is defined as “good” if the relative error falls to category 1. The accuracy is defined as “fair” if the relative error falls to category 2. The accuracy is defined as “bad” if the relative error falls to category 3. Accuracy of the estimated fracture corridor length from the bilinear flow regime is too low in most cases. Thus, there is no point in finding accuracy of the estimated fracture corridor length (section 4.5.1). However, estimated values of matrix permeability and well-corridor distance have very high accuracy. But they can be highly dependent on fracture corridor length. Therefore, this study addresses only the effect of matrix permeability, fracture corridor permeability, well corridor distance, and fracture corridor length on the accuracy of the estimated matrix permeability and well-corridor distance. Cumulative logit models ($\text{logit}[P(Y \leq j)] = \log \left[\frac{P(Y \leq j)}{1 - P(Y \leq j)} \right] = \log \left(\frac{\pi_1 + \dots + \pi_j}{\pi_{j+1} + \dots + \pi_c} \right) = \alpha_j + \beta \mathbf{x}$, ($j = 1, 2, \dots, c - 1$)) are used to estimate the effect of these variables (matrix permeability, fracture corridor permeability, well corridor distance, and fracture corridor length) on the accuracy estimation by predicting the probability of getting the relative error (δ) in each category when the significant variables are given.

It is impossible to get the population (all possible values on which each variable can be measured) of this study to fit the cumulative logit models. In statistics, we use a sample (a subset selected from the population) representing the population to estimate the parameters (α_j and β) of the cumulative logit models. Space-filling design is used to select the sample used in this study,

and the selected sample is shown in Appendix B.1. The sample size is 40. The results obtained by well testing for the selected sample are shown in Appendix B.2.

Before fitting the cumulative logit models, the multicollinearity test must be done to avoid creating an unstable model. The Pearson correlation coefficients for explanatory variables in Table E.1 are very low. The last number of the condition index is 6.85773 (Table E.2), which is much smaller than 40. Small Pearson correlation coefficients and condition index indicate no multicollinearity problem of independent variables. Now, we can have enough confidence to fit the model.

4.6.1. Accuracy of Matrix Permeability Estimation

Initially, we plan to find the effect of matrix permeability (K_m), fracture corridor permeability (K_f), well corridor distance (D), and fracture corridor length (L_f) on the accuracy of the estimated matrix permeability. The initial model (also we can call it the full model here) is

$$\begin{aligned}\text{logit}[P(\text{Category} \leq 1)] &= \log \left[\frac{P(\text{Category} \leq 1)}{1 - P(\text{Category} \leq 1)} \right] = \log \left(\frac{\pi_1}{\pi_2 + \pi_3} \right) \\ &= \alpha_1 + \beta_1 K_m + \beta_2 K_f + \beta_3 D + \beta_4 L_f, \\ \text{logit}[P(\text{Category} \leq 2)] &= \log \left[\frac{P(\text{Category} \leq 2)}{1 - P(\text{Category} \leq 2)} \right] = \log \left(\frac{\pi_1 + \pi_2}{\pi_3} \right) \\ &= \alpha_2 + \beta_1 K_m + \beta_2 K_f + \beta_3 D + \beta_4 L_f,\end{aligned}$$

Where,

$P(\text{Category} \leq 1)$ and π_1 are the probability in category 1 (good accuracy),

π_2 is the probability in category 2 (fair accuracy),

π_3 is the probability in category 3 (bad accuracy),

$P(\text{Category} \leq 1)$ is the probability in category 1 (good accuracy),

$(\text{Category} \leq 2)$ is the probability in categories 1 and 2 (good and fair accuracy),

$\frac{P(\text{Category} \leq 1)}{1 - P(\text{Category} \leq 1)}$ is the odds of the event $\text{Category} \leq 1$,

$\frac{P(\text{Category} \leq 2)}{1 - P(\text{Category} \leq 2)}$ is the odds of the event $\text{Category} \leq 2$.

However, it is possible that one or some of the variables we are interested in (matrix permeability (K_m), fracture corridor permeability (K_f), well corridor distance (D), and fracture corridor length (L_f)) do not affect the accuracy of matrix permeability estimation. The forward selection is used to build the best cumulative logit model for the accuracy of the matrix permeability estimation by SAS (a professional statistics software). The most significant variable, well-corridor distance (D), is chosen to enter the model in step one. Variable matrix permeability (K_m) is then added to the model (based on the t-test of the regression coefficients) until no remaining variables (Table F.1), which means fracture corridor permeability (K_f) and fracture corridor length (L_f)) do not have a significant effect on the accuracy of matrix permeability estimation.

The results show that only the well-corridor distance and matrix permeability significantly affect the accuracy of estimating matrix permeability, with well-corridor distance having a more significant effect than matrix permeability. Parameter approximation for the accuracy of the matrix permeability estimation is showed in Table F.2, provides the cumulative logit model (reduced model) as,

$$\begin{aligned} \text{logit}[P(\text{Category} \leq 1)] &= \log \left[\frac{P(\text{Category} \leq 1)}{1 - P(\text{Category} \leq 1)} \right] = \log \left(\frac{\pi_1}{\pi_2 + \pi_3} \right) \\ &= -2.5186 - 0.4011K_m + 0.012D, \end{aligned}$$

$$\begin{aligned}\text{logit}[P(\text{Category} \leq 2)] &= \log \left[\frac{P(\text{Category} \leq 2)}{1 - P(\text{Category} \leq 2)} \right] = \log \left(\frac{\pi_1 + \pi_2}{\pi_3} \right) \\ &= 0.6984 - 0.4011K_m + 0.012D.\end{aligned}$$

The next question is that if the reduced model is sufficient? In other words, if $\beta_2 = \beta_4 = 0$? A likelihood-ratio test is required to compare the full model and the reduced model. The null hypothesis is that

$$H_0: \beta_2 = \beta_4 = 0.$$

The difference between the deviances is 41.9132, based on $df = 76$, which gives $p\text{-value} = 0.9995 > 0.05$. The large $p\text{-value}$ supports the good fit of the cumulative logit model. So, we do not reject the null hypothesis and conclude that the reduced model is sufficient.

The interpretation of the cumulative logit model for the accuracy of the matrix permeability estimation is given below.

1. The effect of the matrix permeability on the accuracy of the matrix permeability estimation is negative.

For $\text{Category} \leq 1$ with a fixed D and K_m , the logit model is

$$\log \left[\frac{P(\text{Category} \leq 1)}{1 - P(\text{Category} \leq 1)} \right]_1 = -2.5186 - 0.4011K_m + 0.012D$$

The odds of $\text{Category} \leq 1$ with a fixed D and K_m is

$$\left[\frac{P(\text{Category} \leq 1)}{1 - P(\text{Category} \leq 1)} \right]_1 = e^{-2.5186 - 0.4011K_m + 0.012D}$$

For $\text{Category} \leq 1$ with a fixed D and $K_m + 1$ (increase matrix permeability one md),

$$\log \left[\frac{P(\text{Category} \leq 1)}{1 - P(\text{Category} \leq 1)} \right]_2 = -2.5186 - 0.4011(K_m + 1) + 0.012D$$

The odds of Category ≤ 1 with a fixed D and $K_m + 1$ is

$$\left[\frac{P(\text{Category} \leq 1)}{1 - P(\text{Category} \leq 1)} \right]_2 = e^{-2.5186 - 0.4011(K_m + 1) + 0.012D} = e^{-2.5186 - 0.4011K_m + 0.012D} e^{-0.4011}$$

The odds ratio of $\log \left[\frac{P(\text{Category} \leq 1)}{1 - P(\text{Category} \leq 1)} \right]_2$ and $\log \left[\frac{P(\text{Category} \leq 1)}{1 - P(\text{Category} \leq 1)} \right]_1$ is

$$\frac{\left[\frac{P(\text{Category} \leq 1)}{1 - P(\text{Category} \leq 1)} \right]_2}{\left[\frac{P(\text{Category} \leq 1)}{1 - P(\text{Category} \leq 1)} \right]_1} = \frac{e^{-2.5186 - 0.4011K_m + 0.012D} e^{-0.4011}}{e^{-2.5186 - 0.4011K_m + 0.012D}} = e^{-0.4011} = 0.67$$

The same for Category ≤ 2 , the odds ratio of $\log \left[\frac{P(\text{Category} \leq 2)}{1 - P(\text{Category} \leq 2)} \right]_2$ and

$\log \left[\frac{P(\text{Category} \leq 2)}{1 - P(\text{Category} \leq 2)} \right]_1$ is

$$\frac{\left[\frac{P(\text{Category} \leq 2)}{1 - P(\text{Category} \leq 2)} \right]_2}{\left[\frac{P(\text{Category} \leq 2)}{1 - P(\text{Category} \leq 2)} \right]_1} = \frac{e^{0.6984 - 0.4011K_m + 0.012D} e^{-0.4011}}{e^{0.6984 - 0.4011K_m + 0.012D}} = e^{-0.4011} = 0.67$$

It means for fixed well-corridor distance, increase one md matrix permeability, the odds of falling into or below any categories will decrease by 0.67.

2. The effect of well-corridor distance on the accuracy of the matrix permeability estimation is positive. The odds of falling into or below any categories for a fixed matrix permeability will be increased by 1.01 ($e^{0.012}$) with one ft increase in the well-corridor distance.

3. The parameter coefficient estimations (close to 0) are very small because of the unit of the independent variables. In fact, the parameter coefficient estimations' values are significantly different from 0.

4. The cumulative probability of the accuracy of the NFR matrix permeability estimation falling into Category ≤ 1 for a given matrix permeability and well-corridor distance is given by

$$P(\text{Category} \leq 1) = \frac{\exp(-2.5186 - 0.4011K_m + 0.012D)}{1 + \exp(-2.5186 - 0.4011K_m + 0.012D)}$$

The cumulative probability of the accuracy of the NFR matrix permeability estimation falling into Category ≤ 2 for a given matrix permeability and well-corridor distance is given by

$$P(\text{Category} \leq 2) = \frac{\exp(0.6984 - 0.4011K_m + 0.012D)}{1 + \exp(0.6984 - 0.4011K_m + 0.012D)}$$

The cumulative probability of the accuracy of the NFR matrix permeability estimation falling into Category ≤ 3 for a given matrix permeability and well-corridor distance is given by

$$P(\text{Category} \leq 3) = 1$$

5. The probability of the accuracy of the NFR matrix permeability estimation falling into Category = 1 for a given matrix permeability and well-corridor distance is given by

$$P(\text{Category} = 1) = \frac{\exp(-2.5186 - 0.4011K_m + 0.012D)}{1 + \exp(-2.5186 - 0.4011K_m + 0.012D)}$$

The probability of the accuracy of the NFR matrix permeability estimation falling into Category = 2 for a given matrix permeability and well-corridor distance is given by

$$\begin{aligned}
P(\text{Category} = 2) &= P(\text{Category} \leq 2) - P(\text{Category} \leq 1) \\
&= \frac{\exp(0.6984 - 0.4011K_m + 0.012D)}{1 + \exp(0.6984 - 0.4011K_m + 0.012D)} \\
&\quad - \frac{\exp(-2.5186 - 0.4011K_m + 0.012D)}{1 + \exp(-2.5186 - 0.4011K_m + 0.012D)}
\end{aligned}$$

The probability of the accuracy of the NFR matrix permeability estimation falling into Category = 3 for a given matrix permeability and well-corridor distance is given by

$$\begin{aligned}
P(\text{Category} = 3) &= P(\text{Category} \leq 3) - P(\text{Category} \leq 2) \\
&= 1 - \frac{\exp(0.6984 - 0.4011K_m + 0.012D)}{1 + \exp(0.6984 - 0.4011K_m + 0.012D)}
\end{aligned}$$

For example, for $K_m = 1$ md, $D = 1000$ ft, the probability of the accuracy of the NFR matrix permeability estimation falling into Category = 1 is

$$P(\text{Category} = 1) = \frac{\exp(-2.5186 - 0.4011 \times 1 + 0.012 \times 1000)}{1 + \exp(-2.5186 - 0.4011 \times 1 + 0.012 \times 1000)} = 1$$

It means the probability of estimating matrix permeability within a 10% relative error is 100%.

4.6.2. Accuracy of Well-Corridor Distance Estimation

Similarly, the forward selection is selected to build the best cumulative logit model for the accuracy of the well-corridor distance estimation. The most significant variable, fracture corridor length (L_f), was chosen to enter the model in step one. The variable matrix permeability (K_m) was then added to the model based on the t-test of the regression coefficients, until which no remaining variable is significant to the model (Table G.1).

By forward selection, fracture corridor length and matrix permeability significantly influenced the accuracy of estimating the well-corridor distance. Fracture corridor length has a more

significant effect on the accuracy of estimating the well-corridor distance than matrix permeability. Parameter approximation for the accuracy of the well-corridor distance estimation showed in Table G.2, which gave the cumulative logit model below.

$$\begin{aligned}\text{logit}[P(\text{Category} \leq 1)] &= \log \left[\frac{P(\text{Category} \leq 1)}{1 - P(\text{Category} \leq 1)} \right] = \log \left(\frac{\pi_1}{\pi_2 + \pi_3} \right) \\ &= -0.3784 - 0.2543K_m + 0.000945L_f \\ \text{logit}[P(\text{Category} \leq 2)] &= \log \left[\frac{P(\text{Category} \leq 2)}{1 - P(\text{Category} \leq 2)} \right] = \log \left(\frac{\pi_1 + \pi_2}{\pi_3} \right) \\ &= 1.0965 - 0.2543K_m + 0.000945L_f\end{aligned}$$

The likelihood-ratio test (Table G.3) of independence compares the selected reduced model to the full model. The difference between the deviances is 68.4698, based on $df = 76$, which gives $p\text{-value} = 0.7182 > 0.05$. The large $p\text{-value}$ supports the good fit of the cumulative logit model.

The interpretation of the cumulative logit model for the accuracy of the matrix permeability estimation is given below.

1. The effect of the matrix permeability on the accuracy of the matrix permeability estimation is negative. The odds of falling into or below any categories for a fixed fracture corridor length will be decreased by 0.775 ($e^{-0.2543}$) with one md increase in matrix permeability.

2. The effect of fracture corridor length on the accuracy of the matrix permeability estimation is positive. The odds of falling into or below any categories for a fixed permeability will be increased by 1.0000945 ($e^{0.000945}$) with one ft increase in fracture corridor length.

3. The parameter coefficient estimations (close to 0) are very small because of the unit of the independent variables. In fact, the parameter coefficient estimations' values are significantly different from 0.

4. The cumulative probabilities are given by

$$P(\text{Category} \leq 1) = \frac{\exp(-0.3784 - 0.2543K_m + 0.000945L_f)}{1 + \exp(-0.3784 - 0.2543K_m + 0.000945L_f)},$$

$$P(\text{Category} \leq 2) = \frac{\exp(1.0965 - 0.2543K_m + 0.000945L_f)}{1 + \exp(1.0965 - 0.2543K_m + 0.000945L_f)},$$

$$P(\text{Category} \leq 3) = 1.$$

5. The probabilities of the accuracy of well-corridor distance estimation for given values of matrix permeability and fracture corridor length falling into the jth category are given by

$$P(\text{Category} = 1) = \frac{\exp(-0.3784 - 0.2543K_m + 0.000945L_f)}{1 + \exp(-0.3784 - 0.2543K_m + 0.000945L_f)},$$

$$P(\text{Category} = 2) = P(\text{Category} \leq 2) - P(\text{Category} \leq 1)$$

$$= \frac{\exp(1.0965 - 0.2543K_m + 0.000945L_f)}{1 + \exp(1.0965 - 0.2543K_m + 0.000945L_f)} - \frac{\exp(-0.3784 - 0.2543K_m + 0.000945L_f)}{1 + \exp(-0.3784 - 0.2543K_m + 0.000945L_f)},$$

$$P(\text{Category} = 3) = P(\text{Category} \leq 3) - P(\text{Category} \leq 2)$$

$$= 1 - \frac{\exp(1.0965 - 0.2543K_m + 0.000945L_f)}{1 + \exp(1.0965 - 0.2543K_m + 0.000945L_f)}.$$

For example, for $K_m = 1$ md, $L_f = 1000$ ft, the probability of the accuracy of the NFR matrix permeability estimation falling into Category = 1 is

$$\begin{aligned}
P(\text{Category} = 1) &= \frac{\exp(-0.3784 - 0.2543K_m + 0.000945L_f)}{1 + \exp(-0.3784 - 0.2543K_m + 0.000945L_f)} \\
&= \frac{\exp(-0.3784 - 0.2543 \times 1 + 0.000945 \times 1000)}{1 + \exp(-0.3784 - 0.2543 \times 1 + 0.000945 \times 1000)} = 0.4225,
\end{aligned}$$

The probability of the accuracy of the NFR matrix permeability estimation falling into Category = 2 is

$$\begin{aligned}
P(\text{Category} = 2) &= P(\text{Category} \leq 2) - P(\text{Category} \leq 1) \\
&= \frac{\exp(1.0965 - 0.2543 \times 1 + 0.000945 \times 1000)}{1 + \exp(1.0965 - 0.2543 \times 1 + 0.000945 \times 1000)} \\
&\quad - \frac{\exp(-0.3784 - 0.2543 \times 1 + 0.000945 \times 1000)}{1 + \exp(-0.3784 - 0.2543 \times 1 + 0.000945 \times 1000)} = 0.434,
\end{aligned}$$

The probability of the accuracy of the NFR matrix permeability estimation falling into Category = 3 is

$$\begin{aligned}
P(\text{Category} = 3) &= P(\text{Category} \leq 3) - P(\text{Category} \leq 2) \\
&= 1 - \frac{\exp(1.0965 - 0.2543K_m + 0.000945L_f)}{1 + \exp(1.0965 - 0.2543K_m + 0.000945L_f)} = 0.1434.
\end{aligned}$$

The probability that well-corridor length cannot be measured is 14.34%. The probability of estimating well-corridor distance within a 10% relative error is 42.25%. The probability of estimating well-corridor distance with the relative error range between 10% to 20% is 43.4%.

CHAPTER 5. DISCUSSION

5.1. Limitation of Fracture Corridor Length Estimation from Bilinear Flow Regime

In addition to the low accuracy of fracture corridor length estimation from the bilinear flow regime, the estimation is also limited by the well-corridor distance and reservoir size. If the well is far away from the fracture corridor, the bilinear flow regime does not develop (Figure 5.1). Moreover, even if the well is near the fracture corridor, the end time of the bilinear flow regime cannot be determined when the reservoir size is small (Figure 5.2).

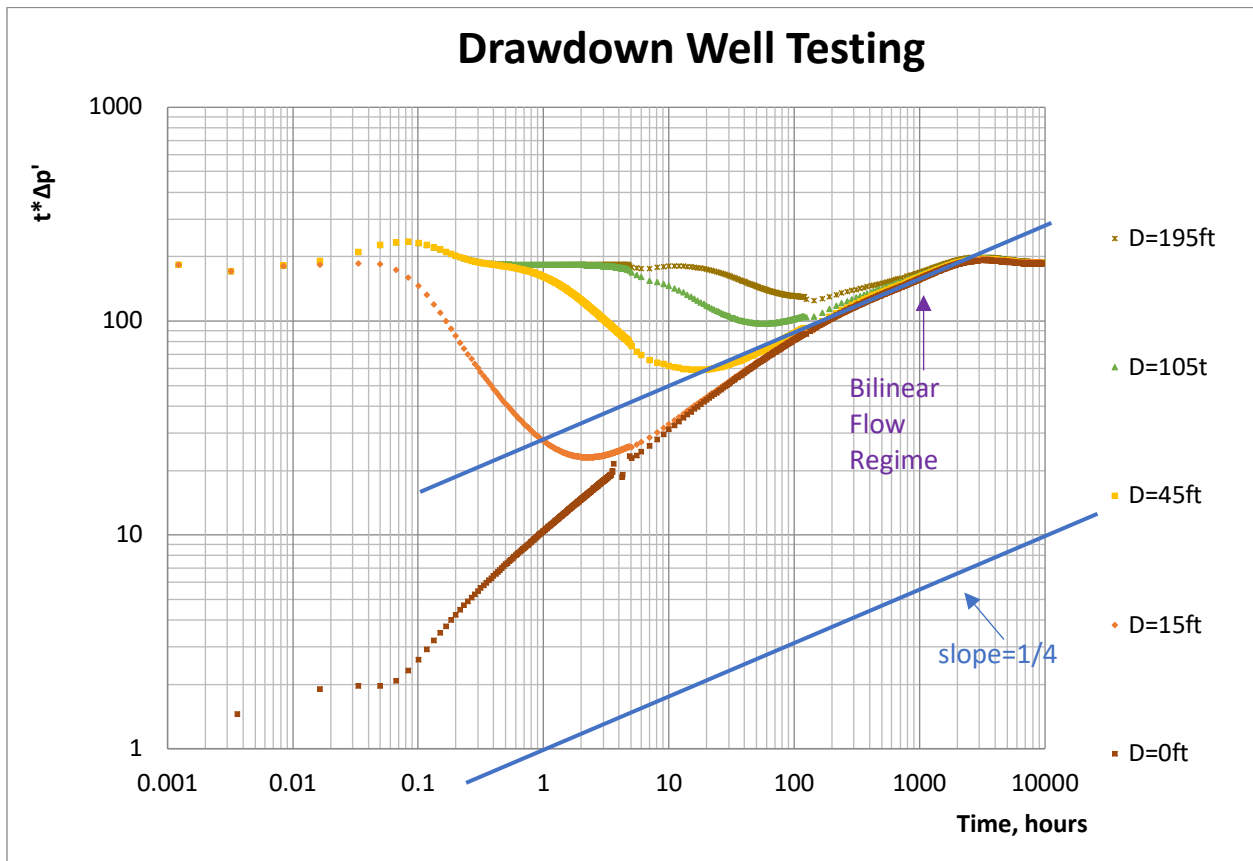


Figure 5.1. Diagnostic plot for fracture and matrix wells in corridor-type NFR (model 1)

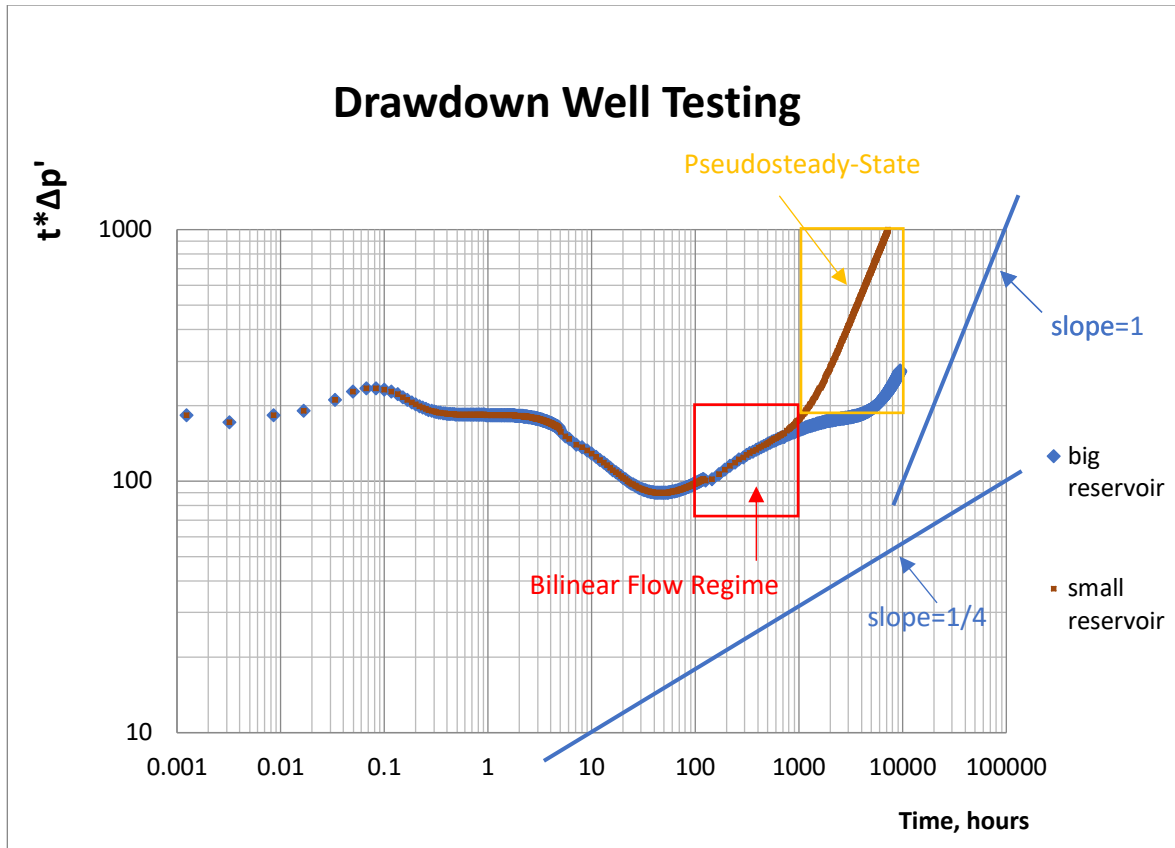


Figure 5.2. Diagnostic plot for matrix well in large and small corridor-type NFR

5.2. Effect of Well-Corridor Configuration on Accuracy of the Fracture Corridor Length Estimation from SSS Flow Regime

In practice, the well position corresponding to the reservoir boundary more or less can be determined, but the fracture corridor position is unknown. The question is if the fracture corridor position or well position would affect the corridor length approximation.

Three positions (Figure 5.3) are tested. The fracture corridor and well are placed in the middle of the reservoir in Position 1. The fracture corridor is located in the middle of the reservoir, and a well is placed at the edge of the corridor in Position 2. The well is nearly the end of a fracture corridor in Position 3. The fracture corridor is parallel to the reservoir boundary for all three position cases, and reservoir properties are in Table 4.3. Well's pressure drawdown ($p_R - p_{wf}$) vs. time for the three cases is shown in Figure Figure 5.4.

As shown in Table 5.1, the error of fracture corridor length approximation for three positions depends on the well-corridor configuration, but its value is acceptable.

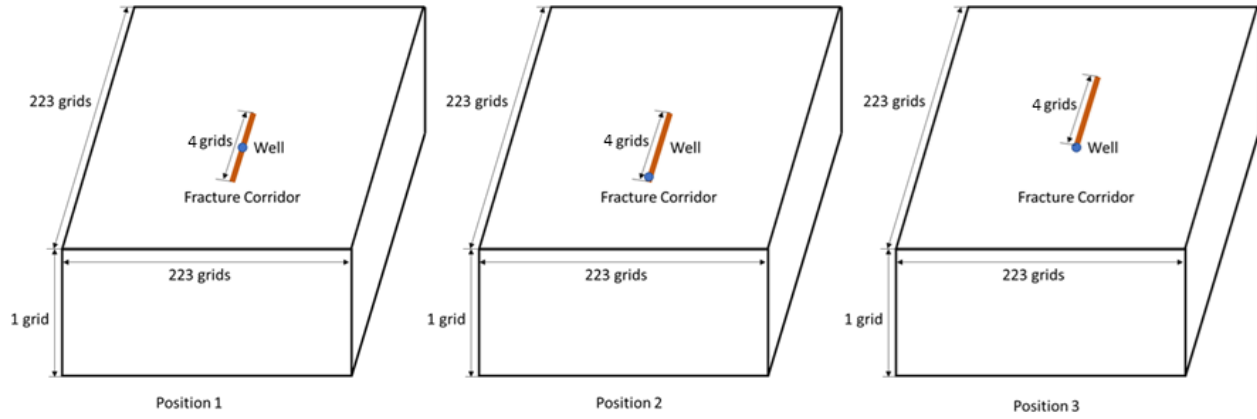


Figure 5.3. Examples of 3 fracture corridor position and well position in the reservoir

Table 5.1. The results of fracture corridor approximation for three positions

Position	$P_R - P_{wf}$, psi	L_f , ft	Relative Error
Position 1	46.1	791	1.14%
Position 2	47.17	759	5.40%
Position 3	48.36	725	10.34%

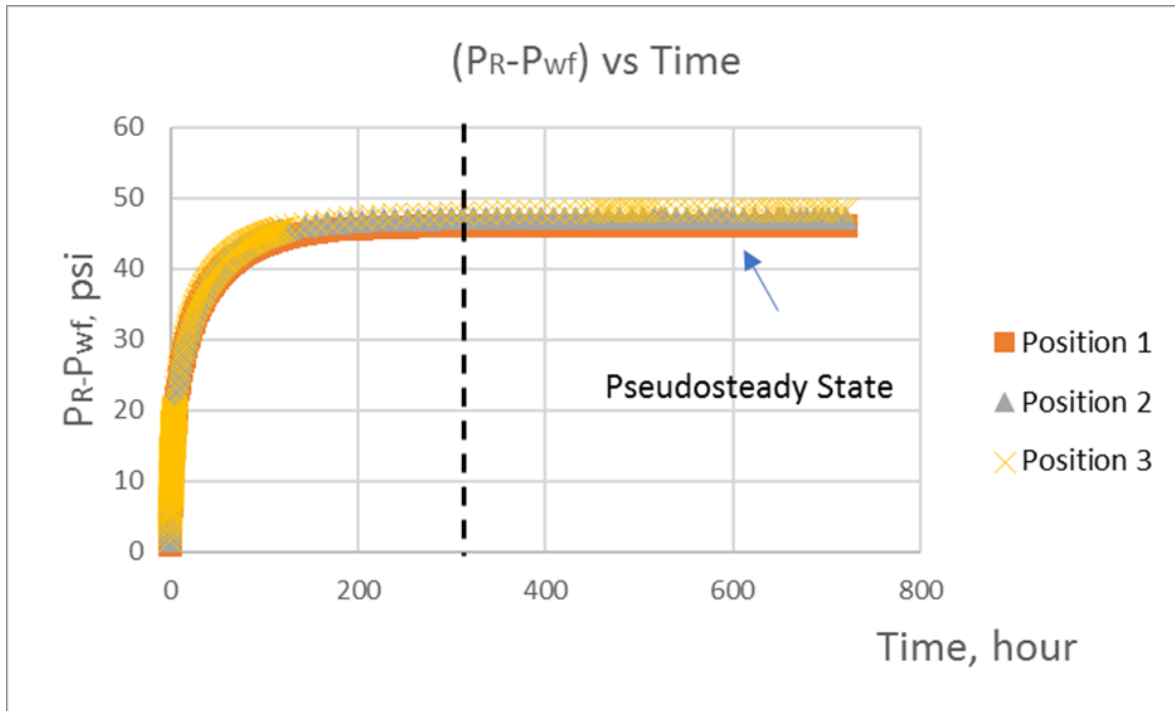


Figure 5.4. $(p_R - p_{wf})$ vs. time for three positions from a fracture well

5.3. Implications for Petroleum Engineering

Compared to other methods, the main advantage of well testing is that it is much cheaper and always available. It can distinguish matrix and fracture corridors through well behavior and distinguish corridor type naturally fractured reservoirs and common naturally fractured reservoirs. The conceptual flow chart of well testing for fracture corridor type naturally fractured reservoirs is shown in Figure 5.5. Additionally, it can be applied to both well-developed oil fields and new fields. What is more, the probability of the accuracy category of estimating the properties of corridor type naturally fractured reservoirs (matrix permeability, well-corridor distance, and fracture corridor length) can be predicted by cumulative logit models first. If it is worthy of doing well testing in a specific oil field can be then determined.

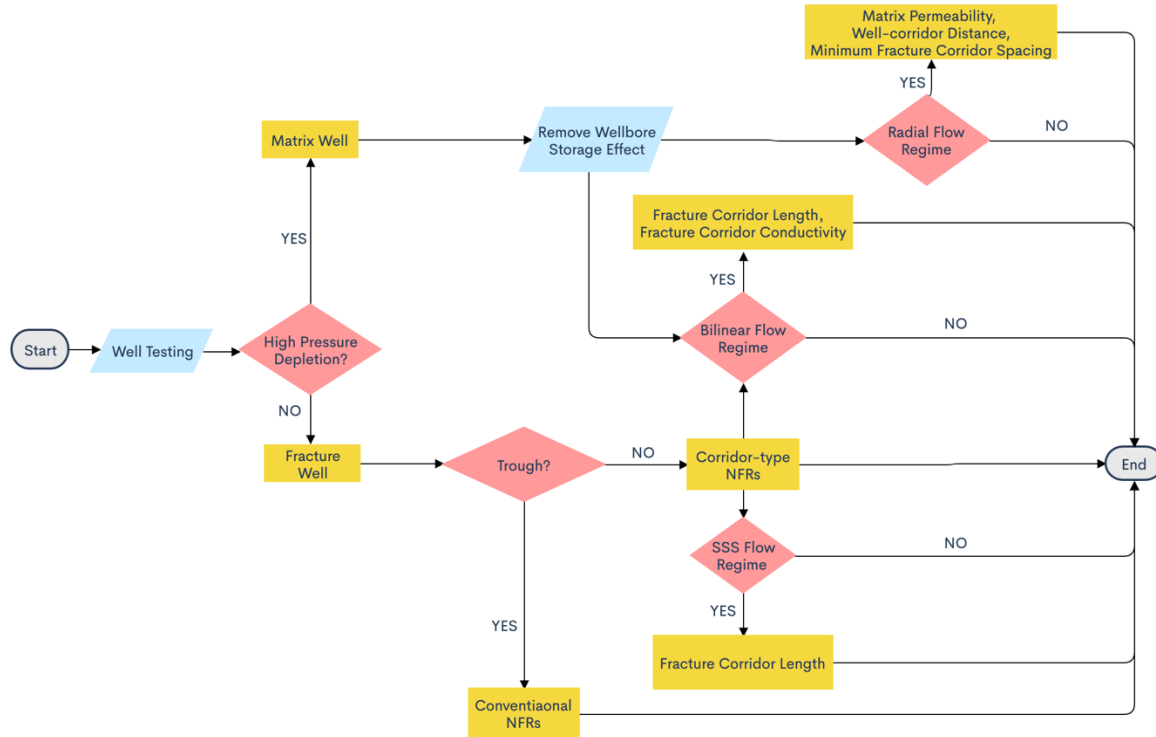


Figure 5.5. Conceptual flow chart of well testing for fracture corridor type naturally fractured reservoirs

5.4. Further Research

The models in this study are ideal. Additional testing utilizing field examples would be necessary to determine if the method would apply to production pressure transient or testing data.

Fracture corridor length cannot be estimated accurately by either bilinear flow regime from the fracture well and matrix well near the fracture corridor or boundary-dominated flow regime from the fracture well. It is better to develop a method to approximate fracture corridor length from matrix well as matrix well is more common. From Figure 5.1, the shape of the trough looks similar. For all the matrix well, the pressure drop will decrease immediately once the pressure transient travels to the fracture corridor (t_1 in Figure 4.9). The pressure drop will then increase immediately once the pressure transient travels to the matrix through the fracture corridor (t_2 in Figure 4.9). The regime from t_1 to t_2 is a good representative of fracture corridor length, but no specific flow regime

developed here. The data mining approach might be useful to predict fracture corridor length from the regime t_1 to t_2 by running a considerable size of CMG models for training.

Well need to be fractured to improve the productivity of the matrix well in corridor type naturally fractured reservoirs. The fracture half length designed by hydraulic fracture should at least be the well-corridor length to connect the well with the fracture corridors. The well performance of the fractured well should be evaluated.

CHAPTER 6. CONCLUSION

The study verifies feasibilities of well test diagnostics for estimating properties of corridor-type NFRs. The approach employs conventional analysis of simulated well tests and categorical data analysis for accuracy evaluation. The findings are summarized below.

- 1) Results of this work are based (limited by) a new, simplified model and a β -deconvolution technique to provide wells testing data in the corridor-type NFR reservoirs for this study based upon analysis of diagnostic plot.
- 2) Diagnostic plots allow distinguishing of corridor-type NFRs from conventional NFRs by estimating permeability from the early radial flow regime.
- 3) The plots also allow detection of well's location either in the exclusion zone or inside a corridor.
- 4) The diagnostic plots for matrix well and fracture well provide sufficient data for the estimation of matrix permeability, fracture corridor conductivity, well-corridor distance, and fracture corridor length.
- 5) Finding fracture corridor length from the bilinear flow regime is not very accurate. The method can only give a rough estimate of the length.
- 6) Fracture corridor length can be accurately estimated by analyzing the SSS flow regime. However, the method is only applicable for long duration production tests.
- 7) Accuracy of diagnostic plot analysis is assessed with cumulative logit model that gives not only values of errors but also probabilities of the errors.
- 8) The more distant the well is from the fracture corridor, and the lower the exclusion zone permeability, the more accurate estimation of exclusion zone permeability

- 9) Accuracy of the well to corridor distance estimation improves for longer corridors and low-permeability exclusion zone.

APPENDIX A. DERIVATION OF EQUATIONS FOR WELLBORE STORAGE REMOVAL

The interval $[0, t]$ is divided into n subintervals. Each of the intervals is denoted as follows, $[0, t_1]$, $[t_1, t_2]$, $[t_2, t_3]$, \dots , $[t_{i-1}, t_i]$, $[t_i, t_{i+1}]$, \dots , $[t_{n-1}, t_n]$.

Assume $(t_{i-1}, \Delta P_{w(i-1)})$, $(t_i, \Delta P_{wi})$, $(t_{i+1}, \Delta P_{w(i+1)})$ pass the small curve $\Delta P_w = at^2 + bt + c$ (Figure A.1), then

$$\Delta P_{w(i-1)} = at_{i-1}^2 + bt_{i-1} + c \quad (A1)$$

$$\Delta P_{wi} = at_i^2 + bt_i + c \quad (A2)$$

$$\Delta P_{w(i+1)} = at_{i+1}^2 + bt_{i+1} + c \quad (A3)$$

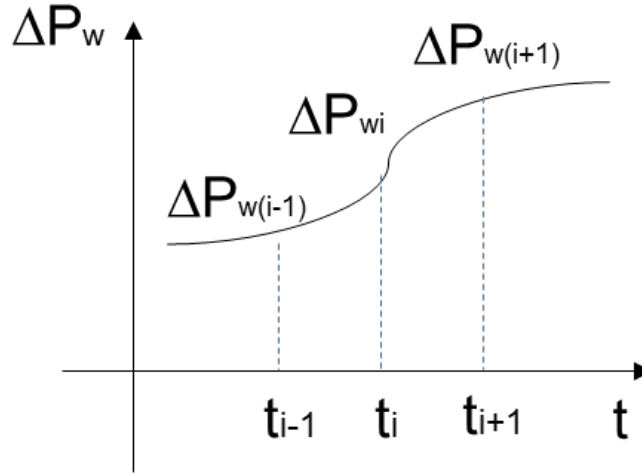


Figure A.1. Sketch of subinterval $[t_{i-1}, t_{i+1}]$ to segment ΔP_w

Combine equation (A1), (A2), (A3), and solve a , b , c , gives

$$a = -\frac{t_{i-1}\Delta P_{wi} - t_{i-1}\Delta P_{w(i+1)} - t_i\Delta P_{w(i-1)} + t_i\Delta P_{w(i+1)} + t_{i+1}\Delta P_{w(i-1)} - t_{i+1}\Delta P_{wi}}{t_{i-1}^2t_i - t_{i-1}^2t_{i+1} - t_{i-1}t_i^2 + t_{i-1}t_{i+1}^2 + t_i^2t_{i+1} - t_it_{i+1}^2} \quad (A4)$$

$$b = -\frac{t_{i-1}^2\Delta P_{wi} - t_{i-1}^2\Delta P_{w(i+1)} - t_i^2\Delta P_{w(i-1)} + t_i^2\Delta P_{w(i+1)} + t_{i+1}^2\Delta P_{w(i-1)} - t_{i+1}^2\Delta P_{wi}}{(t_{i-1} - t_i)(t_{i-1}t_i - t_{i-1}t_{i+1} - t_{i+1}t_i + t_{i+1}^2)} \quad (A5)$$

$$c = -\frac{t_{i-1}^2t_i\Delta P_{w(i+1)} - t_{i-1}^2t_{i+1}\Delta P_{wi} - t_{i-1}t_i^2\Delta P_{w(i+1)} + t_{i-1}t_{i+1}^2\Delta P_{wi} + t_i^2t_{i+1}\Delta P_{w(i-1)} - t_it_{i+1}^2\Delta P_{w(i-1)}}{(t_{i-1} - t_i)(t_{i-1}t_i - t_{i-1}t_{i+1} - t_{i+1}t_i + t_{i+1}^2)} \quad (A6)$$

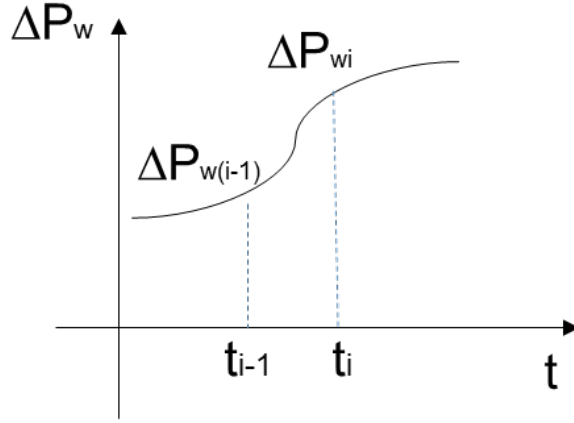


Figure A.2. Sketch of subinterval $[t_{i-1}, t_i]$ for integration

From Figure A.2,

$$\begin{aligned}
 \int_{t_{i-1}}^{t_i} \Delta p_w d\tau &= \int_{t_{i-1}}^{t_i} (at^2 + bt + c) d\tau = \frac{1}{3}a(t_i^3 - t_{i-1}^3) + \frac{1}{2}(t_i^2 - t_{i-1}^2) + (t_i - t_{i-1}) \\
 &= \frac{(t_{i-1}^2 + t_{i-1}t_i + t_i^2) \times (t_{i-1}\Delta P_{wi} - t_{i-1}\Delta P_{w(i+1)} - t_i\Delta P_{w(i-1)} + t_i\Delta P_{w(i+1)} + t_{i+1}\Delta P_{w(i-1)} - t_{i+1}\Delta P_{wi})}{3(t_i - t_{i+1})(t_{i-1} - t_{i+1})} \\
 &\quad - \frac{(t_{i-1} + t_i) \times (t_{i-1}^2\Delta P_{wi} - t_{i-1}^2\Delta P_{w(i+1)} - t_i^2\Delta P_{w(i-1)} + t_i^2\Delta P_{w(i+1)} + t_{i+1}^2\Delta P_{w(i-1)} - t_{i+1}^2\Delta P_{wi})}{2(t_i - t_{i+1})(t_{i-1} - t_{i+1})} \\
 &\quad - \frac{(t_{i-1}^2t_i\Delta P_{w(i+1)} - t_{i-1}^2t_{i+1}\Delta P_{wi} - t_{i-1}t_i^2\Delta P_{w(i+1)} + t_{i-1}t_{i+1}^2\Delta P_{wi} + t_i^2t_{i+1}\Delta P_{w(i-1)} - t_it_{i+1}^2\Delta P_{w(i-1)})}{(t_i - t_{i+1})(t_{i-1} - t_{i+1})} \quad (A7)
 \end{aligned}$$

$$\begin{aligned}
 \int_0^t \Delta p_w d\tau &= \int_0^{t_1} \Delta p_w d\tau + \int_{t_1}^{t_2} \Delta p_w d\tau + \dots + \int_{t_{i-1}}^{t_i} \Delta p_w d\tau + \dots + \int_{t_{n-1}}^{t_n} \Delta p_w d\tau \\
 &= \sum_{i=1}^{t-1} \left[\frac{(t_{i-1}^2 + t_{i-1}t_i + t_i^2) \times (t_{i-1}\Delta P_{wi} - t_{i-1}\Delta P_{w(i+1)} - t_i\Delta P_{w(i-1)} + t_i\Delta P_{w(i+1)} + t_{i+1}\Delta P_{w(i-1)} - t_{i+1}\Delta P_{wi})}{3(t_i - t_{i+1})(t_{i-1} - t_{i+1})} \right. \\
 &\quad - \frac{(t_{i-1} + t_i) \times (t_{i-1}^2\Delta P_{wi} - t_{i-1}^2\Delta P_{w(i+1)} - t_i^2\Delta P_{w(i-1)} + t_i^2\Delta P_{w(i+1)} + t_{i+1}^2\Delta P_{w(i-1)} - t_{i+1}^2\Delta P_{wi})}{2(t_i - t_{i+1})(t_{i-1} - t_{i+1})} \\
 &\quad \left. - \frac{(t_{i-1}^2t_i\Delta P_{w(i+1)} - t_{i-1}^2t_{i+1}\Delta P_{wi} - t_{i-1}t_i^2\Delta P_{w(i+1)} + t_{i-1}t_{i+1}^2\Delta P_{wi} + t_i^2t_{i+1}\Delta P_{w(i-1)} - t_it_{i+1}^2\Delta P_{w(i-1)})}{(t_i - t_{i+1})(t_{i-1} - t_{i+1})} \right] \quad (A8)
 \end{aligned}$$

$$\begin{aligned}
\Delta p_{wi} &= \frac{1}{t} \int_0^t \Delta p_w d\tau \\
&= \frac{1}{t} \sum_{i=1}^{t-1} \left[\frac{(t_{i-1}^2 + t_{i-1}t_i + t_{i+1}^2) \times (t_{i-1}\Delta p_{wi} - t_{i-1}\Delta p_{w(i+1)} - t_i\Delta p_{w(i-1)} + t_i\Delta p_{w(i+1)} + t_{i+1}\Delta p_{w(i-1)} - t_{i+1}\Delta p_{wi})}{3(t_i - t_{i+1})(t_{i-1} - t_{i+1})} \right. \\
&\quad - \frac{(t_{i-1} + t_i) \times (t_{i-1}^2\Delta p_{wi} - t_{i-1}^2\Delta p_{w(i+1)} - t_i^2\Delta p_{w(i-1)} + t_i^2\Delta p_{w(i+1)} + t_{i+1}^2\Delta p_{w(i-1)} - t_{i+1}^2\Delta p_{wi})}{2(t_i - t_{i+1})(t_{i-1} - t_{i+1})} \\
&\quad \left. - \frac{(t_{i-1}^2t_i\Delta p_{w(i+1)} - t_{i-1}^2t_{i+1}\Delta p_{wi} - t_{i-1}t_i^2\Delta p_{w(i+1)} + t_{i-1}t_{i+1}^2\Delta p_{wi} + t_i^2t_{i+1}\Delta p_{w(i-1)} - t_it_{i+1}^2\Delta p_{w(i-1)})}{(t_i - t_{i+1})(t_{i-1} - t_{i+1})} \right] \quad (A9)
\end{aligned}$$

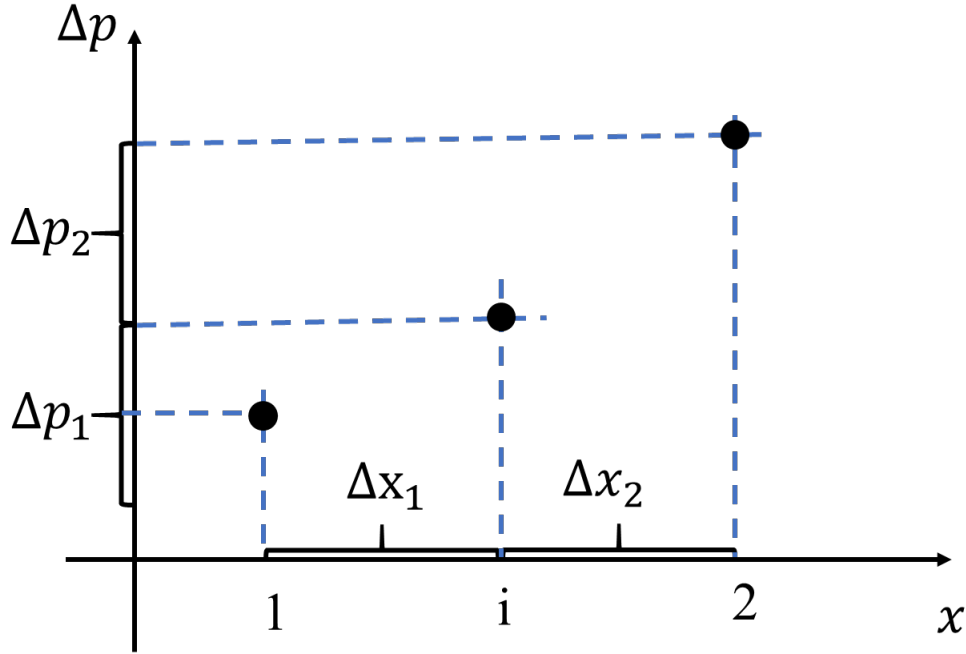


Figure A.3. Sketch of derivative algorithm

From Figure A.3. the derivative is estimated by $\left[\frac{d\Delta p}{dx} \right]_i = \frac{\frac{\Delta p_1}{\Delta x_1} \Delta x_2 + \frac{\Delta p_2}{\Delta x_2} \Delta x_1}{\Delta x_1 + \Delta x_2}$ (A10)

So, $\Delta p_{wd} = t \frac{d\Delta p_w}{dt}$ at each time j can be estimated by

$$\Delta p_{wdj} = \left[t \frac{d\Delta p_w}{dt} \right]_j = \left[\frac{d\Delta p_w}{d \ln t} \right]_j = \frac{\frac{(\Delta p_{wj} - \Delta p_{w(j-1)})}{(\ln t_j - \ln t_{j-1})} (\ln t_{j+1} - \ln t_j) + \frac{(\Delta p_{w(j+1)} - \Delta p_{wj})}{(\ln t_{j+1} - \ln t_j)} (\ln t_j - \ln t_{j-1})}{(\ln t_{j+1} - \ln t_{j-1})} \quad (A11)$$

Plot Δp_{wd} vs. t to get the log-log diagnose plot before removing wellbore storage

Equation $\Delta p_{wid} = t \frac{d\Delta p_{wi}}{dt}$ at each time_j can be estimated by

$$\Delta p_{widj} = \left[t \frac{d\Delta p_{wi}}{dt} \right]_j = \left[\frac{d\Delta p_{wi}}{d\ln t} \right]_j = \frac{\frac{(\Delta p_{wij} - \Delta p_{wi(j-1)})}{(\ln t_j - \ln t_{j-1})} (\ln t_{j+1} - \ln t_j) + \frac{(\Delta p_{wi(j+1)} - \Delta p_{wij})}{(\ln t_{j+1} - \ln t_j)} (\ln t_j - \ln t_{j-1})}{(\ln t_{j+1} - \ln t_{j-1})} \quad (A12)$$

Equation $\Delta p_s = \Delta p_w + \frac{1}{\frac{1}{t}(\Delta p_w - \Delta p_{wd})} \frac{d\Delta p_w}{dt}$ at each time_j can be estimated by

$$\begin{aligned} \Delta p_{sj} &= \left[\Delta p_w + \frac{1}{\frac{1}{t}(\Delta p_w - \Delta p_{wd})} \frac{d\Delta p_w}{dt} \right]_j = \left[\Delta p_w + \frac{1}{\frac{(\Delta p_w - \Delta p_{wd})}{\Delta p_{wid}}} \left(t \frac{d\Delta p_w}{dt} \right) \right]_j \\ &= p_i - p_{wfj} + \frac{1}{\frac{1}{t_j} (p_i - p_{wfj} - \Delta p_{wdj})} \frac{\frac{(\Delta p_{wj} - \Delta p_{w(j-1)})}{(t_j - t_{j-1})} (t_{j+1} - t_j) + \frac{(\Delta p_{w(j+1)} - \Delta p_{wj})}{(t_{j+1} - t_j)} (t_j - t_{j-1})}{(t_{j+1} - t_{j-1})} \quad (A13) \end{aligned}$$

Equation (A9) (A11) (A12) (A13) are applied in Excel to remove wellbore storage.

The derivative of Δp_{sd} is $\Delta p_{sd} = t \frac{d\Delta p_s}{dt}$

$$\Delta p_{sdj} = \left[t \frac{d\Delta p_s}{dt} \right]_j = \left[\frac{d\Delta p_s}{d\ln t} \right]_j = \frac{\frac{(\Delta p_{sj} - \Delta p_{s(j-1)})}{(\ln t_j - \ln t_{j-1})} (\ln t_{j+1} - \ln t_j) + \frac{(\Delta p_{s(j+1)} - \Delta p_{sj})}{(\ln t_{j+1} - \ln t_j)} (\ln t_j - \ln t_{j-1})}{(\ln t_{j+1} - \ln t_{j-1})}$$

Plot Δp_{sd} vs. t to get the log-log diagnose plot after removing wellbore storage.

APPENDIX B. SPACE – FILLING DESIGN DATA AND RESULTS

Table B.1. Space-filling design data generated by JMP (a suite of computer programs for statistical analysis developed by the JMP business unit of SAS Institute)

NO.	Km (md)	Kf (md)	D (ft)	Lf (ft)
1	2	10000	340	1380
2	6	4463	0	30
3	10	1000	270	30
4	1	1000	0	30
5	1	4773	320	3080
6	1	5565	650	1850
7	5	10000	650	1760
8	10	10000	630	3300
9	10	6179	360	560
10	5	5381	210	1680
11	6	10000	0	3300
12	5	5900	580	410
13	10	10000	270	2020
14	9	2491	650	220
15	1	5560	240	350
16	9	2480	0	1400
17	5	3873	0	3300
18	1	2192	650	30
19	2	10000	20	30
20	5	1608	330	30
21	1	7623	0	1810
22	2	1000	0	2130
23	5	4407	650	3300
24	1	9751	650	30
25	10	8077	0	30
26	10	1000	40	3300
27	1	1000	610	3160
28	1	10000	640	3300
29	10	4937	370	3300
30	10	10000	650	30
31	6	9999	10	1290
32	10	1000	650	3150
33	1	1320	380	1540
34	6	8408	380	3110
35	9	5815	650	1900
36	6	10000	320	30
37	10	6349	0	2810
38	5	1000	650	1380
39	1	10000	210	3300
40	8	1000	330	2180

Table B.2. Results

NO.	E_Km (md)	E_D (md)	Reltive Erro_Km	Reltive Error_D	R_Km	R_D
1	1.9	333	6%	2%	1	1
2	-	0	-	0%	3	1
3	9.8	-	2%	-	1	3
4	-	0	-	0%	3	1
5	1.6	312	7%	3%	1	1
6	1.1	667	9%	3%	1	1
7	5	650	8%	0%	1	1
8	9	570	11%	11%	2	2
9	8.7	324	13%	11%	2	2
10	4.5	253	13%	17%	2	2
11	-	0	-	0%	3	1
12	5	-	0%	-	1	3
13	9	233	11%	16%	2	2
14	9	-	4%	-	1	3
15	0.9	215	11%	12%	2	2
16	-	0	-	0%	3	1
17	-	0	-	0%	3	1
18	1	-	0%	-	1	3
19	1.6	-	16%	-	2	3
20	4.5	-	2%	-	1	3
21	-	0	-	0%	3	1
22	-	0	-	0%	3	1
23	5	645	6%	1%	1	1
24	1	-	0%	-	1	3
25	-	0	-	0%	3	1
26	-	-	-	-	3	3
27	1	618	0%	1%	1	1
28	1.1	643	9%	0%	1	1
29	9	333	11%	11%	2	2
30	9.4	-	2%	-	1	3
31	-	-	-	-	3	3
32	8.5	586	13%	11%	2	2
33	1	386	2%	2%	1	1
34	5	341	14%	11%	2	2
35	8	580	13%	12%	2	2
36	6	-	2%	-	1	3
37	-	0	-	0%	3	1
38	5	659	1%	1%	1	1
39	1	217	3%	3%	1	1
40	6.8	285	13%	16%	2	2

APPENDIX C. SAS CODE FOR CUMULATIVE LOGIT MODELS

```
dm 'log; clear; output; clear';
*PETE 8000 project.sas--Guo, Yingying--04/22/2020;
*PETE 8000 project;
options pageno=1
        nodate
        rightmargin=.5in
        leftmargin=.5in
        topmargin=.5in
        bottommargin=.5in
        label;
ods listing;
ods html close;
ods graphics on;
ods rtf file='D:\output_yingying.rtf';
title1 'Guo, Yingying';
title2 'PETE 8000 project';

libname project 'D:\PETE 8000';
libname proxls 'D:\PETE8000.xlsx';

Proc sort data=proxls.'1000$'n
        out=work.data1;
by Km Kf Lf D E_Km E_D R_Km R_D;
label  Km = 'matrix permeability'
        Kf = 'fracture corridor permeability'
        Lf = 'fracture corridor length'
        D = 'well_corridor distance'
        E_Km = 'estimated matrix pereability'
        E_D = 'estimated well_corridor distance'
        R_Km = 'response of estimated matrix pereability'
        R_D = 'response of estimated well_corridor distance';

run;

Proc UNIVARIATE data=work.data1 Normal;
var E_Km E_D;
Title 'normarity test';

run;

Proc corr data=work.data1 nomiss plots=matrix(histogram);
var Km Kf D Lf;
Title 'correlations';

run;

Proc reg data=work.data1;
Title2 'Multicollinearity Test';
Model R_Km =Km Kf D Lf/collin;

Run;
```

```

Proc LOGISTIC data=work.data1;
    MODEL R_Km=Km Kf Lf D/ AGGREGATE influence SCALE=NONE
selection=forward;
    title 'CHOOSE MODEL for R_Km';
run;

Proc LOGISTIC data=work.data1;
    MODEL R_D=Km Kf Lf D/ AGGREGATE SCALE=NONE selection=forward;
    title 'CHOOSE MODEL for R_D';
run;

libname proxls clear;
ods rtf close;

```

APPENDIX D. SAS LOG FOR CUMULATIVE LOGIT MODELS

```
1  dm 'log; clear; output; clear';
2  *PETE 8000 project.sas--Guo, Yingying--04/22/2020;
3  *PETE 8000 project;
4  options pageno=1
5      nodate
6      rightmargin=.5in
7      leftmargin=.5in
8      topmargin=.5in
9      bottommargin=.5in
10  label;
11  ods listing;
12  ods html close;
13  ods graphics on;
14  ods rtf file='D:\output_yingying.rtf';
```

NOTE: Writing RTF Body file: D:\output_yingying.rtf

```
15  title1 'Guo, Yingying';
16  title2 'PETE 8000 project';
17
18  libname project 'D:\PETE 8000';
```

NOTE: Libref PROJECT was successfully assigned as follows:

Engine: V9

Physical Name: D:\PETE 8000

```
19  libname proxls 'D:\PETE8000.xlsx';
```

NOTE: Libref PROXLS was successfully assigned as follows:

Engine: EXCEL

Physical Name: D:\PETE8000.xlsx

20

```

21 Proc sort data=proxls.'1000'$n
22     out=work.data1;
23 by Km Kf Lf D E_Km E_D R_Km R_D;
24 label Km = 'matrix permeability'
25     Kf = 'fracture corridor permeability'
26     Lf = 'fracture corridor length'
27     D = 'well_corridor distance'
28     E_Km = 'estimated matrix pereability'
29     E_D = 'estimated well_corridor distance'
30     R_Km = 'response of estimated matrix pereability'
31     R_D = 'response of estimated well_corridor distance';
32 run;

```

NOTE: Sorting was performed by the data source.

NOTE: There were 40 observations read from the data set PROXLS.'1000'\$n.

NOTE: The data set WORK.DATA1 has 40 observations and 16 variables.

NOTE: PROCEDURE SORT used (Total process time):

real time	0.10 seconds
cpu time	0.07 seconds

```

33
34 Proc UNIVARIATE data=work.data1 Normal;
35     var E_Km E_D;
36     Title 'normarity test';
37 run;

```

NOTE: PROCEDURE UNIVARIATE used (Total process time):

real time 0.12 seconds
cpu time 0.09 seconds

38

39 Proc corr data=work.data1 nomiss plots=matrix(histogram);

40 var Km Kf D Lf;

41 Title 'correlations';

42 run;

NOTE: PROCEDURE CORR used (Total process time):

real time 5.03 seconds
cpu time 1.40 seconds

43

44 Proc reg data=work.data1;

45 Title2 'Multicollinearity Test';

46 Model R_Km =Km Kf D Lf/collin;

47

48 Run;

49

NOTE: PROCEDURE REG used (Total process time):

real time 6.81 seconds
cpu time 1.36 seconds

```

50 Proc LOGISTIC data=work.data1;
51   MODEL R_Km=Km Kf Lf D/ AGGREGATE influence SCALE=NONE
51 ! selection=forward;
52   title 'CHOOSE MODEL for R_Km';
53 run;

```

NOTE: PROC LOGISTIC is fitting the cumulative logit model. The probabilities modeled are summed over the responses having the lower Ordered Values in the Response Profile table. Use the response variable option DESCENDING if you want to reverse the assignment of Ordered Values to the response levels.

NOTE: Convergence criterion (GCONV=1E-8) satisfied in Step 0.

NOTE: Convergence criterion (GCONV=1E-8) satisfied in Step 1.

NOTE: Convergence criterion (GCONV=1E-8) satisfied in Step 2.

NOTE: Since there are more than 2 response levels, the following options have no effect -- INFLUENCE.

NOTE: There were 40 observations read from the data set WORK.DATA1.

NOTE: PROCEDURE LOGISTIC used (Total process time):

real time	0.18 seconds
cpu time	0.10 seconds

54

```

55 Proc LOGISTIC data=work.data1;

```

```

56  MODEL R_D=Km Kf Lf D/ AGGREGATE SCALE=NONE
56 ! selection=forward;
57  title 'CHOOSE MODEL for R_D';
58  run;

```

NOTE: PROC LOGISTIC is fitting the cumulative logit model. The probabilities modeled are summed over the responses having the lower Ordered Values in the Response Profile table. Use the response variable option DESCENDING if you want to reverse the assignment of Ordered Values to the response levels.

NOTE: Convergence criterion (GCONV=1E-8) satisfied in Step 0.

NOTE: Convergence criterion (GCONV=1E-8) satisfied in Step 1.

NOTE: Convergence criterion (GCONV=1E-8) satisfied in Step 2.

NOTE: There were 40 observations read from the data set

WORK.DATA1.

NOTE: PROCEDURE LOGISTIC used (Total process time):

real time 0.14 seconds

cpu time 0.07 seconds

```

59

```

```

60  libname proxls clear;

```

NOTE: Libref PROXLS has been deassigned.

```

61  ods rtf close;

```


APPENDIX E. SAS OUTPUT FOR MULTICOLLINEARITY TEST

Table E.1. Pearson correlation coefficients for independent variables

Pearson Correlation Coefficients, N = 40 Prob > r under H0: Rho=0				
	Km	Kf	D	Lf
Km matrix permeability	1.00000	-0.02424 0.8820	-0.02876 0.8602	0.04652 0.7756
Kf fracture corridor permeability	-0.02424 0.8820	1.00000	0.00236 0.9885	0.01749 0.9147
D well_corridor distance	-0.02876 0.8602	0.00236 0.9885	1.00000	0.03329 0.8384
Lf fracture corridor length	0.04652 0.7756	0.01749 0.9147	0.03329 0.8384	1.00000

Table E.2. Collinearity diagnostics for independent variables

Collinearity Diagnostics							
Number	Eigenvalue	Condition Index	Proportion of Variation				
			Intercept	Km	Kf	D	Lf
1	3.92118	1.00000	0.00667	0.01494	0.01415	0.01737	0.01774
2	0.36762	3.26596	0.00000420	0.05398	0.00027805	0.67277	0.27671
3	0.33282	3.43244	0.00310	0.23169	0.11096	0.09460	0.58360
4	0.29500	3.64583	0.00034096	0.40815	0.53601	0.03911	0.00012407
5	0.08338	6.85773	0.98988	0.29123	0.33860	0.17615	0.12183

APPENDIX F. SAS OUTPUT FOR ACCURACY OF MATRIX PERMEABILITY ESTIMATION

Table F.1. Summary for accuracy of the matrix permeability estimation by forward selection method

Summary of Forward Selection						
Step	Effect Entered	DF	Number In	Score Chi-Square	Pr > ChiSq	Variable Label
1	D	1	1	24.0501	<.0001	well_corridor distance
2	Km	1	2	9.3139	0.0023	matrix permeability

Table F.2. Parameter estimation of the accuracy of the matrix permeability estimation by forward selection method

Analysis of Maximum Likelihood Estimates						
Parameter		DF	Estimate	Standard Error	Wald Chi-Square	Pr > ChiSq
Intercept	1	1	-2.5186	1.0128	6.1840	0.0129
Intercept	2	1	0.6984	0.8490	0.6766	0.4108
Km		1	-0.4011	0.1453	7.6163	0.0058
D		1	0.0120	0.00289	17.3641	<.0001

Table F.3. Likelihood-ratio test for the accuracy of the matrix permeability estimation

Deviance and Pearson Goodness-of-Fit Statistics				
Criterion	Value	DF	Value/DF	Pr > ChiSq
Deviance	41.9132	76	0.5515	0.9995
Pearson	58.2611	76	0.7666	0.9350

APPENDIX G. SAS OUTPUT FOR ACCURACY OF WELL-CORRIDOR DISTANCE ESTIMATION

Table G.1. Summary for accuracy of the well-corridor distance estimation by forward selection method

Summary of Forward Selection						
Step	Effect Entered	DF	Number In	Score Chi-Square	Pr > ChiSq	Variable Label
1	Lf	1	1	7.9005	0.0049	fracture corridor length
2	Km	1	2	6.6903	0.0097	matrix permeability

Table G.2. Parameter estimation of the accuracy of the well-corridor distance estimation by forward selection method

Analysis of Maximum Likelihood Estimates						
Parameter		DF	Estimate	Standard Error	Wald Chi-Square	Pr > ChiSq
Intercept	1	1	-0.3784	0.7063	0.2870	0.5921
Intercept	2	1	1.0965	0.7220	2.3061	0.1289
Km		1	-0.2543	0.1029	6.1082	0.0135
Lf		1	0.000945	0.000299	10.0268	0.0015

Table G.3. Likelihood-ratio test for the accuracy of the well-corridor distance estimation

Deviance and Pearson Goodness-of-Fit Statistics				
Criterion	Value	DF	Value/DF	Pr > ChiSq
Deviance	68.4698	76	0.9009	0.7182
Pearson	80.0703	76	1.0536	0.3526

BIBLIOGRAPHY

- Agar, Susan & Geiger, Sebastian. (2014). Fundamental controls on fluid flow in carbonates: Current workflows to emerging technologies. Geological Society London Special Publications. 406. 10.1144/SP406.18.
- Ahmed Elfeel, M., Couples, G., Geiger, S., & Ma, J. (2010, January 1). Upscaled Multi-Phase Flow Properties of Fracture Corridors. Society of Petroleum Engineers. doi:10.2118/139463-MS
- Al-Kindi, M., 2006. Structural evolution and fracture pattern of Salakh Arch. PhD thesis, University of Leeds.
- Bahabanian, O., Ilk, D., Hosseinpour-Zonoozi, N., & Blasingame, T. A. (2006, January 1). Explicit Deconvolution of Well Test Data Distorted by Wellbore Storage. Society of Petroleum Engineers. doi:10.2118/103216-MS
- Barenblatt GI, Zheltov IP, Kochina IN. Basic concepts in the theory of seepage of homogeneous liquids in fissured rocks [strata]. J Appl Math Mech 1960;24:1286–303.
- Barr D., Arman K., Savory K., McGarrity J. & Fowler S. 2004. Fracture–matrix interaction and its implications for reservoirs and well performance modeling in the Clair field, west of Shetland. Paper presented at the Fractured Reservoirs Conference, London, UK, 16–17 November 2004, 5–6.
- Becker A. & Gross M. R. 1996. Mechanism for joint saturation in mechanically layered rocks: an example from southern Israel. Tectonophysics, 257, 223–237.
- Belayneh M., Matthai S. K. & Cosgrove J. W. 2007. The implications of fracture swarms in the Chalk of SE England on the tectonic history of the basin and their impact on fluid flow in high-porosity, low-permeability rocks. In: Ries A. C., Butler R. W. H. & Graham R. H. (eds) Deformation of the Continental Crust: The Legacy of Mike Coward. Geological Society, London, Special Publications, 272, 499–517.
- Blouin, C. D. 2019. Experimental Design. Department of Experimental Statistics, Louisiana State University, Baton Rouge, Louisiana, US.
- Boro, Herman & Rosero, Enrique & Bertotti, Giovanni. (2014). Fracture-network analysis of the Latemar Platform (northern Italy): Integrating outcrop studies to constrain the hydraulic properties of fractures in reservoir models. Petroleum Geoscience. 20. 79-92. 10.1144/petgeo2013-007.
- Cacas, M. & Daniel, Jean-Marc & Letouzey, J. (2001). Nested geological modeling of naturally fractured reservoirs. Petroleum Geoscience. 7. 10.1144/petgeo.7.S.S43.
- Coats KH. Implicit compositional simulation of single-porosity and dual-porosity reservoirs. In: SPE symposium on reservoir simulation. 1989. <https://doi.org/10.2118/18427-MS>.

- Computer Modeling Group (CMG) Ltd. (2015). IMEX User Guide, Version 2015. Calgary, Alberta, Canada.
- Chatelée, Sébastien & Lamarche, Juliette & Gauthier, Bertrand. (2015). Fracture Corridors in Carbonates. 10.3997/2214-4609.201413528.
- Chen, H. Y. (2013, August). Reservoir Rock Description Handbook. Department of Petroleum Engineering, New Mexico Tech, Socorro, New Mexico, US.
- Chen, H. Y. (2014, January). Engineering Reservoir Mechanics. Department of Petroleum Engineering, New Mexico Tech, Socorro, New Mexico, US.
- Cinco, L., H., Samaniego V., F., & Dominguez, A., N. (1976, January 1). Unsteady-State Flow Behavior for a Well Near a Natural Fracture. Society of Petroleum Engineers. doi:10.2118/6019-MS
- Cinco, L., H., Samaniego V., F., & Dominguez, A., N. (1978, August 1). Transient Pressure Behavior for a Well With a Finite-Conductivity Vertical Fracture. Society of Petroleum Engineers. doi:10.2118/6014-PA
- Cinco-Ley, H., & Samaniego-V., F. (1981, September 1). Transient Pressure Analysis for Fractured Wells. Society of Petroleum Engineers. doi:10.2118/7490-PA
- Denney, D. (2007, February 1). Explicit Deconvolution of Wellbore-Storage-Distorted Well-Test Data. Society of Petroleum Engineers. doi:10.2118/0207-0089-JPT
- El-Gezeery, T. M. ., Al-Saqran, F., Archibong, E. I., & Al-Radhi, S. H. (2008, January 1). Utilizing Real-Time Logging While Drilling Resistivity Imaging to Identify Fracture Corridors in a highly fractured Carbonate Reservoir. Society of Petroleum Engineers. doi:10.2118/118152-MS
- Earlougher, R.C., Jr.: Advances in Well Test Analysis, Monograph Series, Society of Petroleum Engineers (SPE), Richardson, Texas, USA (1977) 5.
- Escobar, F., Martínez, J.A., & Montealegre-Madero, M. (2013). PRESSURE TRANSIENT ANALYSIS FOR A RESERVOIR WITH A FINITE-CONDUCTIVITY FAULT. *Ciencia Tecnología y Futuro*, 5, 5-17.
- Fetkovich, M.J., and Vienot, M.E. : “Rate Normalization of Buildup Pressure By Using Afterflow Data,” JPT (December 1984)2211-24
- Fetkovich, M. J., & Vienot, M. E. (1985, February 1). Shape Factor, CA, Expressed as Skin, sCA. Society of Petroleum Engineers. doi:10.2118/13304-PA
- Fisher, R.A., and Mackenzie. W.A. (1923). Studies in crop variation. II. The manurial response of different potato varieties, *J. Agric. Sci.*, 13, 311–320.

- Fisher, R.A., and Wishart. J. (1930). The arrangement of field experiments and the statistical reduction of the results. Imperial Bur. Soil Sci., Tech. Comm., 10. 23.
- Fisher, R.A. (1935). The Design of Experiments. Oliver and Boyd, Edinburgh.
- Geaghan, P. J., (2014) Statistical Techniques I. Department of Experimental Statistics, Lousinana State University, Baton Rouge, Louisiana, US.
- Geaghan, P. J., (2014) Statistical Techniques II. Department of Experimental Statistics, Lousinana State University, Baton Rouge, Louisiana, US.
- Gilman, J. R., & Kazemi, H. (1983, August 1). Improvements in Simulation of Naturally Fractured Reservoirs. Society of Petroleum Engineers. doi:10.2118/10511-PA
- Gladfelter, R.E., Tracy, G.W., and Wilsey, L.E.: "Selecting Wells Which Will Respond to Production-Stimulation Treatment," Drill.and Prod. Prac., API, Dallas (1955) 117-29
- Gringarten, A. C. (1978, January 1). Reservoir Limit Testing For Fractured Wells. Society of Petroleum Engineers. doi:10.2118/7452-MS
- Guo, B. (2020). Experimental Statistics II. Department of Experimental Statistics, Lousinana State University, Baton Rouge, Louisiana, US.
- Hollis, Cathy & Bastesen, Eivind & Boyce, Adrian & Corlett, Hilary & Gawthorpe, Robert & Hirani, Jesal & Rotevatn, Atle & Whitaker, Fiona. (2017). Fault-controlled dolomitization in a rift basin. *Geology*. 45. 219-222. 10.1130/G38s394.1.
- J.J. Sheng, Formulation of the flow problem in anisotropic porous media using different coordinate transformations, *Journal of Petroleum Science and Engineering*, Volume 75, Issues 1–2, 2010, Pages 203-208, ISSN 0920-4105, <https://doi.org/10.1016/j.petrol.2010.11.010>. (<http://www.sciencedirect.com/science/article/pii/S0920410510002548>)
- Johnston, J.L.: Variable Rate Analysis of Transient Well Test Data Using Semi-Analytical Methods, M.S. Thesis, Texas A&M University, College Station, TX (1992).
- John P. Spivey and W. John Lee. (2013). Applied Well Test Interpretation. Society of Petroleum Engineers, 2013.
- Joseph, J. A., & Koederitz, L. F. (1982, January 1). A Simple Nonlinear Model For Representation Of Field Transient Responses. Society of K.S. Lai and W.K.S. Pao, 2013. Assessment of Different Matrix-fracture Shape Factor in Double Porosity Medium. *Journal of Applied Sciences*, 13:308-314. DOI:10.3923/jas.2013.308.314 URL: <https://scialert.net/abstract/?doi=jas.2013.308.314> Petroleum Engineers.
- J.W. Lee. Well Testing. Society of Petroleum Engineers, 1981. url: <http://site.ebrary.com/lib/ntnu/reader.action?docID=10619584>

- Kong, X. Z. (1999). *Advanced Seepage Mechanics*. China University of Science and Technology Press.
- Lapponi F, Casini G, Sharp I, et al. From outcrop to 3D modelling: a case study of a dolomitized carbonate reservoir, Zagros Mountains, Iran. *PETROLEUM GEOSCIENCE*. 17(3):283-307. doi:10.1144/1354-079310-040.
- Laubach S. E. & Tremain C. M. 1994. Fracture swarms: potential targets for methane exploration in Upper Cretaceous sandstone and coal, northern San Juan Basin, Colorado. In: Ayers W. B. & Kaiser W. R. (eds) *Coalbed Methane in the Upper Cretaceous Sandstone and Coal, Northern San Juan Basin, New Mexico and Colorado*. Bulletin, New Mexico Bureau of Mines and Mineral Resources, 146, 103–118.
- Legrand, N., de Kok, J. H., Neff, P., & Clemens, T. (2010, January 1). Recovery Mechanisms and Oil Recovery From a Tight, Fractured Basement Reservoir, Yemen. *Society of Petroleum Engineers*. doi:10.2118/133086-MS
- Liang, Xing & Liu, Xiao & Shu, HongLin & Xian, Chenggang & Zhang, Zhao & Zhao, ChunDuan & Li, QingFei & ZHANG, Lei. (2015). Characterization of Complex Multiscale Natural Fracture Systems of the Silurian LongMaXi Gas Shale in the Sichuan Basin, China. 10.2118/176938-MS.
- Li, B. (2019). *Experimental Statistics II*. Department of Experimental Statistics, Louisiana State University, Baton Rouge, Louisiana, US.
- Li, B. (2020). *Data Mining*. Department of Experimental Statistics, Louisiana State University, Baton Rouge, Louisiana, US.
- Lim K, Aziz K. Matrix–fracture transfer shape factors for dual-porosity simulators. *J Pet Sci Eng*. 1995;13(3–4):169–78. [https://doi.org/10.1016/0920-4105\(95\)00010-F](https://doi.org/10.1016/0920-4105(95)00010-F).
- Maghsood, A., & Cinco-Ley, H. (1995, March 1). Pressure-Transient Behavior in a Reservoir With a Finite-Conductivity Fault. *Society of Petroleum Engineers*. doi:10.2118/24704-PA
- Marx, B. (2020). *Experimental Statistics 7036*. Department of Experimental Statistics, Louisiana State University, Baton Rouge, Louisiana, US.
- M.R Jalali, & M.B Dusseault. (2012). Coupling Geomechanics and Transport in Naturally Fractured Reservoirs. *International Journal of Mining and Geo-Engineering*, 2, 105.
- Nelson, Ronald A.. (2001). *Geologic Analysis of Naturally Fractured Reservoirs* (2nd Edition). Elsevier. Retrieved from <https://app.knovel.com/hotlink/toc/id:kpGANFRE01/geologic-analysis-naturally/geologic-analysis-naturally>
- N.E. Odling (1997) Scaling and connectivity of joint systems in sandstones from western Norway *J. Struct. Geol.*, 19 (10), pp. 1257-1271

- Ogata K, Senger K, Braathen A, Tveranger J. Fracture corridors as seal-bypass systems in siliciclastic reservoir-cap rock successions: Field-based insights from the Jurassic Entrada Formation (SE Utah, USA). *Journal of Structural Geology*. 2014;66:162-187. doi:10.1016/j.jsg.2014.05.005.
- Ozkaya, S. I., & Bolle, L. (2006, January 1). Modeling and Upscaling Fracture Corridors – Uncertainties. Society of Petroleum Engineers. doi:10.2118/106337-MS
- Ozkaya SI, Lewandoswki HJ, Coskun SB. Fracture study of a horizontal well in a tight reservoir — Kuwait. *Journal of Petroleum Science and Engineering*. 2007;55(1):6-17. doi:10.1016/j.petrol.2006.04.008.
- Ozkaya, S. I. (2007, January 1). Detection of Fracture Corridors from Openhole Logs in Horizontal Wells. Society of Petroleum Engineers. doi:10.2118/110942-MS
- Ozkaya, S. I., & Siyabi, S. (2008, January 1). Detection of Fracture Corridors from Dynamic Data by Factor Analysis. Society of Petroleum Engineers. doi:10.2118/120812-MS
- Ozkaya, S. I. (2008, December 1). Using Probabilistic Decision Trees to Detect Fracture Corridors From Dynamic Data in Mature Oil Fields. Society of Petroleum Engineers. doi:10.2118/105015-PA
- Ozkaya, S. I. (2009, January 1). Use of Exclusion Zones in Mapping and Modeling Fracture Corridors. Society of Petroleum Engineers. doi:10.2118/120136-MS
- Ozkaya, S. I. (2010, August 1). Use of Exclusion Zones in Mapping and Modeling Fracture Corridors. Society of Petroleum Engineers. doi:10.2118/120136-PA
- Ozkaya, S. I. (2013, March 10). Structural controls of fracture corridors in some Middle East Fields. Society of Petroleum Engineers. doi:10.2118/164195-MS
- Ozkaya, S. I. (2019, November 1). Validating Predicted Fracture Corridors by Statistical Comparison With Well Data. Society of Petroleum Engineers. doi:10.2118/195582-PA
- Peaceman, D. W. (1990, January 1). Recalculation Of Dietz Shape Factor For Rectangles. Society of Petroleum Engineers.
- Questiaux J-M, Couples GD, Ruby N. Fractured reservoirs with fracture corridors. *Geophysical Prospecting*. 2010;58(2):279-295. doi:10.1111/j.1365-2478.2009.00810.x.
- Ray, Dipak & Al-Shammeli, Adnan & Verma, Naveen & Matar, Saad & Groen, Vincent & de jousineau, Ghislain & Ghilardini, Laurent & Maux, Thierry & Al-Khamees, Waleed. (2012). Characterizing and modeling natural fracture networks in a tight carbonate reservoir in the Middle East: A methodology. *Bulletin of the Geological Society of Malaysia*. 58. 29-35. 10.7186/bgsm58201205.
- Sanderson DJ, Peacock DCP. Line sampling of fracture swarms and corridors. *Journal of Structural Geology*. 2019;122:27-37. doi:10.1016/j.jsg.2019.02.006.

- Santner T.J., Williams B.J., Notz W.I. (2018) Space-Filling Designs for Computer Experiments. In: The Design and Analysis of Computer Experiments. Springer Series in Statistics. Springer, New York, NY
- Saputra, R., Hidayat, A., & Rahmanto, W. A. (2015, October 20). Adapting Fracture Corridors and Diffuse Fractures in Single Porosity Model of Ujung Pangkah Carbonate Reservoir. Society of Petroleum Engineers. doi:10.2118/176101-MS
- Schaschke, Carl. (2014). Dictionary of Chemical Engineering - economic pipe diameter. Oxford University Press.
- Schlumberger Technology Corporation Granted United States Patent for Streamline Flow Simulation of a Model That Provides a Representation of Fracture Corridors. (2014, January 14). Global IP News (India).
- Schlumberger 2008. Characterization of Fractured Reservoirs – Reliable, Predictive Models to Optimize Carbonate Reservoir Performance, brochure.
- Segall P. & Pollard D. D. 1983. Joint formation in granitic rock of the Sierra Nevada. Geological Society of America Bulletin, 94, 563–575.
- Singh, S. K., Abu-Habbie, H., Khan, B., Akbar, M., Etchecopar, A., & Montaron, B. (2008). Mapping fracture corridors in naturally fractured reservoirs; an example from Middle East carbonates. First Break, 26(5), 109–113.
- Souque C, Knipe RJ, Davies RK, Jones P, Welch MJ, Lorenz J. Fracture corridors and fault reactivation; example from the Chalk, Isle of Thanet, Kent, England. Journal of Structural Geology. 2019;122:11-26. doi:10.1016/j.jsg.2018.12.004.
- Stewart, George. (2011). Well Test Design and Analysis. PennWell. Retrieved from <https://app.knovel.com/hotlink/toc/id:kpWTDA000M/well-test-design-analysis/well-test-design-analysis>
- T. Meyer, H. H. Einstein, and V. Ivanova. Geologic stochastic modeling of fracture systems related to crustal faults. In 9th ISRM Congress. International Society for Rock Mechanics, 1999.
- Tiab, Djebbar Donaldson, Erle C.. (2012). Petrophysics - Theory and Practice of Measuring Reservoir Rock and Fluid Transport Properties (3rd Edition). Elsevier. Retrieved from <https://app.knovel.com/hotlink/toc/id:kpPTPMRR01/petrophysics-theory-practice/petrophysics-theory-practice>
- Tiab, Djebbar Donaldson, Erle C.. (2015). Petrophysics - Theory and Practice of Measuring Reservoir Rock and Fluid Transport Properties (4rd Edition).
- Trocchio, J. T. (1990, August 1). Investigation of Fateh Mishrif Fluid-Conductive Faults. Society of Petroleum Engineers. doi:10.2118/17992-PA

- Uba, M. H., Chiffolleau, Y., Pham, T. R., Divry, V. E., Al-Kaabi, A. U., & Thuwaini, J. (2007, January 1). Application of a Hybrid Dual Porosity Dual Permeability Representation of Large Scale Fractures to the Simulation of a Giant Carbonate Reservoir. Society of Petroleum Engineers. doi:10.2118/105560-MS
- Warren J, Root PJ. The behavior of naturally fractured reservoirs. Soc Petrol Eng J 1963;3:245–55, SPE-426-PA.
- Watkins, Hannah & Healy, Dave & Bond, Clare & Butler, R.W.H.. (2017). Implications of heterogeneous fracture distribution on reservoir quality; an analogue from the Torridon Group sandstone, Moine Thrust Belt, NW Scotland. Journal of Structural Geology. 10.1016/j.jsg.2017.06.002.
- W. Dershowitz, J. Hermanson, S. Follin, and M. Mauldon. Fracture intensity measures in 1-d, 2-d, and 3-d at "asp" o, Sweden. In the 4th North American Rock Mechanics Symposium. American Rock Mechanics Association, 2000.

VITA

Yingying Guo was born in Jingzhou, Hubei Province, China. She started her undergraduate studies at Yangtze University in 2011 before transferring to New Mexico Institute of Mining and Technology, Socorro, NM, from where she earned the degree of Bachelor of Science in Petroleum and Natural Gas Engineering with the Highest Honors in 2015. After that, she continued her education as a graduate student at Louisiana State University in the Craft and Hawkins Department of Petroleum Engineering, Baton Rouge, LA. As her interest in the science of probabilistic data grew, she decided to enter the Department of Experimental Statistics at Louisiana State University in 2018. It was a challenge to open the campus and teach lab courses while keeping all the students, staff, and faculty safe when COVID-19 broke out in the United States. She made 35 professional teaching videos for the course PETE 4059 (mud lab) and EXST 7014 (experimental statistics II) all by herself during the COVID-19 pandemic, which she enjoyed most in her studying at Louisiana State University. Yingying anticipates earning her Master of Science degree in Petroleum Engineering and her Master of Applied Statistics degree in December 2020. Upon completing her master's degrees, she plans to go back to China and establish her own company.

Yingying is a fan of Lego. She built a Lego town and likes to modify Lego sets. She is passionate about painting and baking as well. She spends Saturdays refining her colored pencil drawings. She also makes all kinds of Chinese cake, cookies, and bread, such as mooncakes, egg yolk pastries, and crepe cakes during her free time.

Yingying likes making friends with people all over the world. She appreciates having such a wonderful experience in the United States, which allowed her to work, study, and live with people from different cultures and backgrounds. Her friends taught her many skills, told her always to be herself, and continued her happy life wherever she is in the world.